AN OPTICAL AND ELECTRICAL STUDY OF *a*-Ge-Se-In AND *a*-Ge-Se-In-Bi GLASSY ALLOYS

by

Ishu

A THESIS SUBMITTED IN FULFILLMENT OF THE REQUIREMENTS FOR THE DEGREE OF

DOCTOR OF PHILOSOPHY

IN

PHYSICS

JAYPEE UNIVERSITY OF INFORMATION TECHNOLOGY
WAKNAGHAT
JUNE 2008

For my powerhouse; my loving parents…….

Acknowledgements

It is a pleasure to thank all people collaborated directly or indirectly with my research that made this thesis possible.

First and foremost it is my great privilege to express my deep and sincere gratitude to my PhD supervisors, **Dr. P. B. Barman** and **Dr. S. K. Tripathi** (Panjab University, Chandigarh) for giving me opportunity to research under their combined supervision and sound guidance. With their valuable co-operation, enthusiasm and encouragement they provided me smooth and rewarding research life.

I extend my warm and sincere thanks to Prof. (Dr.) S. C. Katyal (Head, Department of Physics), Dr. S. K. Khah, Mr. Pankaj Sharma, Dr. Vineet Sharma and Mr. Dheeraj Sharma for consistent support.

I truly thank to JUIT authorities especially **Dr. Y. Medury**, **Prof. D. S**. **Chauhan** and **Brig. (Retd.) Balbir Singh** for providing me every kind of financial and administrative assistance during entire course.

I am thankful to our librarian Mr. Shri Ram and Mr. Vipin Sharma for their cooperation during entire work.

I would like to express my deep sense of gratitude and indebtedness to my Better-half, Parents, Ms. Sukanya Raina (*my naani*) and primarily my Brother for their complete association and unflagging love during my research work.

I am really thankful to my friends; Madhu, Sangeeta, Ambika from JUIT and especially Akshay and Sumit from Panjab University, Chandigarh who rendered every type of assistance and provided me a convivial place to work.

Finally, for the completion of this work, I thank to the almighty **God** for fulfilling my desire to complete this study under **HIS** kind blessings.

Date: June 30, 2008 **(*Ishu*)**

Abstract

This thesis work is concerned with the study of optical, electrical and physical properties of *a*-Ge-Se-In and *a*-Ge-Se-In-Bi glassy alloys and their corresponding thin films. Glassy alloys and their thin films prepared and studied are:

I. $Ge_{20}Se_{80-x}In_x$ (x = 0, 5, 10, 15, 20)

II. $Ge_{20}Se_{70-x}In_{10}Bi_x$ (x = 2, 4, 6, 8, 10)

Melt quench technique has been used for the growth of glassy alloys. Thin films of prepared samples were deposited using thermal evaporation technique at base pressure of ~10^{-4} Pa. X-ray diffraction technique has been used to know the nature (amorphous or crystalline) of bulk and deposited films. The optical properties have been estimated by analyzing the transmission spectra (400 – 1800 nm) obtained from ultraviolet-visible-near infrared spectrometer. Swanepoel's method has been used to determine refractive index and extinction coefficient. Optical band gap has been calculated using Tauc extrapolation. The various electrical measurements on the thin films including both the dark and photoconductivity measurements at different temperatures were carried out in a metallic sample holder under a vacuum ~ 10^{-3} mbar throughout the measurements. Steady state photoconductivity has been studied in temperature range 303 – 375 K. Intensity dependent photocurrent has been measured in 3 - 1035 Lux range. Physical parameters of both *a*-Ge-Se-In and *a*-Ge-Se-In-Bi glassy alloys have been estimated.

The thesis has been divided into six chapters;

General introduction of amorphous semiconductors and their classification is described in chapter I. The dawn of chalcogenide glasses (ChG), their binary and ternary compounds and the addition of metal impurities to ChG has been described. A brief introduction of general properties of ChG has also given. Various models applicable to ChG, their applications, motivation and objective of the thesis have also been included.

Chapter II describes the experimental techniques used for the preparation of glasses, deposition of thin films, characterization of bulk and thin films for X-ray

diffraction, optical and electrical properties. Density measurement of bulk glasses has also been described.

Chapter III contains experimental observations and general discussion of various parameters related to optical and electrical properties of *a*-$Ge_{20}Se_{80-x}In_x$ (x = 0, 5, 10, 15, 20) thin films. Optical parameters have been determined from their normal incidence transmission spectra in the wavelength range of 400-1200 nm. Dark and photoconductivity measurements of $Ge_{20}Se_{80-x}In_x$ thin films as a function of temperature in the range 303-375 K have also been studied.

In chapter IV, effect of Bi addition on *a*-Ge-Se-In thin films has been studied. Optical and electrical properties of $Ge_{20}Se_{70-x}In_{10}Bi_x$ (x = 2, 4, 6, 8, 10) vacuum evaporated thin films are determined. Optical parameters, in the wavelength range 400 – 1800 nm, are calculated from their normal incidence transmission spectra. Dark and photoconductivity of $Ge_{20}Se_{70-x}In_{10}Bi_x$ thin films as a function of temperature (300-360 K) have also been investigated.

Chapter V deals with the estimation of physical parameters *viz.* mean bond energy, glass transition temperature, cohesive energy, average single bond energy, density, compactness and molar volume of both *a*-Ge-Se-In and *a*-Ge-Se-In-Bi glassy alloys.

Finally, chapter VI deals with the summary and overall conclusion of the work.

List of Publications

1. **Ishu Sharma**, S. K. Tripathi, A. Monga and P. B. Barman, "*Electrical properties of a-Ge-Se-In thin films*" **Journal of Non-Crystalline Solids** 354 (2008) 3215.

2. **Ishu Sharma**, S. K. Tripathi and P. B. Barman, "*Compositional dependence of physical properties in Ge-Se-In glassy semiconductors"* **Physica B: Condensed Matter** 403 (2008) 624.

3. **Ishu Sharma**, S. K. Tripathi and P. B. Barman, "*An optical study of a-$Ge_{20}Se_{80-x}In_x$ thin films in sub-band gap region*" **Journal of Physics D: Applied Physics** 40 (2007) 4460.

4. **Ishu**, S. K. Tripathi and P. B. Barman, "*Effect of indium incorporation on the physical parameters of Ge-Se glassy alloy*" **Journal of Optoelectronics and Advanced Materials** 9 (2007) 3039.

5. **Ishu**, S. K. Tripathi and P. B. Barman, "*Influence of composition on the optical band gap in a-$Ge_{20}Se_{80-x}In_x$ thin films"* **Chalcogenide Letters** 3 (2006) 121.

6. **Ishu Sharma**, A. Kumar, S. K. Tripathi and P. B. Barman, "*Effect of Bi addition on the electrical properties of a-Ge-Se-In Thin Films*" **Journal of Physics D: Applied Physics** (2008) [Communicated].

7. **Ishu Sharma**, S. K. Tripathi and P. B. Barman, "*Correlation between the physical and optical behavior of a-Ge-Se-In-Bi system*" **Philosophical Magazine** (2008) [Communicated].

8. **Ishu Sharma**, S. K. Tripathi and P. B. Barman, "*Effect of Bi Addition on the Optical Behavior of Thin Films of a-Ge-Se-In Glassy Alloys*" **Applied Surface Science** (2008) [Communicated].

Conferences (National/International)

9. **Ishu Sharma**, Pankaj Sharma, S. K. Tripathi and P. B. Barman, "*Photoconductive measurements of thermally deposited a-$Ge_{20}Se_{80-x}In_x$ thin films*" **Recent advances in innovative materials (RAIM-08)** 57.

10. **Ishu Sharma**, Pankaj Sharma, S. K. Tripathi and P. B. Barman, "*Optical and electrical study of a-Ge-Se-In thin films"* **DAE-SSPS** 52 (2007) 599.

11. **Ishu,** Pankaj Sharma, S. K. Tripathi and P. B. Barman, "*Effect of Indium Incorporation on the Optical Parameters of Germanium Selenide*" **International Conference on IT, 19-21 March, 2007** (HIT, Haldia, W.B.).

Contents

List of Figures

List of Tables

CHAPTER I

Introduction

1.0 Introduction

Solids are a particular state of condensed matter characterized by strong interaction between the constituent particles (atoms, molecules). Solids can be found or prepared either in an ordered (crystalline) state or in a disordered (non-crystalline) state. An ideal crystal corresponds to a regular arrangement of atoms in a lattice with well defined symmetry and a structural unit called unit cell. A real crystal does not exhibit perfect periodicity in space and contains various kinds of imperfections or defects. Solids with irregular arrangements of the atoms are called non-crystalline or amorphous or vitreous or glassy solids. Such a disordered structure manifests itself as a hollow pattern of electron diffraction. It is not always obvious to decode the difference between amorphous and crystalline solids by merely examining the stochiometric compositions in diffraction and spectroscopic measurements. Compositional trends in bond and site signature can provide important clues on their microscopic origin. The differences in the structure stem from the fact that, in glasses, matter is structurally arrested at lower density (or at high molar volume) than in crystals. The structure of solids depends upon the nature of bonding scheme of constituent atoms. For amorphous covalent solids, coordination of the atoms retains short range order. We define short-range order (SRO) as a length scale not longer than the second-nearest-neighbor distance. SRO upto few atomic distances exists in amorphous materials and is an essential aspect which differentiates it from crystalline materials. This loss of long range order (LRO), a characteristic of crystalline solids, is the appearance of fluctuations in angles and distance between the bonds. Variation in bond lengths and bond angles are usually regarded as defects in amorphous solids (*a*-solids). The presence of strained and weak bonds gives rise to band tail which replaces the sharp band edges of crystalline semiconductors. Density of electronic states in crystalline solids decreases sharply to zero at the band edge. Band structure of amorphous solids is shown in figure 1.1. In *a*-semiconductors, the coordination number of atoms varies from site to site implies higher compositional disorder in these materials. The fluctuations in the atomic potential caused by the disorder give rise to localized states which result into tailing of band edges. The tailing depends on the extent of disorder present in the material. If this disorder is large, these tails can overlap in the mobility gap.

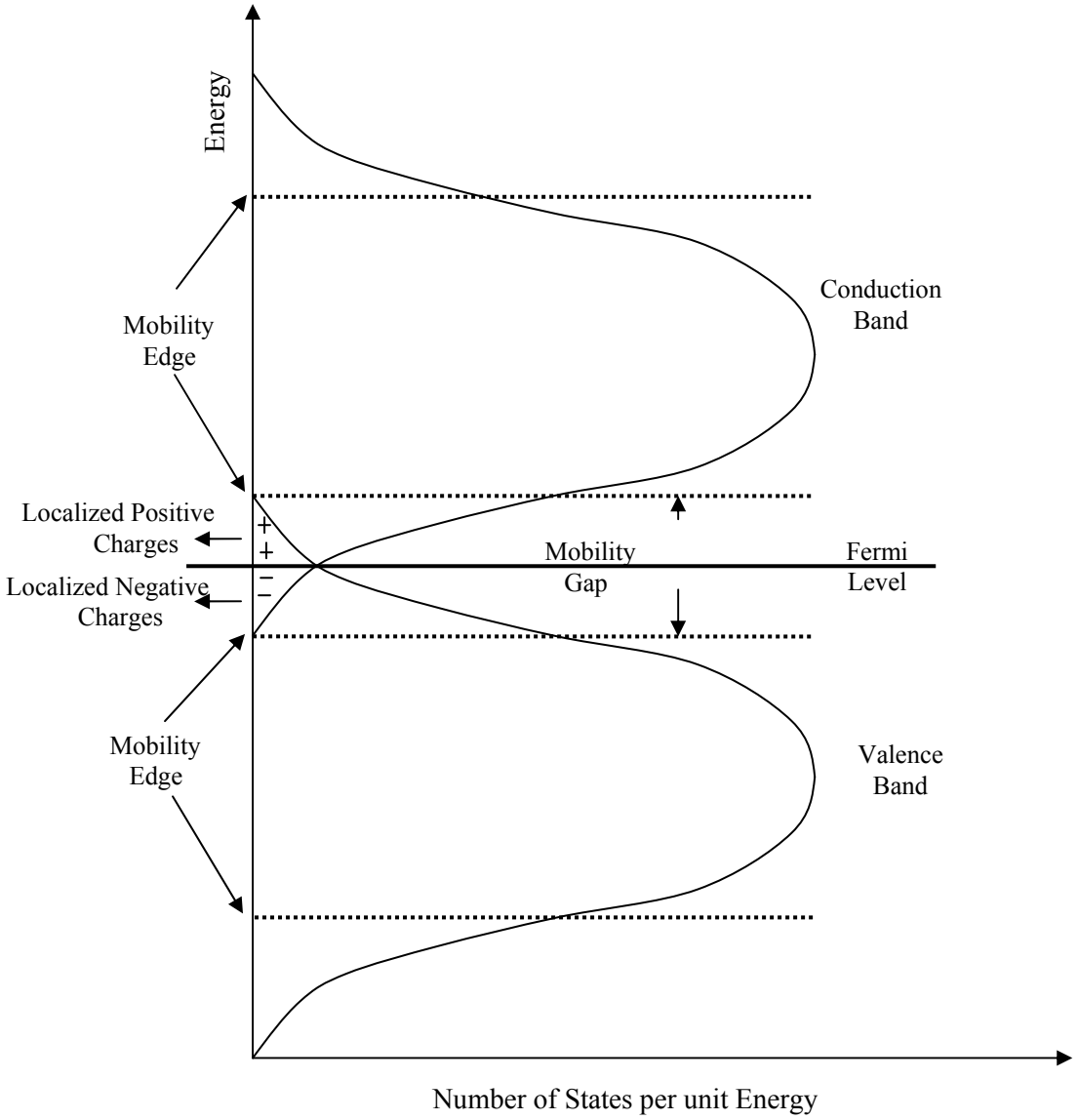

Figure 1.1 Band structure of amorphous semiconductors.

It implies that in some regions of the material, either the stretching or the bending of a bond tends to increase energy of the valance band states and decrease the energy of the conduction band. To lower their energy, such electrons move from valance band tail into the states in conduction band tail. The empty valance states, so formed, give rise to a random distribution of localized positive charges and the occupied conduction band states develop an equal number of localized negative charges. These charged states, above and below the Fermi level, act as efficient trapping centers for electrons and holes.

The crystalline state of a solid is limited to only a few structural forms but disordered material is neither unique nor clearly defined. This lack of understanding of many properties of these materials which differ from crystalline materials, even some of their properties are different from one sample to another, makes it interesting material from the research point of view and the quest of human being pushed him towards the glass sciences. A glass is defined in ASTM [American Society for Testing Materials] as 'an inorganic product of fusion which has been cooled to a rigid condition without crystallization'. In general glass scientists regard the term 'glass' as covering 'all non-crystalline solids that shows a glass transition' irrespective of their preparation methods. However, scientific investigations on amorphous solids started only in this century, about 75 years back. Zachariasen [1] proposed that the structure of vitreous SiO_2 can be described by a continuous random network [*CRN*].

1.1 Classification of Amorphous Semiconductors

There are different modes for the classification of amorphous materials due to their wide spectrum of properties; physical or chemical and the techniques employed for their preparation. On the basis of electrical properties, amorphous materials can be conductors, semiconductors and insulators and in some cases at very low temperature, they can be superconductors. It can be on the basis of their preparation method from solid, liquid or vapor phases leading to amorphous solid, glass and films respectively. On the basis of difference in their chemical bonding, amorphous materials can be classified into three major categories followed by their sub categories and are tabulated in table 1.1.

Table 1.1 Classification of amorphous materials.

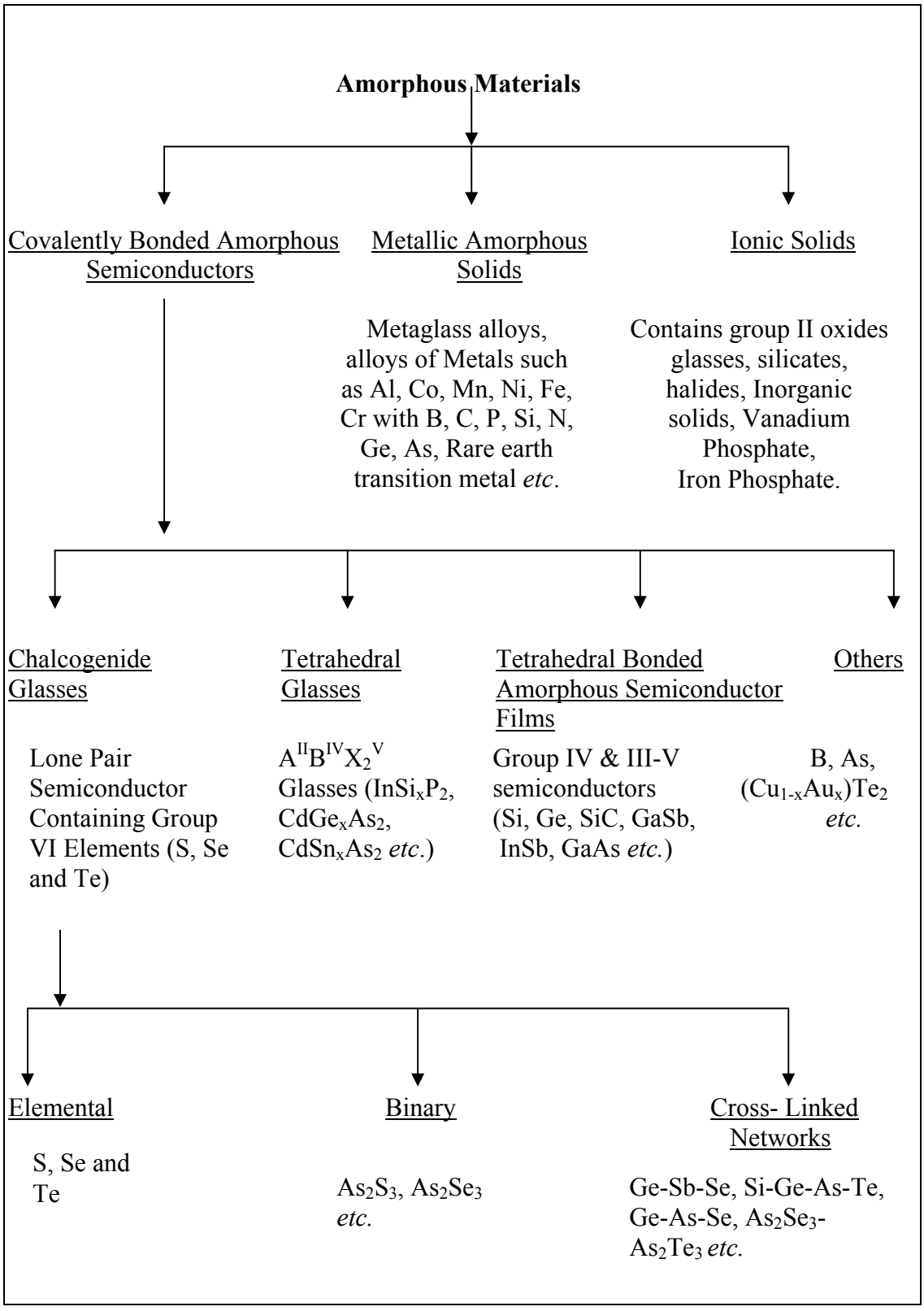

1.1.1 Dawn of Chalcogenide Glasses

Chalcogenide glasses are the chains of random lengths and random orientations formed by bonding of chalcogen elements sulphur (S), selenium (Se) and tellurium (Te) and alloys containing these chalcogen as the major constituents. Systematic research on chalcogenide glasses started at the middle of the twentieth century. Chalcogenide glasses have been of enormous interest for infrared optics since 1950 [2]. In 1968, S.R. Ovshinsky [3], made an outstanding discovery; the memory and switching effects exhibited by certain chalcogenide films subjected to electrical fields.

The structure of a glass is very important because many properties depend on it. In 1978 Popescu [4] and in 1979 Phillips [5] demonstrated that in many non-crystalline solids an 'ordering at not too large scale but more extended than the short-range order' must be admitted in order to explain the first sharp diffraction peak (FSDP). Thus the concept of medium-range order or intermediate-range order was born. The glass structure consists of covalently bonded molecules, as opposed to the ionic bonding of other glasses and these are weakly bound via a combination of covalent and vander Waal like attraction [6,7]. The amorphous chalcogenide field continued to develop both from fundamental and applications point of view. New phenomena were discovered, new applications emerged. The recent discovery of intermediate, self-organized phases in chalcogenides and other glasses [8,9] will have high impact not only in glass science but also in many other fields of research *viz.* protein folding, thin-film gate dielectrics and high-temperature superconductivity. The freedom allowed in the preparation of glasses in varied compositions brings about changes in their short range order and thus results in variation of their physical properties. Therefore, it is possible to tailor their various properties, as desired, for technological applications. They have well defined niches in passive and active applications like grating fabrication, phase change optical disk, glass waveguide for IR evanescent wave sensor, photoinduced waveguide, fiber fabrication, fiber amplifiers and lasers, IR micro lens arrays, optical switching, optical computing, regeneration, efficient femtosecond devices *etc*. [10-17], many of which have been realized or anticipated but still a lot of work is needed for complete understanding of these materials.

1.2 Band Models for Amorphous Semiconductors

The key to understanding of the electronic properties of the materials is knowledge of their electronic band structure. In case of crystalline semiconductors, sophisticated theoretical models are available for their structure. In case of *a*-semiconductors, theories of band structure are crude and qualitative because long range periodicity is absent. Different models have been proposed to explain the electrical and optical properties of non-crystalline semiconductors in terms of 'states in gap', which are normally due to defects *i.e.* the presence of strained and weak bonds. For a rigid network, conduction (or valence) band differs from that in a crystal in having a 'tail' of states localized in the sense of Anderson [18] and any charge carriers created in these states will be localized on some weak, strained or dangling bonds. These localized states are inevitable in the amorphous materials. The localized states being separated from the extended states by an energy known as mobility edge [19].

Electronic energy states of a semiconductor consist of delocalized states like valence and conduction bands, commonly known as extended states and the localized states like tails and dangling bond states. The extended states are due to short range order and the tail states are due to translational and compositional disorder which is assumed to cause fluctuations of the potential of sufficient magnitude such that they give rise to localized states extended from the conduction and valence bands in the gap. The extended states are quantum mechanical states of motion in which electron may be found anywhere in space with equal probability. A single model can not describe the essential features of all amorphous materials. So, various models and even their modifications have been proposed to give appropriate understanding of the vital features of these semiconductors. To describe the properties of amorphous materials, three basic models are given below.

1.2.1 CFO Model / Mott - CFO Model

For alloy glasses which contains compositional as well as potential disorder the '*CFO*' model was put forward by Cohen, Fritzsche and Ovshinsky [20] shown in figure 1.2. They investigated the tails of localized states pulled out of the conduction

and valence band by the disorder and some overlap between these tails. Such overlapping states would pin the Fermi level. The principal concept of this model was the existence of mobility edges, identical with the critical energies 'E_c' and 'E_v', introduced earlier by Mott [21], so also known as Mott – CFO Model. The character of wave function changes at 'E_c' and 'E_v', separating localized states from extended states. In extended states, the electron and hole mobility drops sharply as compared to high density states, so called 'mobility edges'. It also defines mobility gap *i.e.* E_c - E_v, which contains only localized states.

1.2.2 Davis – Mott Model

This model was proposed by Davis and Mott [22] and band model is shown in figure 1.3. According to this model the mobility edges for electron and holes lie again at 'E_c' and 'E_v'. A strong distinction is made between localized states which originate from lack of long range order and others which are due to defects in the structure. The defect states form longer tails but of insufficient density to pin the Fermi level, but author proposed a bend of compensated levels near the gap centre in order to pin the Fermi level. Thermally assisted hopping may also take place in these ranges.

1.2.3 Mott, Davis and Street Model

This model is a further amendment of Mott and Davis model. According to Mott, Davis and Street model the centre band further splits into two levels forming donor and acceptor bands as shown in figure 1.4. According to Mott [23], the bands of localized states originate due to the dangling bonds. These bonds can take zero, one or two electrons and are, therefore, designated as D^+, D^0 and D^- states respectively. The dangling bond energy levels depend mainly on the lattice distortion and the energy level involved. In actual case two electrons are shared in a chemical bond between atoms. In certain configuration, the atoms are not able to share the electrons and the bond breaks. Because of this unstable situation, the dangling bond emerges out. If a dangling bond is singly occupied *i.e.* D^0, it is neutral, indicating that an electron spin resonance signal is expected. If an additional electron is attracted by the dangling bond, thus providing a lone pair, designated as D^-, indicating that there will

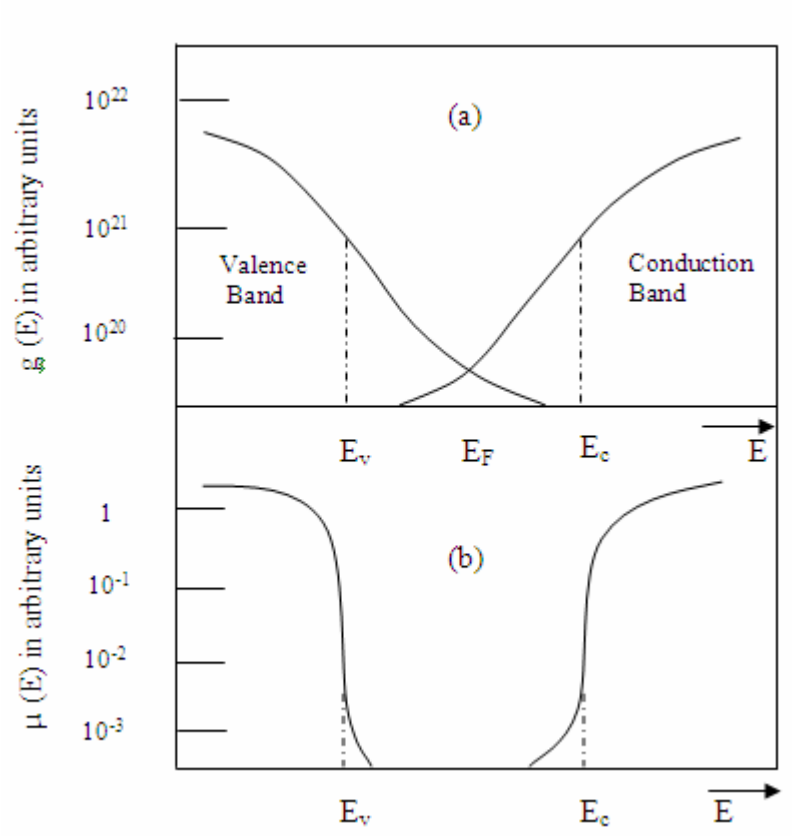

Figure 1.2 Sketch of (a) the partial densities of states of the valence and conduction bands and (b) the electron and hole mobility, respectively.

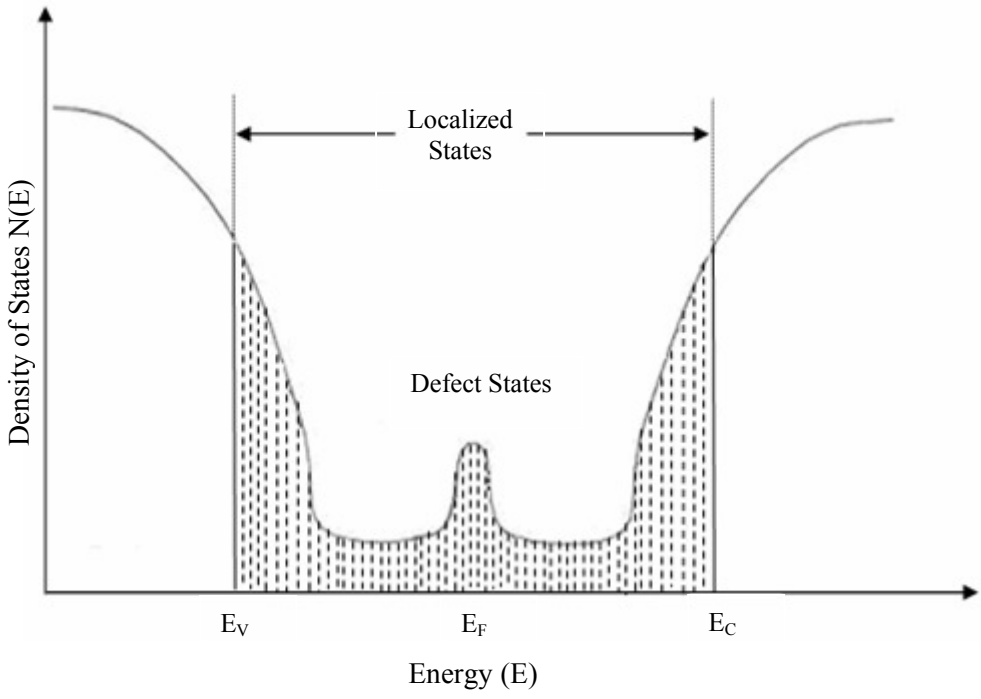

Figure 1.3 Sketch of Mott and Davis Model.

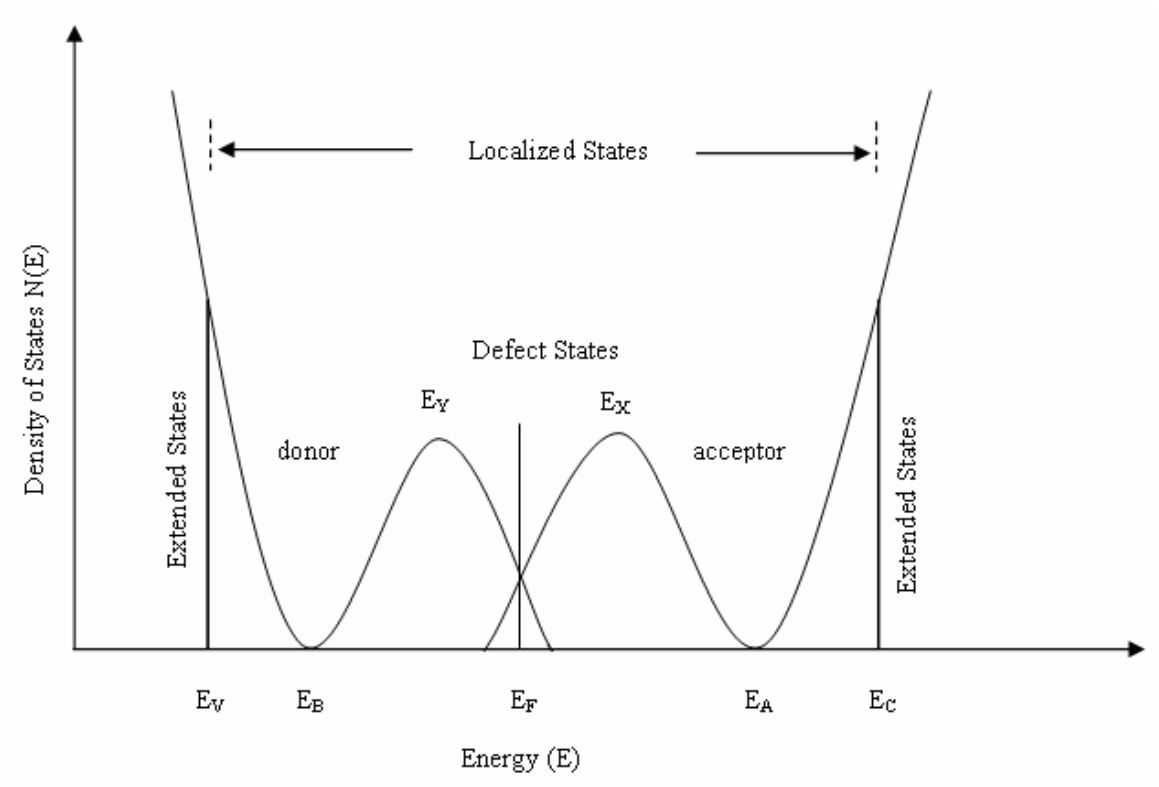

Figure 1.4 Sketch of Mott, Davis and Street Model.

be no ESR signal and when the bond even loses the single electron it will be D^+, giving rise to a hole representing a bond without any spin. The model is based on the assumption that only paired states *i.e.* D^+ and D^- are preferred in chalcogenide glasses.

1.3 Defect States in Amorphous Semiconductors

In amorphous semiconductors defect is defined as a departure from the fully coordinated random network. One type of point defect concerns the atomic coordination, which occurs due to either under or over – coordination. 'Under coordinated defects' are simply known as dangling bonds or broken bonds. A neutral dangling bond normally contains one electron but under certain conditions (*e.g.* chemical or electronic doping), the electronic occupancy can be changed to create negatively or positively charged dangling bonds. Photoluminescence study [24], photoconductivity measurements [25] and pinned Fermi level gives the evidences that chalcogenide glasses contain high concentration of defect states. Paramagnetism study at lower temperature [26] and absence of ESR signal shows the absence of unpaired electrons which is a characteristic feature of broken bonds. In amorphous chalcogenides, the electron – phonon coupling causes the network to relax to a new equilibrium state at a lower total energy. The addition of an electron into a dangling bond *i.e.* spin pairing of electron at a defect centre, may cause a change in the bonding, which lowers the electronic energy by an amount U_r. Now the effective correlation energy for two spin paired electrons at a same site, is given by

$$U_{eff} = U_c - U_r = U_c - \frac{\lambda^2}{c}, \tag{1.1}$$

where, λ is the electron – phonon coupling constant and the force constant c is related to phonon frequency as $\omega = \sqrt{c/m}$, which is taken to be constant. U_{eff} is negative if $U_c < U_r$, *i.e.*, for strong electron - lattice coupling. This spin pairing defect is called the negative U defect. This idea proposed by Anderson [27] was first applied to defect in amorphous chalcogen by Mott and Street [28] and later by Kastner *et al*. [29]. These defects are often called as *charged-dangling bond* (*CDB*) as defect of dangling bond is charged due to pairing of electrons and holes. The feature of *CDB* in

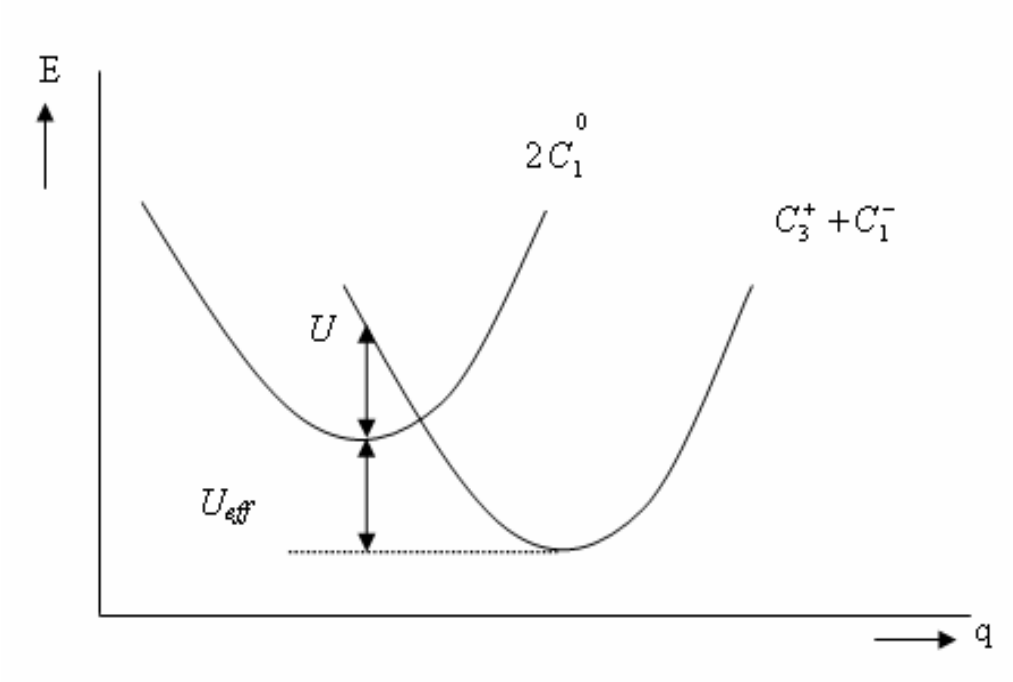

Figure 1.5 Configuration-coordinate diagram for the formation of a $D^+(C_3^+)$ - $D^-(C_1^-)$ pair.

a-Se can be presented by a model as shown in figure 1.5.

The structure of Se is two fold coordinated and is believed to consist mostly of chains. The dangling bond will contain an unpaired electron if electron – phonon interaction is not strong and is written as C_1^0. However, electron pairing should occur at C_1^0 centre due to low atomic coordination resulting in a high degree of network flexibility (strong electron – phonon interaction). There are also non-bonding $p\pi$ orbitals at chalcogen atom (Se or S) and hence the transfer of an electron from one C_1^0 centre to another produces a negatively charged C_1^- (electron spin paired) and a three-fold-coordinated positively-charged dangling bond C_3^+ (hole spin paired). The reaction

$$2C_1^0 = C_1^- + C_3^+, \tag{1.2}$$

is thus exothermic with an effective negative correlation energy. Using configuration coordinate diagram, this process is illustrated in figure 1.5. Thus the neutral C_1^0 is unstable and $2\,C_1^0$ transform into a pair of C_1^- and C_3^+, which is called a *valence – alteration pair* (VAP) by Kastner *et al.*

1.4 Ge-Se Glassy System / $Ge_{20}Se_{80}$ System

Current research deals with the ternary and quaternary alloys for which basic system consist of Ge-Se network. Se is the best in many respects in the chalcogen series. Among the glasses, only Se vitrifies as an elemental glass which is fairly stable at room temperature. Besides the wide commercial/device applications like switching memory, xerography *etc*., Se also exhibits a unique property of reversible transformation [30]. This very property makes it very useful in optical memory devices but pure Se has also some shortcomings like short life time and low sensitivity. On addition of Ge to Se, Ge atoms act as bond modifiers. Se based chalcogenide glasses in which the linear polymeric structure of two fold coordinate, Se atoms can be modified by introducing atom of higher coordination number such as Ge having *CN* = 4. They strengthen the average bond by cross linking the Se chain structure, thereby increasing the glass transition temperature and resistivity [31] and also overcome some difficulties of pure Se. Upon introducing the Ge content to the Se

polymeric chain, the structure leads progressively to a 3-*D* network. A completely cross-linked network is reached at the compound composition $GeSe_2$ – tetrahedra – bearing back bone of the glasses. The concentration of disordered bonds (Ge-Ge and Se-Se) is very less in $GeSe_2$ glass. Because of the small concentration of homopolar bonds, the structure of the stochiometric glass has often been assumed to be [32,33] defected continuous random network (*CRN*). At higher Ge concentration, the structure gets weakened by increasing number of weaker Ge-Ge bonds. Ge_xSe_{1-x} glasses are among the best covalent glass formers. Ge-Se glasses have been particularly studied because of their ready glass formation, easy synthesis requirements and good chemical stability. By studying this system, fundamental glass properties may be understood more easily without complications arising from ionic forces such as those in canonical glasses like the silicon oxides since in chalcogenide glasses maximum fraction of ionic bond is only about 9 %. The Ge-Se glasses show some very remarkable thermal and photo-induced structural transformations. Recently, it has been observed that under suitable excitation condition, some of the photo-induced transformations may be reversible. These materials are potential technologically-important photo resist [34-36].

The Ge-Se system was the first in which formation of an intermediate phase was demonstrated experimentally by Boolchand *et al.* [37] and further developed theoretically by Thorpe *et al.* [38]. In binary Ge_xSe_{1-x} glasses, the self-organized phase exists in the $0.20 < x < 0.254$ range. In this phase, glass compositions are configurationally close to their liquid counterparts while glasses with $x < 0.20$ are regarded as floppy and those with $x < 0.26$ are stressed rigid. Dynamic calorimetric measurements on the intermediate phase have led to the conclusion that such materials do not age, [9,39] a feature that might be of importance in application of these materials.

For a covalently bonded network constrained by bond stretching (α) and bond bending (β), Phillips [5,40] suggested that the glass forming tendency will be optimized when the number of constraints per atom (N_c) equal the degree of freedom (N_d). Enumeration of α and β constraints for three dimensional network showed that condition is satisfied when the mean coordination number $< r >$ of a network

acquires a critical value $< r >$ = 2.4. To explain the strong glass forming property of some chalcogenide system, Phillips advanced that the covalent bonding in glasses may be optimized when the average coordination number $< r >$ = 2.4. When, $N_c < N_d$, the unconstrained glass is floppy in nature. At this stage the connectivity of the glass is diluted. Here the average coordination number is nearly two. Network has begun to fall apart into disconnected chain segment. On adding cross-linking bonds at random, the number of such floppy modes, whose number per atom f is $N_d - N_c$, decreases and it extrapolates to zero at average coordination number of 2.4, corresponding to $Ge_{20}Se_{80}$ composition. This transition is a new glassy phase, the 'intermediate phase', which is strictly a topological phase. The phase has no special symmetry, but it does have a characteristic connectivity. This glassy phase is not an equilibrium phase; it is not a true phase in the sense of equilibrium thermodynamics. Two transitions define the limits of an intermediate phase that separates the floppy from the stressed rigid phase. It has lead to a structure based classification of glasses in terms of their elastic response; floppy-intermediate-stressed rigid. When, $N_c = N_d$, the network is rigid and yet stress free and if $N_c > N_d$, the glass network is rigid and stressed.

Glasses of Ge_xSe_{1-x} system can be obtained in the whole range $0 < x < 42$, if a sufficiently small amount of material is quenched [41]. The glass of composition $Ge_{20}Se_{80}$ was characterized on the basis of radial distribution measurements, as a definite compound with chemical formula $GeSe_4$ and structure where $GeSe_4$ tetrahedra are linked through Se-Se bonds in the covalent network [42].

The structure of chalcogenide glasses consists of chalcogen chain, $[\text{-Se-}]_n$, that are cross-linked by four linked (Ge) metalloid atoms. In such glasses, the amount of cross linking is important. The average coordination number defined by [5]

$$< r >= 2(x+1), \qquad (1.3)$$

allows for a simple description of the expected amount of cross linking of Ge_xSe_{1-x} glass network ($x \leq 1$), provided germanium and selenium are four fold and two-fold coordinated respectively. For $< r >$ values between 2.2 and 2.4 (corresponding to $GeSe_4$ stoichiometry), the glass network is built on $GeSe_4$ units, two germanium atoms being separated by selenium chains of at least two atoms. This structure

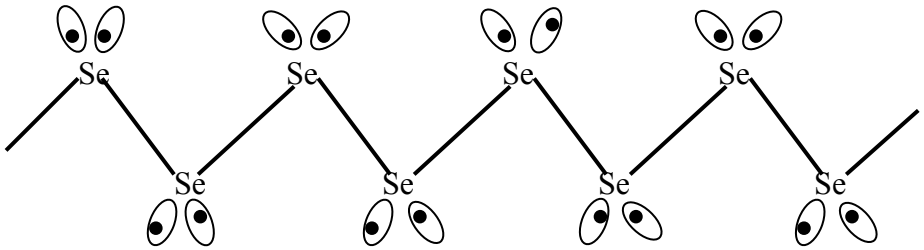

$(Se)_n$

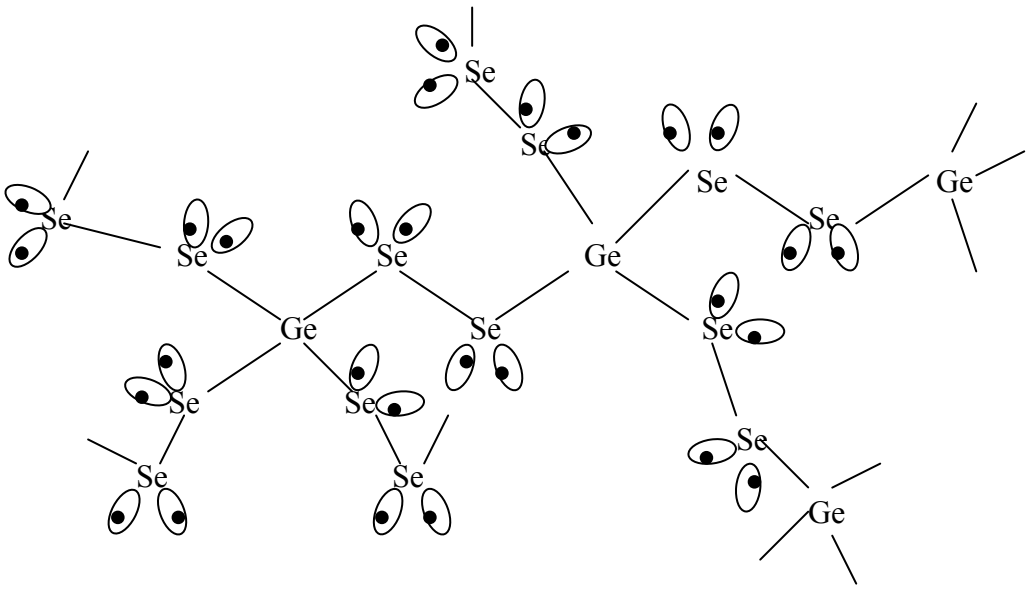

$Ge_{20}Se_{80}$

Figure 1.6 Schematic drawings of the structure of $(Se)_n$ and Ge-Se glasses at atomic scale.

organizes to form tri-layer units, where the two outside layers contain the chalcogen anion and centre layer contains germanium. A rigidity percolation threshold is associated with $< r >= 2.4$ corresponds to a fully cross-linked network with two selenium atom segments between germanium atoms as shown in figure 1.6.

Ample experimental evidence in support of the existence of this threshold in the property-composition dependence for chalcogenide glasses comes from thermal, physicochemical [43-45], neutron [46,47], Mossbauer [48,49], mechanical [50], electronic [51], vibrational [52,53] measurements. Furthermore, its existence has been confirmed by computer simulations of bond-depleted diamond network [54], 2*D* triangular central force networks [55] and self-organizing networks [56].

1.5 General Properties of Ge-Se System

In tetrahedral semiconductors (Si, Ge, III-V compound *etc*.), bonding band forms the valence band and antibonding bands forms the conduction band, but the situation is quite different in chalcogenide glasses. In chalcogenide glasses, the valence band (σ-bonding) originates from lone-pair (*LP*) electron states whereas the conduction band arises from antibonding (σ^*) states.

Ge in four fold coordination has hybridized sp^3 orbitals which split into bonding (σ) and antibonding (σ^*) states. In solid, these molecular states are broadened into bands. Thus in tetrahedral semiconductor bonding bands forms the valence band and antibonding bands form the conduction band. In Se, on the other hand, s-state lie well below the p-states and need not be considered. Se is normally two fold coordinated because only two of the p-states are utilized for the bonding. So leaves one non-bonding electron pair. These unshared or lone pair electrons form a band near the original p-state energy as shown in figure 1.7. σ and σ^* bands split symmetrically. Both σ and lone pair bands are occupied. Thus bonding band is no longer the VB; this role is played by lone pair band. Here lone – pair band determines the conduction properties, these materials might appropriable be called as Lone Pair Semiconductors. In both cases, a filled state is pulled out of the σ band and an unoccupied state forms σ^* band. In tetrahedral materials, these produce localized states in the gap. Considering Coulomb interaction and correlation, one estimates that

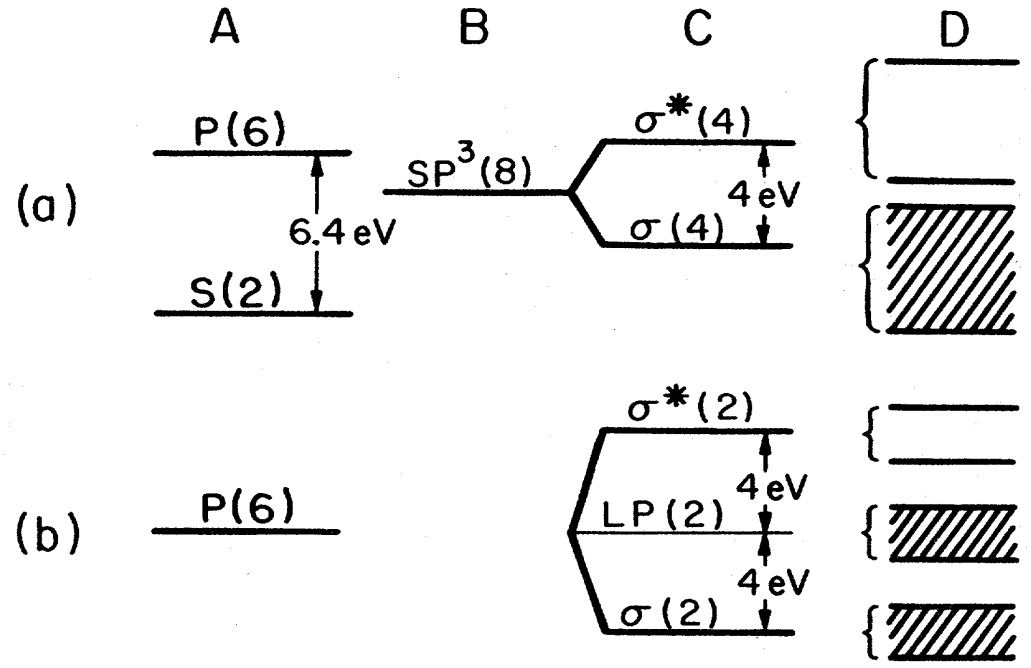

Figure 1.7 Bonding in (a) Ge and (b) Se. (A) atomic states, (B) hybridized states, (C) molecular states, (D) broadening of states into bands in the solids.

a donor is formed near the gap centre and acceptor above it. In chalcogenide materials, the lone pair band lies in the energy region between the σ and σ^* bands. The occupied state from σ bands falls into the lone pair bands. The unoccupied state probably forms acceptors above the lone pair bands. It is also possible, particularly at a high concentration of dangling bonds, that the unoccupied state lie within the lone pair band.

1.6 Effect of Metallic Additives

Earlier work by Kolomiets and co-workers [57,58] on amorphous semiconductors suggested that the electrical properties of chalcogenide glasses are comparatively insensitive to composition variations and presence of impurities. This is explained by Mott [59] using his 8 - *N* rule. According to this rule, impurities in these glasses are coordinated in such a way that covalent bonding requirements are satisfied, therefore, they do not form donors and acceptors. However, some experiments show that certain impurities can cause significant changes in the behavior of chalcogenide glasses. The concept of charged dangling bonds and valence alteration pairs [60,61] have been used by several workers to explain the behavior of chalcogenide glasses. It is postulated that the impurities may either destroy the dangling bond centers of one sign or form charged centers which are compensated by centers if opposite sign. Under such circumstances, activation energy may either increase or decrease. The addition of certain elements to a glass can alter the density of valence alteration centers [62].

The defect-chemistry in lone pair semiconductors is governed by the quite unusual inter-conversion property of the valence-alteration centers. At equilibrium, the valence-alteration centers reduce the influence of foreign atoms on the conductivity in two ways: (*i*) they retard the occurrence of charged additives and (*ii*) they increase in number such that their concentration always exceeds that of charged additives. Consequently, the valence-alteration centers remain the source of charge carriers. They are allowed to establish equilibrium by annealing the chalcogenide glass near glass-transition temperature or by adding third element, *i.e.* additive to the base melt. It is interesting to note from the experimental investigations that the metal atoms are mostly three - fold coordinated in glassy selenides such as As-Se-Ag,

Ge-Se-Ag and Ge-Se-In [63-65]. Chalcogenide bulk glasses exhibiting *n*-type conduction were first prepared by quenching the melts of a mixture of Ge, Se and Bi_2Se_3 or Bi by Tohge *et al.* [66]. They noticed that Seebeck coefficient 'S' is negative, suggesting the electrons are dominant carriers in these glasses ($Ge_{20}Bi_{10}Se_{70}$). Thin films of $Ge_{20}Bi_xSe_{70-x}Te_{10}$ (x = 7, 9, 11, 13) were studied for their switching properties [67] and it was observed that films with $x \geq 9$ exhibited electronic switching.

These amorphous semiconductors with tailored properties have a potential for thermoelectric and photovoltaic device application. To explore the possibility of such applications, it is necessary to obtain these materials in thin film form and to understand their physical properties. Some attempts have been made to prepare and study the properties of Bi-Ge-Se [68] and Bi-Ge-Se-Te [69,70] thin films. Study of the electronic structure of *p*-type and *n*-type amorphous Ge-Se-Bi films and the density of states in the conduction band as well as that in the valence band has been investigated by inverse-photoemission and ultraviolet photoemission spectroscopy by Matsuda *et al*. [71]. It was found that, with increasing Bi content, the conduction band minimum approaches the Fermi level, while the valence band maximum remains unchanged with respect to the Fermi level. Thus it was concluded that the mixture of Ge-Se and Bi-Se anti-bonding orbits compose the conduction band of the Ge-Se-Bi system. The origin of the *n*-type conduction in the high Bi concentration is attributed to this conduction band which appears just above the Fermi level. Carrier type reversal (*p* to *n*) has been observed Pb-Ge-Se-Te glasses at 8 at. % of lead. Electrical properties are found to exhibit notable change at $p \rightarrow n$ transition threshold [72]. Effect of annealing rate on the crystallization process in $Ge_5Bi_{18}Se_{77}$ thin films and a detailed analysis of the structural properties has been presented by Rajagopalan *et al.* [73]. Bhat *et al.* [74] proposed a consistent approach to understand the mechanism of three-fold coordinated Bi doping in Ge–Se glasses by carrying out specific heat (C_p) measurement in $Ge_{20}Se_{70-x}Te_{10}Bi_x$ system for $0 \leq x \leq 11$. The two softening temperatures exhibited by heat treated samples are explained on the basis of 'microscopic phase separation'. The minimum in 'configurational heat capacity' at *x* = 7.5 is related to be a feature of chemical threshold.

Effect of Sn content on the electrical and optical properties of Ge-Se-Sn glasses is studied by Fadel *et al.* [75]. Optical properties of amorphous Ge-Se-Tl have been studied by Aziz *et al.* [76]. They found that optical band gap decrease with increase in tail width with the increase of Tl content. Effect of Ag on the $Ge_{15}Se_{85}$ glassy alloy on ac-conductivity was investigated by Fouad *et al.* [77]. Ac-conductivity is found to be temperature dependent. The effect of both the chalcogenide composition and the nature of the chemical bonding of Ge-Se-Ag samples are analyzed using a simple consideration based on coordination number.

Electrical transport properties of amorphous $Se_{78-x}Te_{22}Bi_x$ films have been carried out by Khan *et al.* [78]. By alloying Bi to Se-Te base alloy, dark conductivity increases. Effect of Cu on the structure of Ge-Se is studied by Tecklenburg *et al.* [79]. Presence of Cu extinguishes the photoconductivity effect exhibited by Ge-Se_2. Density increases with addition of Cu. Cu affects the defects (Ge-Ge bonds) but does not affect the Ge-Se_2 chain. Photoconductivity in $Se_{90}Ge_{10-x}In_x$ (x = 2, 4, 6, 8, 10) as studied by Singh *et al.* [80] found that the conductivity is thermally activated process and activation energy is found to decreases with increasing intensity.

Electrical and optical system on Pb modified amorphous Ge-Se-Te film was carried out by Pattanaik *et al.* [81]. *p* to *n* type conduction was observed by the addition of lead with 9 at. %. Activation energy and optical gap decreases with the addition of Pb content.

Space charge limited conduction on $Se_{78-x}Te_{22}Bi_x$ where $0 \le x \le 4$ thin films have been studied by Khan *et al.* [82]. The calculated values of density of stated $N(E_F)$, calculated by fitting the data to the theory of SCLC assuming uniform distribution of localized state, increases with increasing Bi concentration. Effect of Bi addition to Ge-Se on the ac-conductivity is studied by Singh *et al.* [83]. The value of ac-conductivity decreases at low concentration of Bi (4 at. %) and increases at higher concentration of Bi (10 at. %). The value of frequency exponent decreases as the temperature increases. Electrical properties of amorphous $Se_{70}Ge_{30-x}M_x$ (x = 0, 5); (M = Ag, Cd, Pb) thin films have been investigated by Afifi *et al.* [84]. They found that increase in conductivity with Pb is higher than that of Cd which in turn is higher than that of Ag. I-V curves of the investigated samples are typically for a memory switch. In $(Ge_{20}Se_{80-x})_{1-x}Sn_x$ glassy alloys the dc conducting measurements at high electric

field have been studied. Non-ohmic behavior is observed. Experimental data confirms the presence of SCLC in this glassy material [85]. A peculiar role of Sn as an impurity in $Ge_{20}Se_{80-x}$ is studied.

Saffarini *et al.* [86] used DSC to establish the heat capacity jump, ΔC_p at T_g [$\Delta C_p = C_{pl} - C_{pg}$, C_{pl} is C_p value of super cooled liquid and C_{pg} is of glassy state] for Ge-Se-In glasses and concluded that ΔC_p possess a local minimum in the vicinity of $< r > \approx 2.4$ *i.e.* minimum fragility. Thus strongest thermodynamic character is reached at about $< r > \approx 2.4$ or glass forming liquid has a minimum crystallization tendency by virtue of having reduced accessible structural or configurational reordering in the super cooled region.

Thin amorphous chalcogenide films from the $GeSe_x$ (x = 1-5), $(GeSe_4)_{100-y}Ga_y$ and $(GeSe_5)_{100-y}Ga(Tl, B)_y$ (y = 5, 10, 15, 20) systems have been prepared by thermal evaporation and characterized with respect to their internal stress using a cantilever technique [87]. The correlations between the stress, the composition and the structure of the films were investigated. The obtained results were related with some structural and mechanical parameters of the glasses like mean coordination number, number of constrains per atom, density, compactness *etc*. With the addition of Ag in the Ge-Se glassy alloy, refractive index is found to increase with the subsequent decrease of optical band gap [88].

Effect of Bi impurity on the ac-conductivity of $Ge_{20}Se_{80}$ glassy alloy has been done by Singh *et al.* [89]. The value of ac-conductivity decreases at low concentration of Bi (4 at. %) but increase for higher Bi content (10 at. %). DC conductivity and switching phenomenon of $Se_{80}Te_{20-x}Ge_x$ amorphous system has been investigated by Afifi *et al.* [90]. The observed switching phenomenon for these compositions was of memory type. Electrical measurements on $(Ge_{20}Se_{80})_{100-x}Cu_x$ has also been carried out by Thakur *et al.* [91]. They showed that value of dark conductivity and photoconductivity increases and activating energy decreases upto 1 at. % of Cu addition to $Ge_{20}Se_{80}$ glassy alloy. Photosensitivity increases and decay time constant decreases upto 1 at. % of Cu addition. With the further increase of Cu conc. (> 1 at. %), reverse trend takes place.

Effect of In incorporation on the optical properties of *a*-Se-Ge thin films $Se_{90}Ge_{10-x}In_x$ (x = 2, 4 and 6) have been reported by Pandey *et al*. [92]. Authors have

observed from optical transmission measurements that optical band gap decreases with In content while refractive index and real dielectric constant decreases with increasing wavelength. Marquez *et al.* [93] studied the optical dispersion and absorption of Ag-photodoped $Ge_xSb_{40-x}S_{60}$ chalcogenide glass thin films. The film thickness and optical constants have been determined by envelope method and dispersion of linear refractive index of Ag-photodoped chalcogenide film is analyzed in terms of Wemple-DiDomenico oscillator model. Effect of Te on the Ge-Se glassy alloy has been studied by Sharma *et al.* [94,95]. They found that optical gap decreases with increase of Te. With the increase in thickness, optical gap decreases.

Pre-exponential factor of Arrhenius equation for the isothermal crystallization of Se-Ge, Se-In and Se-Te chalcogenide glasses has been reported by Mehta *et al.* [96]. They observed the Meyer-Neldel rule between pre-exponential factor and activation energy of crystallization in these systems.

Thermal stability and percolation threshold of $Ge_xSe_{100-x-y}Fe_y$ (y = 2, 4, 6) glasses have been discussed by Saffarini *et al.* [97]. DSC and DTA have been used for their determination. They observed that the maximum stability of network is just obtained if the percolation threshold limit is reached. The overall mean bond energies and their correlation with T_g have been discussed.

Thermal stability and crystallization kinetics of $As_{14}Ge_{14}Se_{72-x}Sb_x$ (x = 3, 6, 9, 12, 15) glasses are studied using DSC by Dahshan [98]. The values of T_g and peak temperature of crystallization (T_p) are found to be dependent on heating rate and antimony content. They found that thermal stability decreases with increase of Sb content. Thermal properties of $GeSe_2$-As_2Se_3-CdSe glasses were investigated via DSC measurements. The dependence of T_g and thermal stability on glass composition were discussed by Zhao *et al.* [99].

Optical and thermo-mechanical properties of new Ge-Ga-Se-AgI glasses are studied by Roze *et al*. [100]. They found that the possibility of shaping and drawing these glasses give them a great interest in ion exchange experiments to achieve gradient of refractive index. Thermally and optically induced irreversible changes in the optical gap and refractive index were studied for sulphur rich and sulphur poor Ge-As-S system by Kincl *et al*. [101]. They found that with illumination optical gap decreases and refractive index increases. The influence of light illumination on the

optical parameters of Ge-Sb-Te thin films is studied by spectral ellipsometry in visible ranges of light. It was found that illumination of films leads to the decrease of refractive index. With increase of Ge content optical gap increases [102].

Glasses and glass-ceramics based on $GeSe_2$-Sb_2Se_3 and halides for far infrared transmission have been studied by Calvez *et al.* [103]. Glasses forming region and thermo-mechanical properties have been investigated. They showed that shaped glass ceramics are still transparent and show improved mechanical properties. Seedek *et al.* [104] studied the effect of laser irradiation on the electronic structure of *a*-$Ge_{36}Se_{64}$ films by detecting variation of bond length (r) and coordination number (CN). Study of variation of r and CN values induced by subsequent annealing of thin films is also given. Singh *et al.* [105] has shown that with the addition of Pb content to $Ge_{20}Se_{80}$ system, ac-conductivity and static permittivity increases. Effect of annealing on the optical and electrical properties of *a*-$Ge_{30}S_{10}Se_{60}$ thin films have been investigated by Aly *et al.* [106]. Annealing at $T \leq T_g$ results in the slight increase in optical gap and dark activation energy where as for $T > T_g$, optical gap and dark activation energy decreases with further increase of annealing temperature. Nano phase separation (observed by SEM and supported by XRD) and effect on the properties of Ge-As-Se chalcogenide glasses has been carried out by Xia *et al.* [107]. It was established that nano phase separation becomes more intensive when $< r > > 2.64$.

1.7 Selection of the Problem

Ge-Se chalcogenide glasses are transparent in 8-12 μm range and have good thermal, mechanical and chemical properties. Being a glass, chalcogenides are versatile platform mainly for optical devices. Main motivation of this thesis work is to carry out and expand the range of certain properties (mainly optical and electrical) of multicomponent chalcogenide glasses by the alteration of their chemical compositions. One of the most important properties of any amorphous solid is its optical properties. There are two reasons for this, (*i*) optical properties of crystalline semiconductor are well studied, so the optical properties of amorphous semiconductors can easily be related and compared. (*ii*) Optical properties are directly related to the structural and electronic properties of solids and hence very important in device application. So, a detailed knowledge of some important and related

parameters can provide huge information on material about their structure and opto-electronic behavior. These measurements give valuable information regarding the defect states and other mechanism responsible for electrical conductivity and photoconductivity behavior of alloy. These materials exhibit unique physical properties that make them good candidates for several potential applications such as infrared transmission and detection, threshold and memory switching *etc*. [108,109]. The addition of third element as an impurity has a pronounced effect on the optical, electrical and physical properties.

Though a scattered literature is there on the Ge-Se-In and Ge-Se-In-Bi system, but many features of these compounds still remain unexplored. There is no report on the detailed study of optical, electrical and physical properties of these systems in the literature. In view of all these observations, we proposed in this thesis to study the role played by metallic indium, belonging to group III of periodic table with atomic number 49 on Ge-Se glassy alloy and the effect of bismuth (group V, Z = 83) on the Ge-Se-In glassy alloy. The first system under investigation is $Ge_{20}Se_{80-x}In_x$ (x = 0, 5, 10, 15, 20) and second system is $Ge_{20}Se_{70-x}In_{10}Bi_x$ (x = 2, 4, 6, 8, 10).

The aim of this study is to undertake a systematic investigation of these systems and to lighten the new features of their optical, electrical and physical behavior.

References

1. Zachariasen W H 1932 *J. Am. Chem. Soc.* **54** 3841
2. Hilton A R 1970 *J. Non-Cryst. Solids* **2** 28
3. Ovshinsky S R 1968 *Phys. Rev. Lett.* **21 (20)** 1450
4. Popescu M 1978 *Proc. Intern. Conf Amorphous Semiconductors '78' Pardubice, Czechoslovakia* **1** 185
5. Phillips J C 1979 *J. Non-Cryst. Solids* **34** 153
6. Elliott S R 1986 *J. Non-Cryst. Solids* **81** 71
7. Yamane M and Asahara 2000 *Glasses for photonics* (Cambridge: University press)
8. Wang F, Mamedov S, Boolchand P, Goodman B and Chandrasekhar M 2005 *Phys. Rev. B* **71** 174201
9. Chakravarty S, Georgiev D G, Boolchand P and Micoulaut M 2005 *J. Phys.: Condens. Mat.* **17** L1
10. Zakery A 2002 *J. Phys. D: Appl. Phys.* **35** 2909
11. Taeed V G, Baker N J, Fu L, Finsterbusch K, Lamont M R E, Moss D J, Nguyen H C, Eggleton B J, Choi D Y, Madden S and Luther-Davies B 2007 *Optics Express* **15** 9205
12. Trnovcona V, Furar I and Lezal D 2007 *J. Non-Cryst. Solids* **353** 1311
13. Lyubin V, Klebanov M, Feigel A and Sfez B 2004 *Thin Solid Films* **459** 183
14. Babeva Tz., Dimitrov D , Kitova S and Konstantinov I 2000 *Vacuum* **58** 496
15. Ganjoo A, Jain H, Yu C and Pantano C G 2006 *J. Non-Cryst. Solids* **352** 584
16. Fu L B, Fuerbach A, Littler I C M and Eggleton B J 2006 *Appl. Phys. Lett.* **88** 081116
17. Lankhorst M H R 2005 *Nat. Mater.* **4** 347
18. Anderson P W 1958 *Phys. Rev.* **109** 1492
19. Mott N F 1967 *Adv. Phys.* **16** 49
20. Cohen M H, Fritzsche H and Ovshinsky S 1969 *Phys. Rev. Lett.* **22** 1065
21. Mott N F 1966 *Phil. Mag.* **13** 989

22. Davis E A and Mott N F 1970 *Phil. Mag.* **22** 903
23. Mott N F 1971 *Phil. Mag.* **24** 911
24. Bhat N A, Sangunni K S and Rao K S R K 2003 *J. Non-Cryst. Solids* **319** 192
25. Sharma I, Tripathi S K, Monga A and Barman P B 2008 *J. Non-Cryst. Solids* **354** 3215
26. Marshall J M and Owen A E 1971 *Phil. Mag.* **24** 1281
27. Anderson P W 1975 *Phys. Rev. Lett.* **34** 953
28. Street R A and Mott N F 1975 *Phys. Rev. Lett.* **35** 1293
29. Kastner M, Adler D and Fritzsche F 1976 *Phys. Rev. Lett.* **37** 1504
30. Tanaka K 1989 *Phys. Rev. B* **39** 1270
31. Sarrach D J, De Neufiville J P and Hawoth W L 1976 *J. Non-Cryst. Solids* **22** 245
32. Elliott S R 1993 *Glasses and Amorphous Materials* ed. Zarzycki J (New York: VCH)
33. Petri I, Salmon P S and Fischer H E 2000 *Phys. Rev. Lett.* **84** 2413
34. Fayek S A 2000 *Mat. Chem. Phys.* **62** 95
35. Shiryaev V S, Adam J L and Zhang X H 2004 *J. Phys. Chem.* **65** 1737
36. Veinguer M, Feigel A, Sfez B, Klebanov M and Lyubin V 2003 *J. Optoelectron. Adv. Mater.* **5** 1361
37. Boolchand P, Georgiev D G and Goodman B 2001 *J. Optoelectron. Adv. Mater.* **3** 703
38. Thorpe M F, Jacobs D J, Chubynsky M V and Phillips J C 2000 *J. Non-Cryst. Solids* **266** 859
39. Boolchand P, Georgiev D G and Micoulaut M 2002 *J. Optoelectron. Adv. Mater*. **4** 823
40. Phillips J C 1981 *J. Non-Cryst. Solids* **44** 17
41. Feltz A 1993 *Amorphous Inorganic Materials and Glasses* (Germany: VCH Weinheim)
42. Malaurent J C and Dixmier J 1980 *J. Non-Cryst. Solids* **35** 1227
43. Senapati U and Varshneya A K 1995 *J. Non-Cryst. Solids* **185** 289

44. Tatsumisaga M, Halfpap B L, Green J L, Lindsay S M and Angell C A 1990 *Phys. Rev. Lett.* **64** 1549
45. Feltz A, Aust H and Blayer A 1983 *J. Non-Cryst. Solids* **55** 179
46. Kamitakahara W A, Cappelletti R L, Boolchand P, Halfpap B, Gompf F, Neumann D A and Mutka H 1991 *Phys. Rev. B* **44** 94
47. Boolchand P, Enzweiler R N, Cappelletti R L, Kamitakahara W A, Cai Y and Thorpe M F 1990 *Solid State Ion.* **39** 81
48. Boolchand P, Norban B, Persing D, Enzweiler R N, Griffiths J E and Phillips J C 1987 *Phys. Rev. B* **36** 8109
49. Zhang M and Boolchand P 1994 *Science* **266** 1355
50. Bohmer R and Angell C A 1992 *Phys. Rev. B* **45** 10091
51. Asokan S, Parthasarathy G and Gopal E S R 1988 *Phil. Mag. B* **57** 49
52. Feng X, Bresser W J and Boolchand P 1997 *Phys. Rev. Lett.* **78** 4422
53. Phillips J C 1996 *Phys. Rev. B* **54** R6807
54. Franzblau D S and Tersoff J 1992 *Phys. Rev. Lett.* **68** 2172
55. Jacobs D J and Thorpe M F 1995 *Phys. Rev. Lett.* **75** 4051
56. Thorpe M F, Jacobs D J, Chubynsky M V and Phillips J C 2000 *J. Non-Cryst. Solids* **266–269** 859
57. Kolomiets B T 1976 *Thin Solid Films* **34** 1
58. Kolomiets B T and Raspopova E M 1973 *J. Non-Cryst. Solids* **11** 350
59. Mott N F 1969 *Phil. Mag.* **19** 835
60. Kastner M 1972 *Phys. Rev. Lett.* **28** 355
61. Elliot S R 1977 *Phil. Mag.* **36** 1291
62. Kastner M 1978 *Phil. Mag. B* **37** 127
63. Dejus R J, Susman S, Volin K J, Montague D G and Price D L 1992 *J. Non-Cryst. Solids* **143** 162
64. Benmore C J and Salmon P S 1993 *J. Non-Cryst. Solids* **156-158** 720
65. Saffarini G 1999 *Phys. Stat. Soli. B* **213** 261
66. Tohge N, Yamamoto Y, Minami T and Tanaka M 1979 *Appl. Phys. Lett.* **34(10)** 640
67. Rahman S and Sastry G S 1992 *Mat. Sci. Eng.* **B 12** 219
68. Kumar S, Kashyap S C and Chopra K L 1986 *J. Non-Cryst. Solids* **85** 100

69. Rahman S, Muralidhar K V and Sastry G S 1993 *Phys. Chem. Glasses* **34** 176
70. Rahman S and Kumar K S 1996 *Phys. Chem. Glasses* **37** 76
71. Matsuda O, Ohba T, Murase K, Ono I, Grekos P, Kouchi T, Nakatake M, Tamura M, Namatame H, Hosokawa S and Taniguchi M 1996 *J. Non-Cryst. Solids* **198-200** 688
72. Murugavel S and Asokan S 1998 *Phys. Rev. B* **58** 4449
73. Rajagopalan T and Reddy G B 1999 *Thin Solid Films* **353** 254
74. Bhat N A and Sangunni K S 2000 *Solid State Commun.* **116** 297
75. Fadel M, Sedeek K and Hegab N A 2000 *Vacuum* **57** 307
76. Abdel-Aziz M M, El-Metwally E G, Fadel M, Labib H H and Afifi M A 2001 *Thin Solid Film* **386** 99
77. Fouad S S, Bekheet A E and Farid A M 2002 *Physica B: Condensed Matter* **322** 163
78. Khan M A M, Zulfequar M and Husain M 2003 *J. Mater. Sci.* **38** 549
79. Tecklenburg M M J, Larsen E, Lita B and Qadir D I 2003 *J. Non-Cryst. Solids* **328** 40
80. Singh S, Sharma R S, Shukla R K and Kumar A 2004 *Vacuum* **72** 1
81. Pattanaik A K and Srinivasan A 2004 *Semicond. Sci. Technol.* **19** 157
82. Khan M A M, Zulfequar M and Husain M 2005 *Physica B* **366** 1
83. Singh G, Sharma J, Thakur A, Goyal N, Saini G S S and Tripathi S K 2005 *J. Optoelectr. Adv. Mater.* **7(4)** 2069
84. Afifi M A, Fadel M, El-Metwally E G and Shakra A M 2005 *Vacuum* **77** 259
85. Singh R, Tripathi S K, Kumar S 2006 *J. Non-Cryst. Solids* **352** 3230
86. Saffarini G and Saiter J M 2004 *J. Mater. Sci.* **39** 6141
87. Popov C, Boycheva S, Petkov P, Nedeva Y, Monchev B and Parvanov S 2006 *Thin Solid Films* **496** 718
88. Thakur A, Singh G, Saini G S S, Goyal N and Tripathi S K 2007 *Optical Materials* **30** 565
89. Singh G, Goyal N, Saini G S S and Tripathi S K 2007 *J. Non-Cryst. Solids* **353** 1322

90. Afifi M A, Hegab N A, Atyia H E and Farid A S 2007 *Journal of Alloys and Compounds* doi : 10.1016/j.jallcom.2007.09.011
91. Thakur A, Saini G S S, Goyal N and Tripathi S K 2007 *J. Non-Cryst. Solids* **353** 1326
92. Pandey V, Tripathi S K and Kumar A 2007 *Physica B: Condensed Matter* **388** 200
93. Marquez E, Gonzalez J M, Bernal-Oliva1 A M, Wagner T and Garay R J 2007 *J. Phys. D: App. Phys.* **40** 5351
94. Sharma P and Katyal S C 2007 *Thin Solid Films* **515 (20)** 7966
95. Sharma P and Katyal S C 2007 *Mater. Lett.* **61** 4516
96. Mehta N and Kumar A 2007 *J. Mater. Sci.* **42** 490
97. Saffarini G, Saiter J M and Matthiesen J 2007 *Mater. Lett.* **61** 432
98. Dahshan A 2008 *J. Non-Cryst. Solids* **354 (26)** 3034
99. Zhao D, Zhang X, Wang H, Zeng H, Ma H, Adam J L and Chen G 2008 *J. Non-Cryst. Solids* **354** 1281
100. Roze M, Calvez L, Ledemi Y, Ma H L, Lucas J and Zhang X H 2008 *J. Optoelectron. Advance. Mater.* **10** 141
101. Kincl M and Tichy L 2008 *Mater. Chem. Phys.* **110** 322
102. Pamukchieva V and Szekeres A 2008 *Optical Material* **30** 1088
103. Calvez L, Ma H L, Lucas J and Zang X H 2008 *J. Non-Cryst. Solids* **354** 1123
104. Sedeek K, Adam A, Balboul M R, Wahab L A and Makram N 2008 *Mater. Res. Bull.* **43** 1355
105. Singh G, Goyal N, Saini G S S and Tripathi S K 2008 *Physica B: Condensed Matter* **403** 599
106. Aly K A, Abousehly A M, Osman M A and Othman A A 2008 *Physica B: Condensed Matter* **403** 1848
107. Xia F, Baccaro S, Wang W, Pilloni L, Zang X, Zeng H and Chem G 2008 *J. Non-Cryst. Solids* **354 (12-13)** 1137
108. Saffarini G and Saiter J M 2004 *J. Mater. Sci.* **39** 6141
109. Savage J A 1985 *Infrared Optical materials and their antireflecting coatings* (London: A. Hilger)

CHAPTER II

Experimental Techniques

2.0 Introduction

Development of the techniques of fabricating and studying thin films have set a fairly clear picture of the nature of such films to be obtained and have led to an understanding of their electrical, thermal and most importantly their optical behavior. This chapter is dedicated to the fabrication and characterization techniques utilized for the bulk glasses and their corresponding thin films, prepared and used in this study. The preparation of amorphous materials is much easier than growing crystalline material. This feature makes them more suitable for making devices for commercial and research purpose at a comparatively cheaper rate than the crystalline materials. All the amorphous solids are thermodynamically unstable and tend to relax towards a stable or metastable phase. The time scale, on which these changes occur varies enormously, is usually a sensitive function of temperature. A class of non-crystalline solids prepared from the liquid state is called glass. These are characterized by being structurally continuous with liquid state and are prepared by quenching the molten liquid to a temperature far below their equilibrium melting point, without crystallizing and they can remain in their metastable states indefinitely. When the temperature decreases from the liquid phase, some materials do not crystallize below their melting point, but they become a super cooled liquid. As the temperature keeps decreasing, glass transition occurs at a certain temperature, 'T_g', below which they become glass. These behaviors are explained by volume versus temperature curve as shown in figure 2.1. T_g is defined by the temperature at which the extrapolations of the liquid and glassy lines are intersected. This shows that when the cooling rate is fast, T_g becomes higher or vice versa. The slower the rate of cooling, larger is the region for which liquid is super-cooled and hence lower is the glass transition temperature. The glass transition of a particular material partly depends on its thermal history. The value of T_g is influenced by the prevailing experimental conditions to a large extent, *e.g*. the cooling rate of the melt. Glass formation becomes more probable, when the cooling rate is greater, the sample volume is smaller and the crystallization rate is slower. However, fast quenching to avoid crystallization introduces a volume change which results in a large density fluctuation and vice-versa.

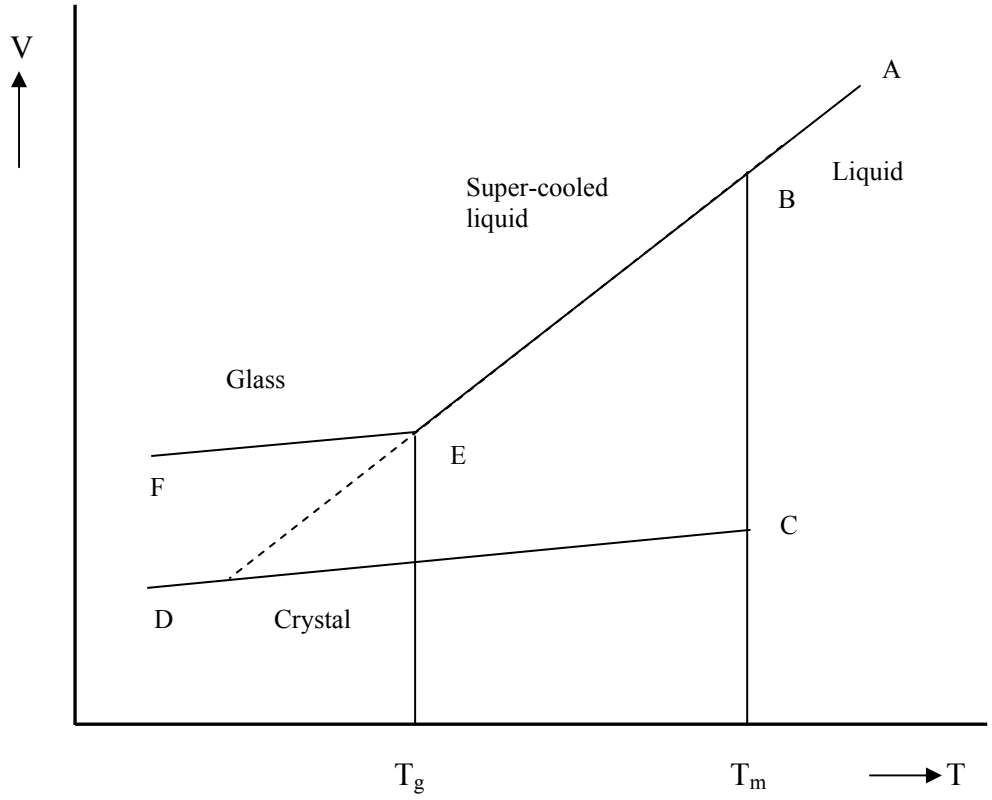

Figure 2.1 Schematic illustration of volume versus temperature curve: transition from the crystalline state to glassy state.

$T_g = 2T_m/3$, where T_m is the melting temperature [1]. The nature of glass transition is poorly understood, while there are numerous studies devoted to this topic [2]. Factors which determines the glass transition temperature are still not known, while correlation between the T_g and the average coordination number is given by [3]

$$\ln T_g \approx 1.6 < \mathrm{r} > + 2.3 \tag{2.1}$$

Tichy and Ticha [4] were the first to point out that the value of glass transition temperature should not be only related to the average coordination number $(< r >)$ but should also be related to the quality of connections, *i.e.* the mean bond energy $(< E >)$ between the atoms of the network.

$$T_g = 311[< E > -0.9] \tag{2.2}$$

2.1 Glass Formation

Glass formation has been discussed for a long time from the view point of thermodynamics, kinetics and structural properties. The most convenient and conventional technique for the bulk glass formation is melt quenching. During quenching of molten material, the glass forming ability depends on viscosity of melt as the amorphous solid is formed by continuous hardening (increase in viscosity). On cooling, viscous liquid does not provide the atomic mobility necessary for forming crystallites. Glass formation from the rapid cooling melts requires prevention of the nucleation and growth process which is responsible for crystallization. The extent of glass forming region is slightly dependent on the quenching rate or the amount of material used in sample preparation. Amorphous materials can be prepared by several other techniques such as thermal quenching of melts, glow discharge, RF sputtering, chemical vapor deposition and sol-gel processes, but melt quenching was widely used technique to get bulk sample. The advantage of melt quenching technique over other techniques is the large flexibility of compositions. Since quenching of melt does not require stoichiometry among constituents, the preparation of glasses with a wide variety of compositions, consisting of sometimes up to ten kinds of constituents at various ratios from a few to several ten of percent, is possible.

In this experimental work melt quench method has been used to grow various samples of chalcogenide glasses. Chalcogenide glasses can be prepared by elemental precursors like S, Te, Se, Ge, As, Ga *etc.* and from compound precursors like sulphides and selenides. For obtaining high quality glasses, 5*N* pure raw materials are used. Prior to batching and melting, quartz ampoules (with outer diameter = 1.0 cm, inner diameter = 0.8 cm), were etched with chromic acid. The degreasing of these ampoules has been done by using tri-chloro-ethylene (TCE), acetone and methanol followed by thorough wash with double distilled water and then heat treated in vacuum for eight hours, in order to remove adsorbed water and inorganic contaminants.

First materials are weighed in batch of 4 g, according to their atomic weight percentages followed by sealing of these materials in an evacuated (~ 10^{-4} Pa) quartz ampoule. Resulting chalcogenide glass melts have high vapor pressure at the melting temperature so melting is carried out in a properly sealed system. Thus, after batching, the quartz ampoule is sealed off by an oxy fuel burner, while being evacuated to a vacuum ~ 10^{-4} Pa.

For melting, the sealed ampoule is transferred to an electric furnace and heated gradually, in steps, at a heating rate of 3-4 ^{o}C/min to the melting temperature in order to prevent explosion due to high vapor pressure of the batch components. To ensure homogenization of viscous melts, the melt is agitated by rocking the quartz ampoule. Melting temperature is maintained for 24 hours to make the melt homogeneous. In case of $Ge_{20}Se_{80-x}In_x$, the temperature of the furnace is raised to 250 ^{o}C for two hours, so the Se (T_m = 217 ^{o}C) and In (T_m = 157 ^{o}C) diffuse into the rest of the constituents. The temperature is then raised to 1000 ^{o}C, so that the Ge (T_m = 938 ^{o}C) thoroughly mixes with other constituents. For $Ge_{20}Se_{70-x}In_{10}Bi_x$, the temperature step is given at 300 ^{o}C, for two hours because for Bi, T_m = 271 ^{o}C. The quenching was done in ice-cold water to get the glassy alloys.

2.2 Thin Film Deposition

Development of techniques of producing and studying thin films, lead to better understanding of their optical, electrical, photoelectrical properties. There is an

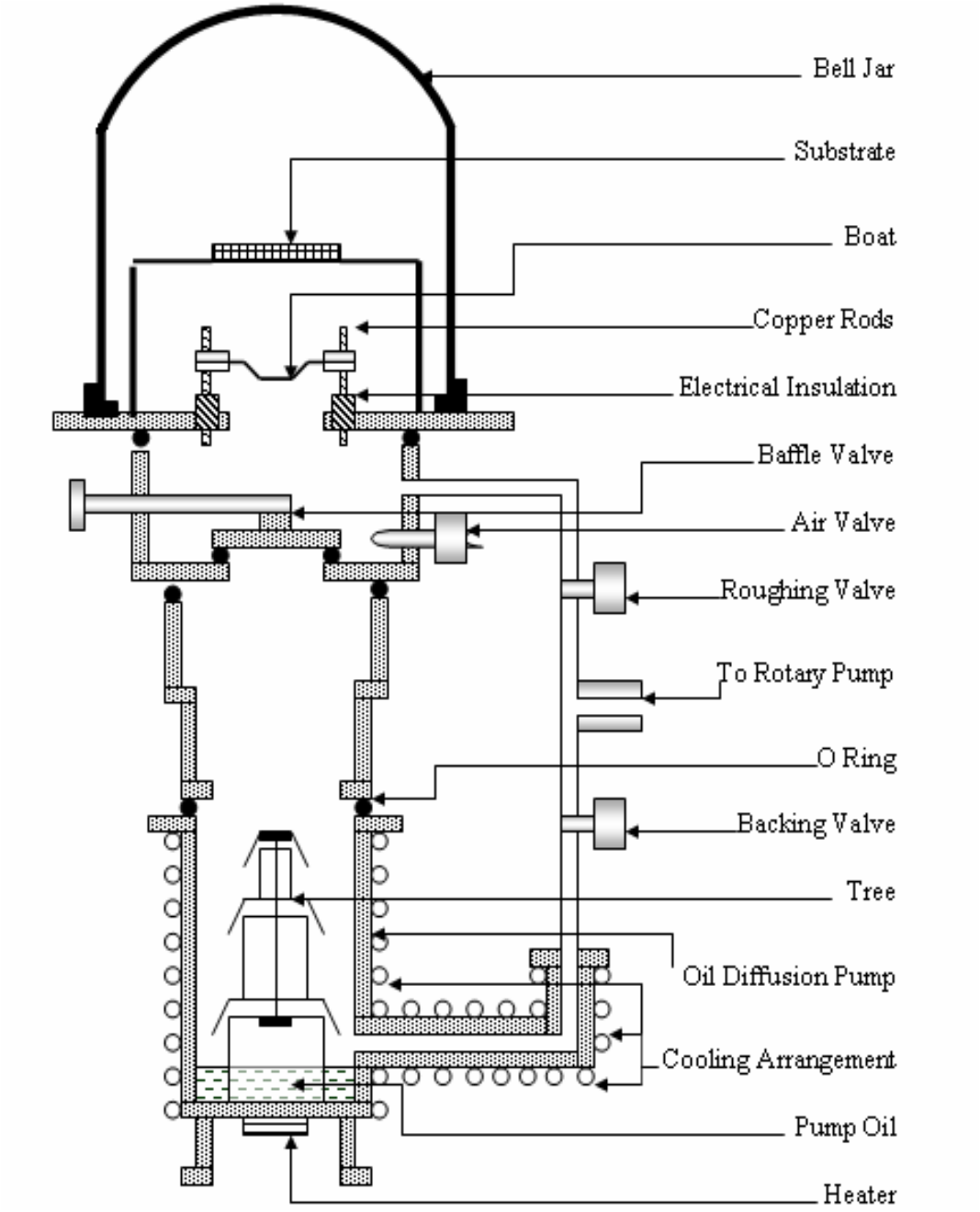

Figure 2.2 Schematic diagram of thin film coating unit.

appreciable dependence of film properties on the condition of formation of thin films. Among the factors which are liable to influence the properties of thin films are; rate of deposition, velocity of impinging atoms, structure and condition of target surface, history of film between deposition and examination *etc.* Lack of information on these and many other variables which may determine the nature of film makes difficult to compare the results of various workers.

Thin films of the materials can be prepared using various techniques; physical and chemical. Physical methods are vacuum evaporation, electron-beam evaporation, flash evaporation, RF sputtering, multi-source evaporation, ion beam evaporation, laser beam evaporation, resistive evaporation *etc.* Some chemical methods, which essentially depend on electrical separation of ions, thermal effect or thermal growth, are anode electrolytic deposition, chemical bath deposition, cathode electrolytic deposition, chemical vapor deposition and plasma-enhanced chemical vapor deposition *etc.*

The increasing use and study of thin films are in part due to the rapid strides which have been made in vacuum techniques. In the present work, thermal deposition in vacuum by resistive heating method is used. This is the most commonly used technique adopted for deposition of metals, alloys and also many compounds. The primary requirement for this method is a high vacuum deposition system at a pressure of about 10^{-4} Pa or even less. The attainment of low pressure necessary for the production and study of films has been so facilitated that rapid progress has been made possible. Most widely used method of depositing films, particularly for use in optical system, is that of thermal evaporation.

Prior to deposition of thin films, it is essential to clean the surface of the substrate because thin films readily adhere to a clean insulating surface. Tendency for the films to crack and peel increases, if the surface is contaminated with foreign impurities since the adhesion of the films is degraded. Cleaning of the substrate is done in three steps: (*i*) soap solution cleaning and (*ii*) cleaning with acetone (vapor cleaning) and (*iii*) with methanol. Soap solution cleaning basically involves scrubbing the substrate in the soap solution, then rinsing it thoroughly with double distilled water. This procedure is repeated 3 - 4 times for cleaning single substrate. Soap solution cleaning is used to remove any visible oil, grease and dust impurities. Vapor

cleaning procedure is mainly used to remove the organic impurities, which are present on the surface of substrate. Acetone vapor is used for the removal of organic impurities. For the removal of inorganic impurities methanol is used. After all this cleaning the substrates are subjected to dry in vacuum oven at a temperature approximately 110 ^{o}C and then put into deposition chamber. The schematic diagram of the coating unit is shown in figure 2.2.

Fine powder of the material which has to be deposited is put into the flash cleaned molybdenum (Mo) boat. Flash cleaning is done by passing a heavy current through the boat so as to make it white hot or incandescent for a short period. Then the system was evacuated to a base pressure of 10^{-4} Pa. A shutter was incorporated in between the source and the substrate so that no vapor stream of the material can reach the substrate directly prior to attaining the required deposition conditions. After establishing the required source temperature, substrate temperature and vacuum in the chamber, the shutter was removed to start the deposition of film on the cleaned substrate. When the required film thickness was obtained the shutter was brought back to the original position. Thin films were kept in the deposition chamber in the dark for 24 h to attain thermodynamic equilibrium as stressed by Abkowitz *et al.* [5]. The vacuum evaporation process was carried out in a coating system (HINDHIVAC model 12A4D India). The rate of evaporation of deposited thin films and thickness of the films deposited has been measured by thickness monitor (Model DTM-101).

For the electrical measurements, indium electrodes were deposited using a mask so that the desired electrode gap is left for the deposition of thin films between the electrodes. Thin films of the required sample were deposited on to the electrode gap by passing low voltage and high current through the molybdenum (Mo) boat containing the material. These films of the glassy alloys are used to make the necessary electrical measurements. The films thus deposited are kept in the deposition chamber in dark for 24 hours so that the deposited films attain thermodynamic equilibrium before making any measurements on them. The deposition parameters are kept identical for all alloys (binary, ternary and quaternary) to make the analysis and comparison of the various properties, parameters and change in them under identical conditions.

2.3 Characterization of Thin Films

2.3.1 X-Ray Diffraction

XRD is presently the most widely used technique to characterize the amorphous nature of bulk glasses and their thin films. The powder method was used to check the nature (*i.e.* amorphous or polycrystalline or crystalline) of the bulk samples. The bulk samples were crushed to fine powder with a pestle and mortar and then this powder was used for taking XRD pattern. Philips PW 1710 X-ray diffractometer (Radiation used was Cu-Kα, λ = 1.540598 A^o, 40 KV and 25 mA) was used to plot the XRD patterns of the samples. Data acquisition was made in the 2θ range from 5^o to 60^o with a step size of 0.05^o. Thin films of the bulk samples deposited on the microscopic glass slides were also characterized to check the crystalline or amorphous nature of the films.

2.3.2 Electrical Characterization

To carry out the various electrical measurements on the thin films (dc and photoconductivity measurements) at different temperatures, a specially designed metallic sample holder, as shown in figure 2.3, is fabricated in the laboratory. Stainless steel is used for making the sample holder to take care of surface currents and unwanted disturbances in the measurements of small currents (pA). It also helps to provide proper shielding to the thin film samples for the accurate current measurements during various experimental observations. At low and high temperature, stainless steel is highly durable and corrosion free. The sample holder is fitted with a Chromel-Alumel thermocouple through teflon tape. During different measurements, this thermocouple gives the exact temperature reading to which thin film is subjected. The junction of the thermocouple is placed on copper block very near to thin film so that the chance of error in the temperature measurement of thin film is very rare. A small circular glass window is installed in the sample holder directly above the space at which film is placed on the copper block. This copper block is connected to the base of the sample holder through a copper rod. By this arrangement, the temperature gradient is very small between the copper block and base of the sample holder. The light could be shone through the glass window to carry

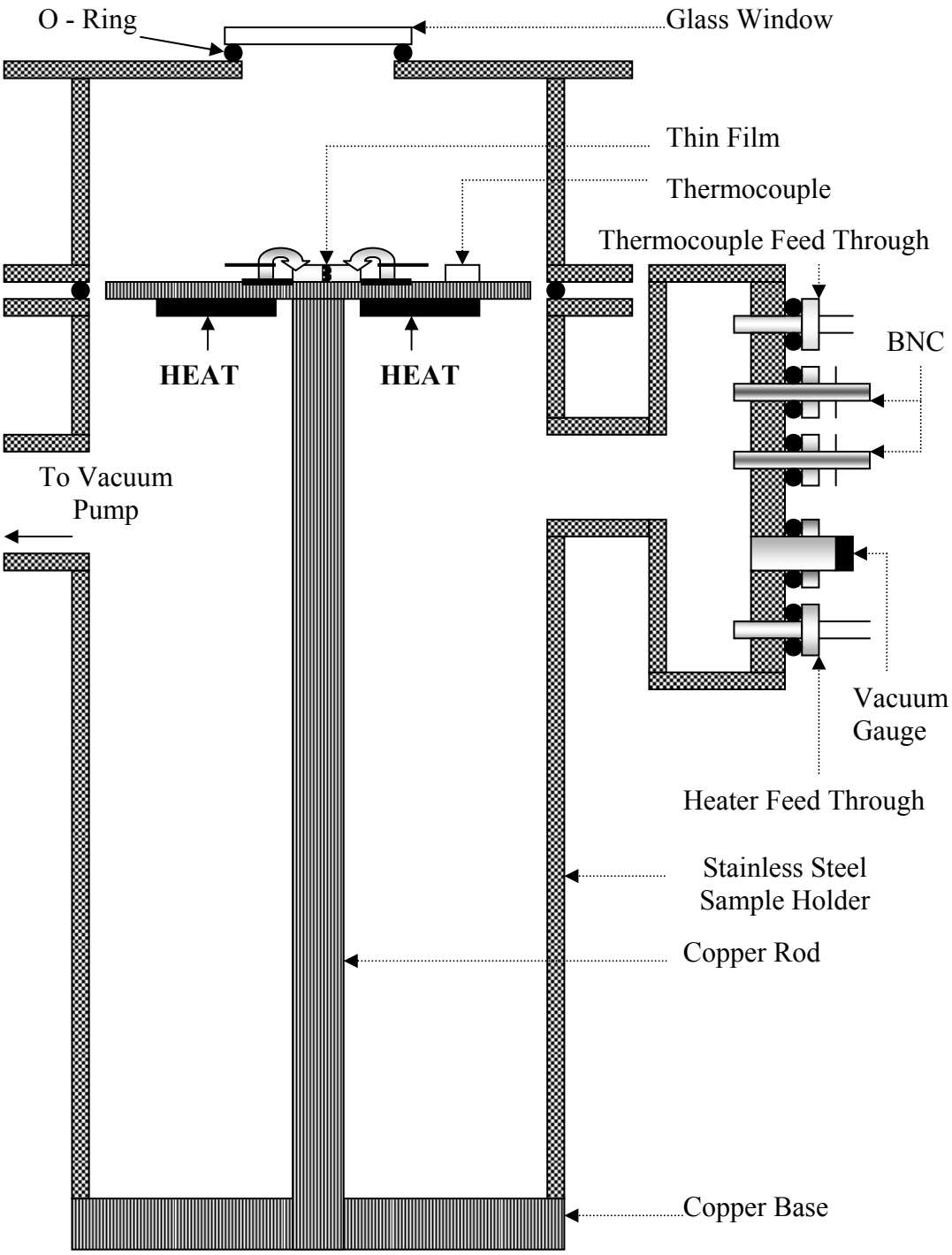

Figure 2.3 Stainless steel metallic sample holder.

out the photoconductivity measurements on thin films. To cut off the IR part of the light, water in transparent petri dish is kept above the glass window while taking the various photoconductivity measurements. The Cu block from lower side is fitted with heater to anneal the films and to study their behavior with rise in temperature. These heaters are connected to a variac through Teflon feed from outside the sample holder to vary the rate of heating. The rate is monitored through the display of the digital panel meter which is connected to the thermocouple. The current is measured by a digital pico-ammeter (DPM-111) with an accuracy of 1pA. The intensity of light is measured using a digital Luxmeter (TES-1332). Photocurrent (I_{ph}) is measured after subtracting the dark current (I_d) from the current measured in the presence of light (I). The sample holder is connected to rotary vacuum pump to maintain a vacuum ~ 10^{-3} mbar throughout the measurements. The pressure inside the sample holder is measured by using a vacuum gauge that is connected to the sample holder. These measurements are also carried out in a vacuum ~ 10^{-5} mbar using an oil diffusion pump but the results are found to be same in both the cases. So, all these measurements are performed in a vacuum of ~ 10^{-3} mbar.

Thin films of the glassy alloys after deposition and attainment of the thermodynamic equilibrium on being characterized for their amorphous nature using XRD are mounted on the sample holder, as mentioned earlier. Various electrical and photoconductivity measurements are carried out in the same sample holder in continuity without disturbing the particular film under investigation. The present measurements are found to be of the same nature in the films deposited in different runs. Therefore, the conclusion of the present work will not be much affected by the surface effects, as most of the explanations given are qualitative in nature. The deposition parameters are kept almost identical in case of binary, ternary and quaternary systems, so that a comparison of the results could be made for almost identical conditions. This confirms that the composition of the evaporated films is not very different from the corresponding glassy alloys prepared by quenching techniques.

2.3.3 Optical Characterization

No material is fully transparent in all optical frequencies and hence there always be some absorption in some region of the spectra. When light is incident on a thin film some of its energy is reflected, some is absorbed and rest is transmitted. Thin films are studied more accurately by acquiring transmission instead of absorption as was the case for bulk glasses. The transmission spectra of the thin films in the spectral range 400 – 1800 nm are obtained using a double beam ultraviolet - visible - near infrared spectrophotometer (Hitachi-330 and Perkin Elmer Lambda - 750). The spectrophotometer is set with a slit width of 1 nm in the spectral range. Therefore, it is unnecessary to make slit width corrections because of a small slit width value in comparison with different line widths. Typical interference fringes were obtained and the signal is used to calculate the refractive index dispersion curves using Swanepoel's technique [6] which is based on the approach of Manificier *et al.* [7]. This technique additionally allows the calculation of thickness of deposited thin films, optical absorbance and absorption coefficient.

References

1. Mott N F and Davis E A 1979 *Electronic Processes in Non-Crystalline Materials* (Oxford: Clarendon Press)
2. Elliot S R 1990 *Physics of Amorphous Materials* (London: Longman)
3. Tanaka K 1989 *Phys. Rev. B* **39** 1270
4. M. F. Thorpe and L. Tichy 2001 *Properties and Applications of Amorphous Materials* (London: Kluwer Academic)
5. Abkowitz M, Foley G M T, Markovics J M and Palumbo A C 1984 *Optical Effects in amorphous Semiconductors* (*AIP Conf. Proc.* vol 120) ed. Taylor P C and Bishop S G (New York: American Institute for Physics) 117
6. Swanepoel R 1983 *J. Phys. E : Sci. Instrum* **16** 1214
7. Manificier J C, Gasiot J and Fillard J P 1976 *J. Phys. E: Sci. Instrum* **9** 1002

CHAPTER III*

Effect of Indium on Optical and Electrical Properties of *a*-Ge-Se Thin Films

* • **Ishu Sharma**, S. K. Tripathi and P. B. Barman, "*An optical study of a-$Ge_{20}Se_{80-x}In_x$ thin films in sub-band gap region*" **Journal of Physics D: Applied Physics** 40 (2007) 4460.

• **Ishu Sharma**, S. K. Tripathi, A. Monga and P. B. Barman, "*Electrical properties of a-Ge-Se-In thin films*" **Journal of Non-Crystalline Solids** 354 (2008) 3215.

3.0 Introduction

In contrast to traditional oxide glasses, chalcogenide glasses based on the chalcogen elements S, Se and Te are versatile platform. They are attractive and widely investigated materials as they possess high optical transparency in IR region. The range of the IR transparency, controlled by higher atom masses and lower bonding force constraints in the chalcogenides combination, is essentially broadened towards higher wavelengths. Chalcogenide glasses have low phonon energy, high photosensitivity, easy fabrication and processing, good chemical durability and special second/third order optical non linearity due to their high refractive index ($2.0 \leq n \leq 3.7$). Their non-linearity (hundred times larger than silica), making them excellent and unique for ultrafast all-optical devices. So, it has a wide variety in photonic applications such as ultrafast optical switches, frequency converters, optical amplifiers, optical recording devices, integrated optics, infrared lasers and infrared transmitting optical fibers [1-6].

Ge-Se system is a widely studied system for its optical and electrical properties. $Ge_{20}Se_{80}$ glassy alloy lies at the threshold *i.e.* floppy ↔ intermediate region having an average coordination number $< r > = 2.4$ [7]. The energy band gap and lattice perfections play a major role in the preparation of devices for a particular wavelength, which can be modified by the addition of dopants [8, 9]. The optical and photoconductive properties of chalcogenide glasses depend on the structural configuration of the system and addition of metallic additive creates the structural disorder. Ovshinsky [10] and Fritzsche [11] discovered a way of incorporating certain additives into chalcogenides and other amorphous semiconductors which increase their conductivity in a drastic manner. Generally, the binary alloys are covalent in nature and the addition of third element creates iono-covalent bond and consequently conduction increases [12]. The alloying of third element in Ge-Se glassy alloy in varying proportion may help to find the suitable material from the basic physics and application point of view. The addition of Indium (In) to $Ge_{20}Se_{80}$ system in an effective way, control it's electrical and optical properties which leads the system towards intermediate region. Moreover, Ge-Se-In system is of special interest because of the fact that it form glasses over a wide domain of compositions [13] and the incorporation of In to Ge-Se alloy expands the glass forming area and creates

compositional and configurational disorder in the system. The addition of In creates the structural disorder. Alloying In with Ge-Se base is associated with the change in optical constants, allowing the vast use of these materials in the fabrication of large number of optical devices.

In this chapter we have discussed the effect of In addition on the optical and electrical properties of $Ge_{20}Se_{80-x}In_x$ system (x = 0, 5, 10, 15, 20) in detail, not only in order to know the basic mechanism underlying these phenomena, but also to exploit their technological and potential applications.

3.1 Optical Properties of Ge-Se-In Thin Films

Optics explain optical phenomenon. It describes the behavior of light and interaction of light with matter. Optical characterization are of unsurpassed importance because they provide a non-destructive means to identify many optical behaviors in terms of their absorption, reflection, refraction and transmission characterization *i.e.* it is able to predict and even allows to alter their response.

In this section optical band gap (E_g^{opt}), absorption coefficient (α), refractive index (n) and extinction coefficient (k) for $Ge_{20}Se_{80-x}In_x$ (x = 0, 5, 10, 15, 20) thin films have been determined by analyzing transmission spectrum in the wavelength range from $400-1200$ nm. The dispersion of refractive index was analyzed with Wemple - DiDomenico single oscillator model. The dielectric constants and optical conductivity are analyzed using n, k and α.

3.1.1 Experimental Details

Bulk samples of $Ge_{20}Se_{80-x}In_x$ (x = 0, 5, 10, 15, 20) alloys were prepared using melt quench technique. Thin films of the alloys were prepared by thermal evaporation technique [Vacuum coating unit HINDHIVAC 12A4D Model] at room temperature and base pressure of $\sim 10^{-4}$ Pa using a molybdenum boat. The thickness of the deposited films has been measured by thickness monitor (DTM-101). Amorphous nature of the bulk samples and thin films were confirmed by XRD technique. No prominent peak was observed in the bulk as well as in films. The normal incidence transmission spectra of $Ge_{20}Se_{80-x}In_x$ thin films were obtained by a double beam

ultraviolet-visible-near infrared spectrophotometer [Hitachi-330], in the transmission range 400-1200 nm. Repeated characterizations on the thin films of same composition (grown at different times), were carried out and the results only varied within ± 1-2 %. All optical measurements were performed at room temperature (300 K).

3.1.2 Methods to Determine Optical Properties

A light beam experiences both refraction and dispersion as it passes through some medium. Refraction occurs when the direction of light beam is bent at all interfaces and dispersion occurs when the degree of bending depends on the wavelength. The techniques used to calculate the optical parameters like refractive index (n), extinction coefficient (k), absorption coefficient (α), thickness of thin film (d) and optical band gap (E_g^{opt}) are described below.

3.1.2.1 Refractive Index and Extinction Coefficient

Light that is transmitted into the interior of transparent materials experiences a decrease in velocity and as a consequence bends at the interface. This phenomenon is termed as refraction. The index of refraction (n) of a material is defined as the ratio of velocity of light in a vacuum (c) to the velocity of light in the medium (v) *i.e.* $n = c / v$.

The magnitude of n or the degree of bending will depend on the wavelength of light and this effect is graphically demonstrated by the familiar dispersion of a beam of white light. Not only does the index of refraction affect the optical path of light, but it also influences the fraction of incident light that is reflected at the surface. The refractive index is given by

$$n = c/v = \frac{\sqrt{\mu\varepsilon}}{\sqrt{\mu_0\varepsilon_0}} = \sqrt{\varepsilon_r \mu_r} \tag{3.1}$$

where μ and ε are permittivity and permeability respectively. Phenomenon of refraction is related to electronic polarization of relatively high frequencies for visible light; thus the electronic component of the dielectric constant may be determined from the index of refraction. Since the retardation of electromagnetic radiation in medium results from electronic polarization, the size of the constituent atoms or ions have a

considerable influence on the magnitude of this effect. Generally, the larger an atom or ion, the greater will be the electronic polarizability, the slower the velocity and greater the index of refraction. From the Maxwell's equations, the complex refractive index (n^*) related to complex dielectric constant can be resolved into real and imaginary components as

$$n^* = n - ik \tag{3.2}$$

It is customary to define n as the refractive index and k as the extinction coefficient or absorption index. This index is a function of the wavelength, so that two beams with different colors (or frequencies) travel at different speeds.

The knowledge of accurate value of wavelength dependent refractive index of the thin films is very important from technological point of view. It yields fundamental information for the design and modeling of optical components and optical coating such as interference filters. There are various methods to estimate the optical parameters n and k but here we are concerned only with those which are applicable to thin films only. Since films are not self supporting, a suitable supporting substrate is used for deposition. This results in a system consisting of three dielectrics namely air, film and substrate. It is also possible that both the film and substrate may be transparent or partly opaque to the incident light. Hence the methods will considerably depend on the optical nature of film. There are number of methods for the calculation of optical constants of thin films like depending on the mode used such as (*i*) both reflection and transmission (*ii*) only reflection (*iii*) only transmission. But transmission method which was basically proposed by J. C. Manificier [14] and extended by Swanepoel [15] is easiest to apply, if thin film does not show much localised absorption band in between interference extremes. Thin films show very low absorption so that interference fringes are visible. Film should have optical thickness high enough (> 400 nm) to yield a few interference extremes for visible and near infrared spectra.

This method considers only transmission spectra of thin films for the calculation of optical parameters. Swanepoel's method has advantage due to its non-destructive nature and yields the dispersion relation over a large range of wavelength without any prior knowledge of film's thickness and no parameters have to be

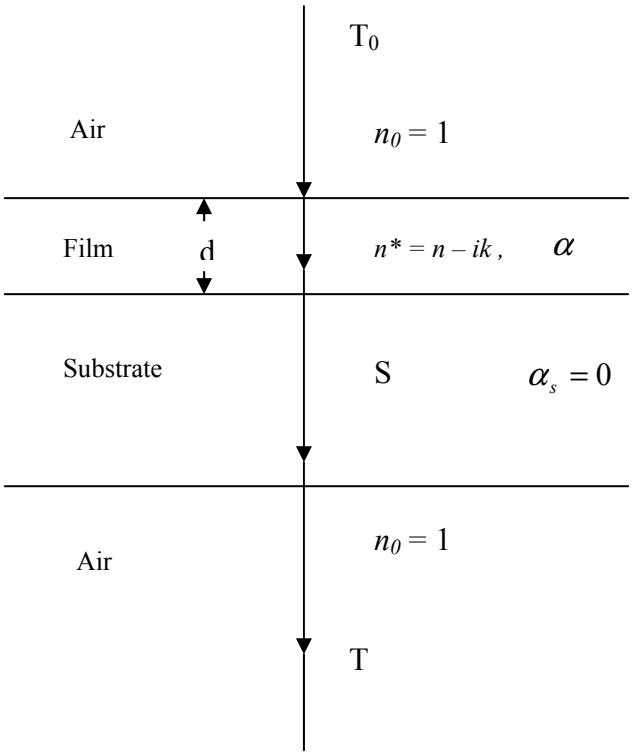

Figure 3.1 System of an absorbing thin film on a thick finite transparent substrate.

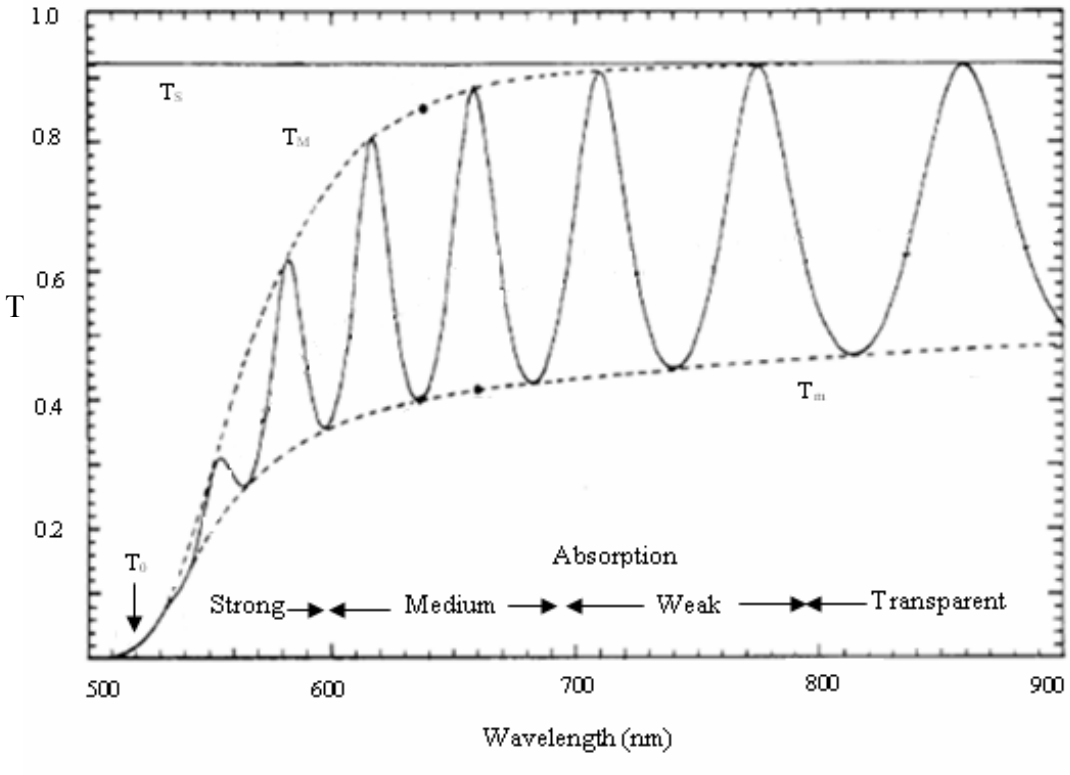

Figure 3.2 Different absorption regions in the transmission spectrum.

introduced. Consider a thin film having thickness *d* and complex refractive index $n^* = n - ik$, where *n* is the real part of the refractive index and *k* is the extinction coefficient. The index of the surrounding air is $n_a \approx 1$.

The glass substrate is several orders of magnitude thicker than the film and has a refractive index $s = 1.51$. All the multiple reflections at the three interfaces, figure 3.1, are taken into account when calculating transmittance *T*.

If the thickness *d* is uniform and comparable with wavelength of light which goes through the thin film, interference effect gives rise to a typical spectrum as shown in figure 3.2. Beginning at the long wavelength end and moving to shorter wavelength, we can divide the spectrum following Swanepoel [15] into different regions according to their transmission intensities. In the transparent spectral region of the film $\alpha \approx 0$, the transmission is determined by n and s through multiple reflections. In the region of weak absorption, α is small so the transmission starts to decrease. In the region of medium absorption, α is large and hence determines the overall transmission.

In the region of strong absorption, the transmission decreases drastically almost exclusively due to the influence of α. In the transparent region, transmission fringe minima T_m can be used to calculate the refractive index of the film which is given by

$$n = [M + (M^2 - s^2)^{1/2}]^{1/2} \tag{3.3}$$

where $M = \frac{2s}{T_m} - \frac{(s^2 + 1)}{2}$ (3.4)

If there are insufficient fringes in the transparent region, one may have option to using fringes from the region of weak and medium absorption, where $\alpha \neq 0$. Both extremes, T_M and T_m, are used to determine the film's refractive index (n), then *M* in equation (3.3) is given by

$$M = 2s\frac{T_M - T_m}{T_M T_m} + \frac{(s^2 + 1)}{2} \tag{3.5}$$

This optical characterization method provides values for refractive index of films at particular wavelengths where transmission spectra are tangential to their corresponding top and bottom envelops. A distinct advantage of using the envelopes

of the transmission spectrum rather than only the transmission spectrum is that the envelopes are slow-changing functions of wavelength (λ), whereas the spectrum oscillates rapidly with λ. In the strong absorption region, the transmittance decreases drastically due to the influence of α and the refractive index can be estimated by extrapolating the values of n calculated in the other regions of the spectrum. Thus we can evaluate the spectral dependence of the absorbance (x) and finally spectral dependence of absorption coefficient (α). Therefore, we first apply Cauchy's formula [15] to estimate n

$$n = A + \frac{B}{\lambda^2} \tag{3.6}$$

where A and B are material dependent constants. Therefore, the resulting solid line of n in interference region is extrapolated onto the refractive index axis to obtain the value of n in strong absorption region [16] and then the value of absorbance can be calculated from

$$x = \frac{(n+1)^3(n+s^2)}{16n^2 s} T_0 \tag{3.7}$$

where T_0 represents the transmission in the region of strong absorption. In the region of weak and medium absorption using the transmission maxima, x can be calculated by

$$x = \frac{E_M - [E_M^2 - (n^2-1)^3(n^2-s^4)]^{0.5}}{(n-1)^3(n-s^2)} \tag{3.8}$$

where

$$E_M = \frac{8n^2 s}{T_M} + (n^2-1)(n^2-s^2) \tag{3.9}$$

The extinction coefficient also called absorption index is a measure of the fraction of light lost due to scattering and absorption per unit distance of the participating medium. The extinction coefficient (k) can be calculated using the relation

$$k = \frac{\lambda}{4\pi d} \ln(1/x) \tag{3.10}$$

where d is the thickness of the film.

3.1.2.2 Thickness of Film

Thickness of film can be determined from the envelope method proposed by Swanepoel [15]. If n_1 and n_2 are the refractive indices of two adjacent maxima or minima at wavelengths λ_1 and λ_2, then the thickness *d* of the film is given by

$$d = \lambda_1\lambda_2 / 2(\lambda_1 n_2 - \lambda_2 n_1) \tag{3.11}$$

3.1.2.3 Absorption Coefficient

An electronic transition between the valence and conduction bands in the crystal starts at the absorption edge which corresponds to the minimum energy difference between the lowest minimum of the conduction band and highest maximum of the valence band. If these extrema lie at the same point of the *k*-space then the transition is called direct. If this is not the case, the possible transitions are phonon assisted and are called indirect. In most of the amorphous compound semiconductors, the absorption curve appears similar. Optical absorption is characterized in terms of the absorption coefficient (α).

It is crucial to determine the absorption characteristics of glasses and thin films, especially when comes to optical materials in order to evaluate their potential applications. When light is incident on a thin film, some of its energy is reflected, some is absorbed and rest is transmitted. The optical absorption of thin films varies with thickness and wavelength and is a function of its physical and chemical structure. The absorption coefficient (α) measures the spatial decrease in intensity of a propagating beam of light due to progressive conversion of the beam into different forms of energy. The values of absorption coefficient from the transmission spectra have been calculated using the equation.

$$\alpha = (1/d)\ln(1/x) \tag{3.12}$$

where *d* is the thickness of the film and *x* is the absorbance. The absorption coefficient of chalcogenide glasses is known to change rapidly for photon energies close to their band gap and for many glassy and amorphous non-metallic materials, the absorption edge can be divided into three regions;

(*i*) For high absorption coefficient ($\alpha \geq 10^4$ cm^{-1}); Tauc's power law [17] states that

$$\alpha h\nu = B(h\nu - E_g^{opt})^n \tag{3.13}$$

where B is the slope of Tauc edge called band tailing parameter that depends on the width of localized states in the band gap which are attributed to homopolar bonds in chalcogenide glasses. In the above equation, n = 1/2 for a direct allowed transition, n = 3/2 for a direct forbidden transition, n = 2 for an indirect allowed transition and n = 3 for an indirect forbidden transition. E_g^{opt} is the optical band gap.

(*ii*) For intermediate absorption coefficient (10^1 cm^{-1} $< \alpha <$ 10^4 cm^{-1}); the absorption coefficient follows the Urbach's exponential relation [18,19] *i.e.*

$$\alpha = \alpha_0 \exp(h\nu / E_e), \tag{3.14}$$

where ν is the frequency of the radiation, α_0 is a constant, h is Planck's constant and E_e is an energy which is often interpreted as the width of the tail of localized states in the gap region or Urbach energy. The parameter E_e is thought to provide information about the extent of disorder or randomness in amorphous chalcogenide glasses. Absorption in this region is related to the transition between extended states in one band and localized states in the exponential tail of the other band; hence disorder here refers more towards that of electronic states with in the material as compared to irregularity in atomic arrangement. This relation was first proposed by Urbach [18] to describe the absorption edge in alkali halide crystals at high absorption levels. The relation has been found to hold for many amorphous or glassy materials. Tauc [17] believes that it arises from electronic transitions between localized states in the band edge tails and the density of which is assumed to fall off exponentially with energy. Davis and Mott [20] were uncertain about the precise explanation of the exponential dependence and suggested that the slopes of the observed exponential edges obtained from equation (3.12) are very much same in many semiconductors and the value of E_e for a range of amorphous semiconductors [21] lies between 0.045 and 0.67 eV.

(*iii*) For weak absorption region ($\alpha < 1\,\mathrm{cm}^{-1}$); the strength and shape of absorption edge were found to depend on the preparation, purity and thermal history of the material.

3.1.2.4 Optical Band Gap

The band gap is the energy difference between the lowest minimum of the conduction band and highest maximum of the valence band is called the band or forbidden gap or simply energy gap. When this energy gap is calculated using optical methods then it is called optical band gap. The optical band gap of most of the chalcogenide glasses varies in the range 0.7 to 3.0 eV [22]. By knowing the values of absorption coefficient, optical band gap can be calculated by the method proposed by Tauc [17]. For different transitions from valence to conduction band the following relation is used;

$$\alpha h\nu = B(h\nu - E_g^{opt})^n \tag{3.13}$$

This relationship allows us to estimate the value of optical band gap by plotting $(\alpha h\nu)^{0.5}$ against $h\nu$. The values of E_g^{opt} can readily be calculated from the plot of $(\alpha h\nu)^{0.5}$ as a function of $h\nu$. The value of E_g^{opt} can be estimated by the intercept of the extrapolations to zero absorption with the photon energy axis $(\alpha h\nu)^{0.5} \to 0$.

Theoretically, the optical band gap can be calculated for the amorphous alloys from the Shimakawa's relation [23]

$$E_g(AB)(Y) = YE_g(A) + (1-Y)E_g(B) \tag{3.15}$$

where Y is the volume fraction of element A, $E_g(A)$ and $E_g(B)$ are the optical gaps for A and B elements, respectively. The conversion from atomic composition (at. %) or molecular composition (mol. %) to volume fraction (Y) is made using atomic or molecular mass and density.

3.1.2.5 Dielectric Constants

The complex dielectric constant is fundamental intrinsic material property. The real part of it is associated with the term that how much it will slow down the speed of light in the material and imaginary part gives that how a dielectric absorb

energy from electric field due to dipole motion. The knowledge of real and imaginary part of dielectric constant provides information about the loss factor which is the ratio of imaginary part of dielectric constant to real part of dielectric constant *i.e.* larger the imaginary part of dielectric constant or smaller the real part of dielectric constant, larger is the loss factor.

The complex refractive index is given by the relation

$$(n^*)^2 = \varepsilon^* \times \mu^* \tag{3.16}$$

where ε^* is complex dielectric constant (or complex permittivity) and μ^* is complex permeability. For non-magnetic materials, $\mu^* = 1$. Then above equation can be written as

$$(n - ik)^2 = \varepsilon_r - i\varepsilon_i \tag{3.17}$$

So, the real and imaginary parts of the dielectric constant can be determined using the relations derived from above equation

$$\varepsilon_r = n^2 - k^2 \tag{3.18}$$

and

$$\varepsilon_i = 2nk. \tag{3.19}$$

3.1.2.6 Optical Conductivity

The optical response of a material is most conveniently studied in terms of the optical conductivity. It has dimensions of frequency which is valid only in Gaussian system of units. The optical conductivity (σ) has been determined from the relation [24]

$$\sigma = \alpha nc/4\pi \tag{3.20}$$

where c is the velocity of light, α is absorption coefficient and n is the refractive index.

3.1.2.7 Wemple – DiDomenico Model

According to single oscillator model proposed by Wemple-DiDomenico (WDD) model [25,26], the optical data could be described to an excellent approximation by the following expression;

$$n^2(h\nu) = 1 + \frac{E_0 E_d}{E_0^2 - (h\nu)^2} \tag{3.21}$$

where $h\nu$ is photon energy, E_0 is single oscillator energy and E_d is dispersion energy which is a measure of the average strength of interband optical transitions (interband transition energy or also called dispersion energy). Experimental verification of equation (3.21) can be obtained by plotting $(n^2 - 1)^{-1}$ against $(h\nu)^2$. The resulting straight line yields values of parameters E_0 and E_d.

3.1.3 Results and Discussion

Optical transmission (T) is a very complex function and is strongly dependent on the absorption coefficient (α). Figures 3.3 and 3.4 show the variation of transmission (T) with wavelength (λ) for $Ge_{20}Se_{80-x}In_x$ (x = 0, 5) and (x = 10, 15, 20) thin films respectively.

According to Swanepoel's method [15], the envelope of the interference maxima and minima of transmission spectra can be used for deducing optical parameters *viz.* the values of the thickness (d), refractive index (n), extinction coefficient (k) of the thin films. The extinction coefficient can be neglected in the region of weak and medium absorption $(\alpha \neq 0)$. Therefore, this approximation is valid over most part of the spectra. The presence of maxima and minima on nearly same wavelength position confirms the optical homogeneity of the deposited film *i.e.* very - very small scattering or absorption occurs at long wavelength.

The thickness of the films calculated from the transmission spectrum is reported in table 3.1. The variation of refractive index and extinction coefficient with wavelength is shown in figures 3.5 and 3.6 respectively. From figures 3.5 and 3.6 it is clear that both refractive index and extinction coefficient decrease with the increase of wavelength for the thin films under investigation. This decrease in the values of refractive index and the extinction coefficient with the increase in wavelength attributes to the significant normal dispersion behavior of the material. Moreover, this decrease in the extinction coefficient with an increase in wavelength also shows that

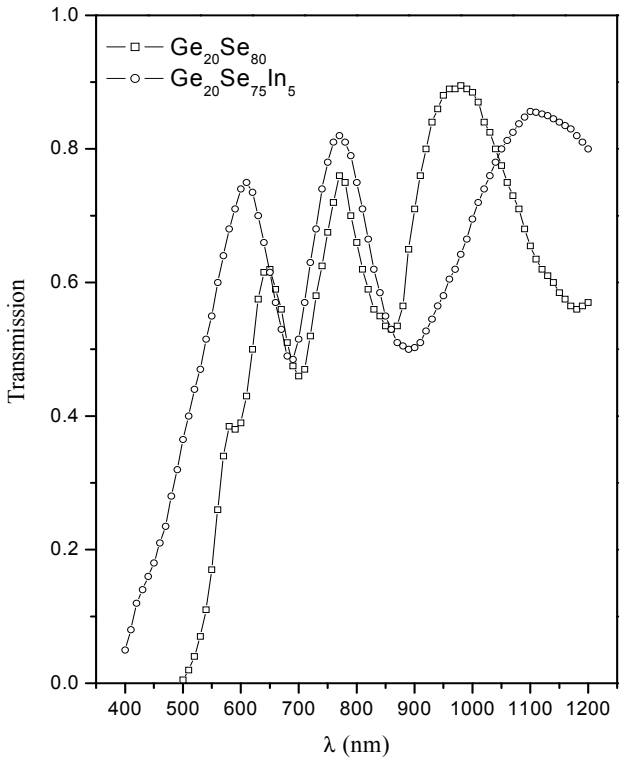

Figure 3.3 Plot of optical transmission versus wavelength for $Ge_{20}Se_{80-x}In_x$ (x = 0, 5) thin films.

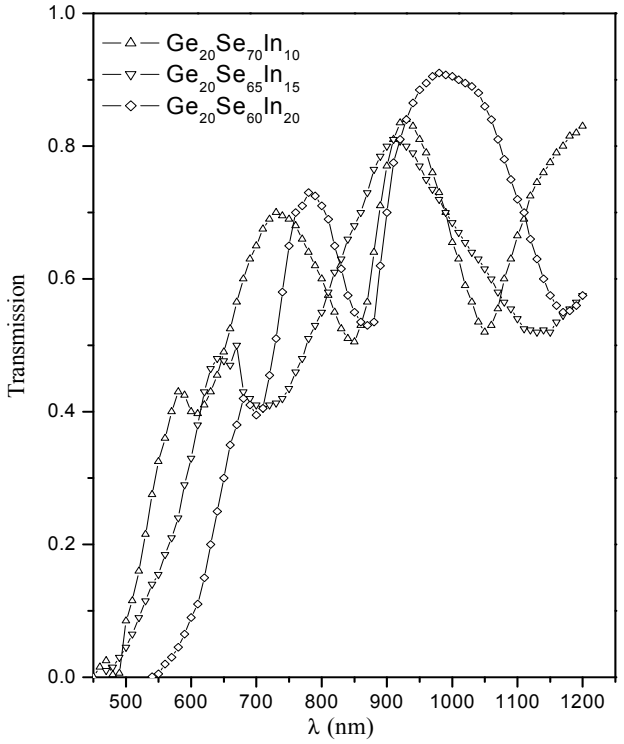

Figure 3.4 Plot of optical transmission versus wavelength for $Ge_{20}Se_{80-x}In_x$ (x = 10, 15, 20) thin films.

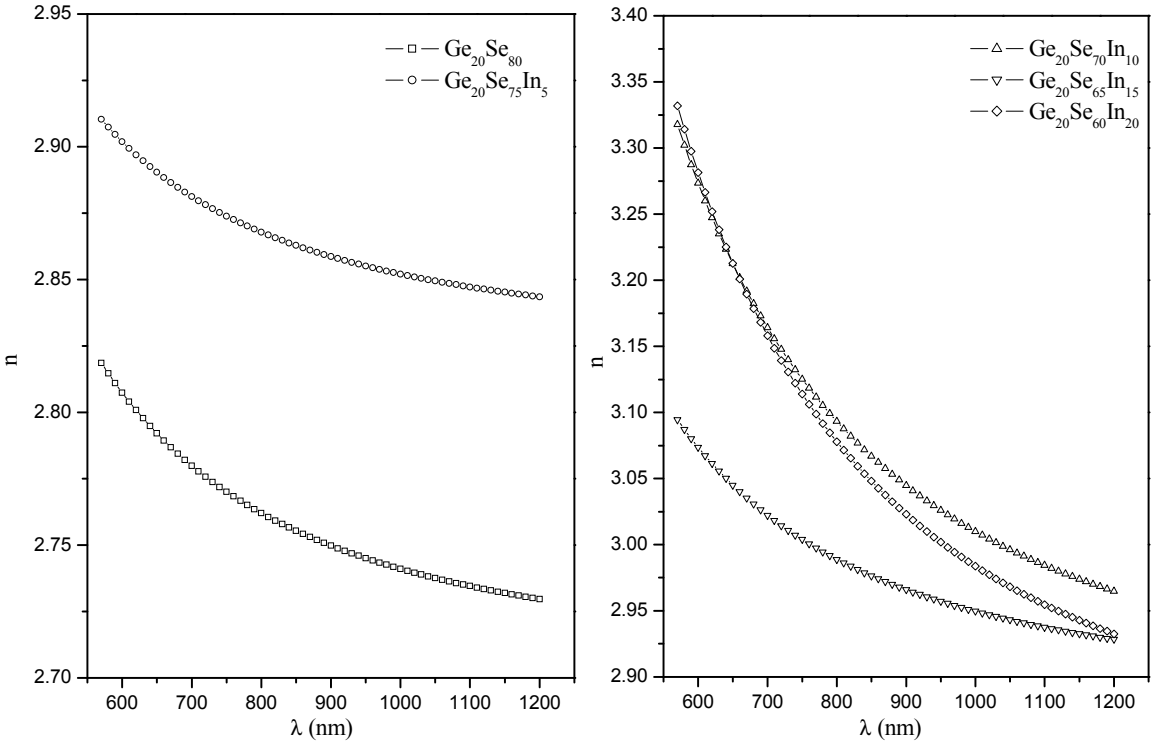

Figure 3.5 Plot of refractive index versus λ (nm) for $Ge_{20}Se_{80-x}In_x$ (x = 0, 5, 10, 15, 20) thin films.

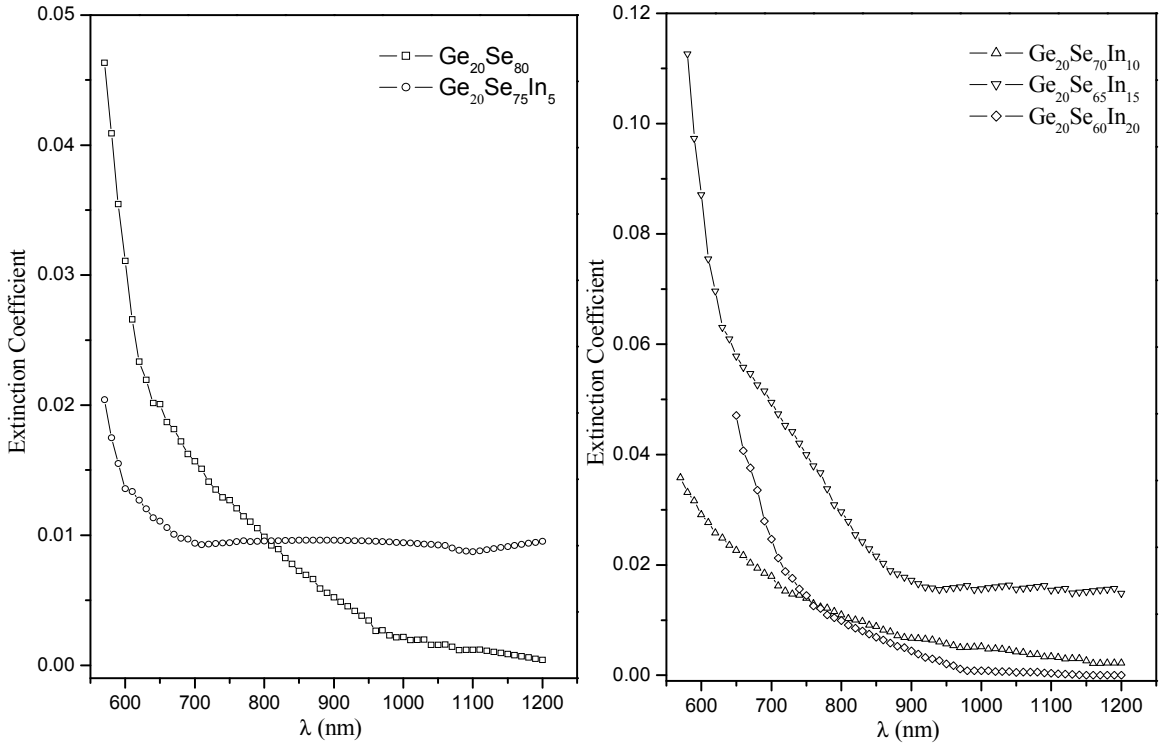

Figure 3.6 Plot of extinction coefficient versus λ (nm) for $Ge_{20}Se_{80-x}In_x$ (x = 0, 5, 10, 15, 20) thin films.

Table 3.1 Values of thickness (d), refractive index (n), extinction coefficient (k), dispersion energy (E_d), oscillator strength (E_0) at 1000 nm and static refractive index (n_0) for $Ge_{20}Se_{80-x}In_x$ (x = 0, 5, 10, 15, 20) thin films.

x	d (nm)	n	k	E_d (eV)	E_0 (eV)	n_0
0	799	2.74	0.00216	42.6	6.73	2.71
5	562	2.85	0.00942	47.56	6.87	2.82
10	777	3.01	0.00517	54.22	7.15	2.93
15	414	2.9	0.01572	41.96	5.58	2.92
20	952	2.98	0.00085	28.8	3.76	2.91

the fraction of light lost due to scattering and absorbance process decreases. The values of n and k for all the compositions at $\lambda = 1000$ nm are tabulated in table 3.1.

The spectral dependence (dispersion) of refractive index for each sample have been fitted to Wemple - DiDomenico single-oscillator model [25,26]. The optical data could be described to an excellent approximation by the relation

$$n^2(h\nu) = 1 + \frac{E_0 E_d}{E_0^2 - (h\nu)^2} \tag{3.21}$$

where $h\nu$ is the photon energy, n is refractive index, E_0 is the energy of the effective dispersion oscillator also called average energy gap or 'WDD gap', E_d is the dispersion energy. Plotting $(n^2 - 1)^{-1}$ against $(h\nu)^2$ allows us to determine the oscillator parameters by fitting a straight line to the points. The value of E_0 and E_d can be directly determined from the slope and the intercept on the vertical axis. In the figure 3.7, the slope = $(E_0 E_d)^{-1}$ and the intercept on vertical axis = (E_0 / E_d). The calculated values of E_0 and E_d are also given in table 3.1. E_0 is related to the bond energy of the different chemical bonds present in the material. Thus, the increase observed in the values of E_0 with the addition of In content (upto 10 at. %) and then consequent decrease (>10 at. %) for the films under study, is presumably due to the change in bond energies of the system which are discussed later. According to Tanaka [27], the single-oscillator energy E_0 approximately equals twice the optical band - gap (E_g^{opt}). This is quite reasonably supported by our results also. The value of static refractive indices (n_0) for $Ge_{20}Se_{80-x}In_x$ thin films are calculated from WDD dispersion parameters E_0 and E_d by using the formula

$$n_0 = \left(1 + \frac{E_d}{E_0}\right)^{1/2} \tag{3.22}$$

The values of n_0 are calculated by extrapolating the WDD dispersion equation to $h\nu \to 0$ {equation (3.21) and figure 3.7} and the values of n_0 are given in table 3.1.

The absorption coefficient (α) of $Ge_{20}Se_{80-x}In_x$ thin films can be calculated using the well-known relation (equation 3.12). The variation of absorption coefficient

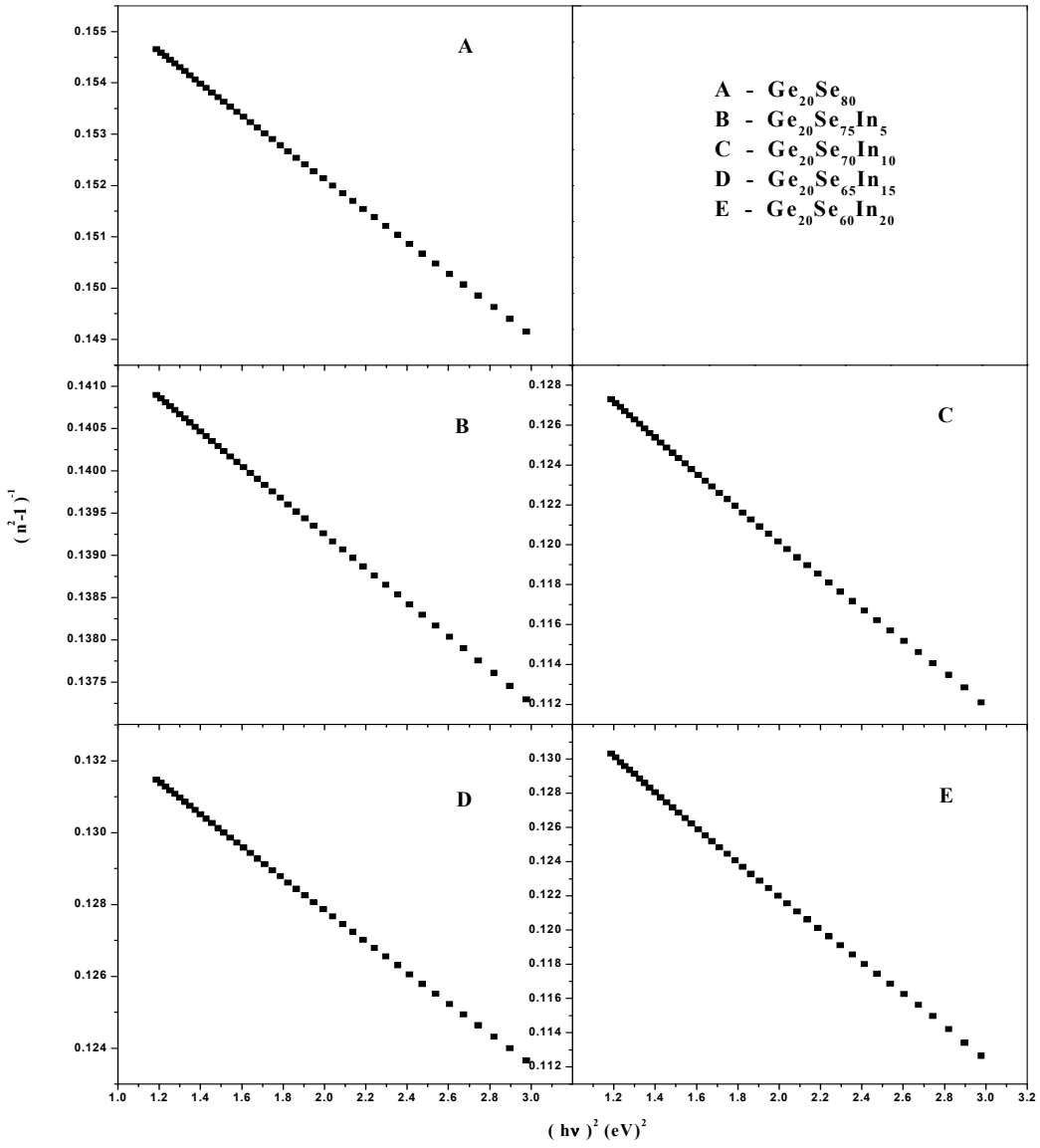

Figure 3.7 Plot of $(n^2-1)^{-1}$ versus $(h\nu)^2$ for $Ge_{20}Se_{80-x}In_x$ (x = 0, 5, 10, 15, 20) thin films.

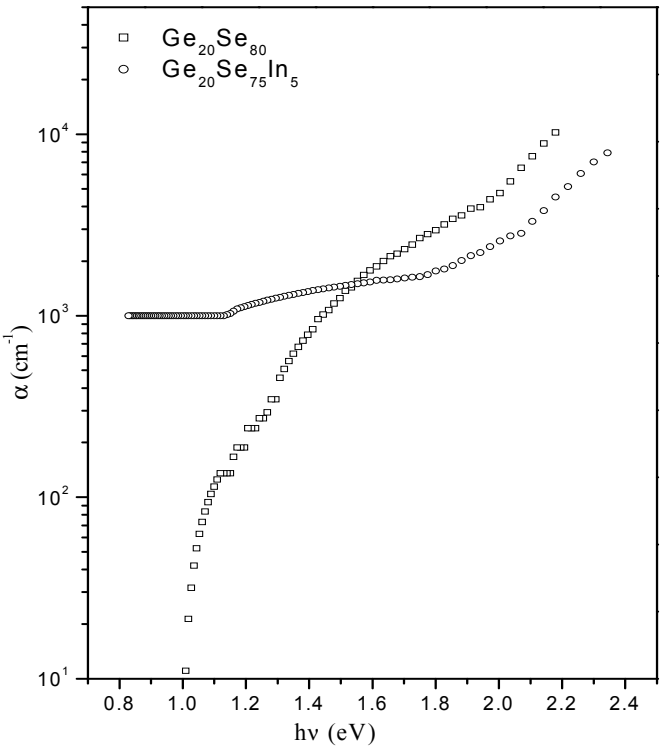

Figure 3.8 Plot of absorption coefficient versus $h\nu$ for $Ge_{20}Se_{80-x}In_x$ (x = 0, 5) thin films.

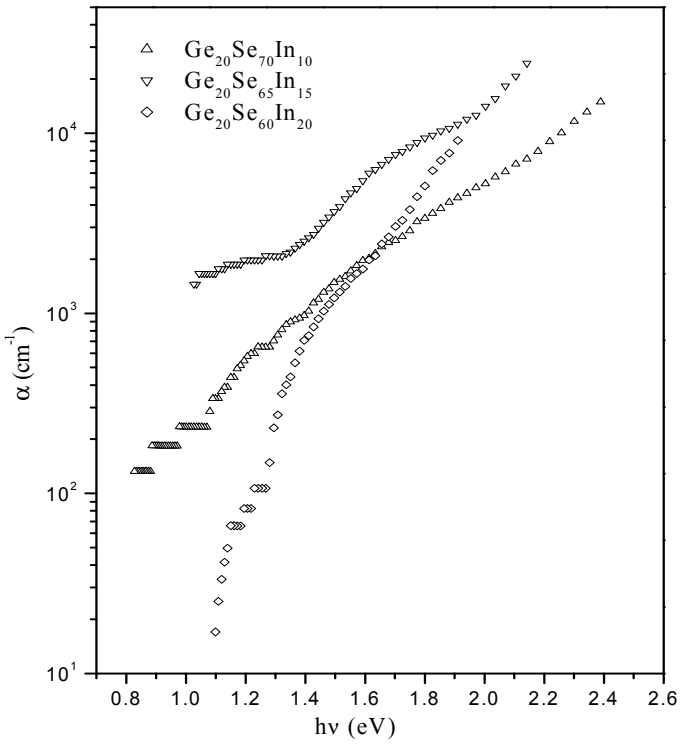

Figure 3.9 Plot of absorption coefficient versus $h\nu$ for $Ge_{20}Se_{80-x}In_x$ (x = 10, 15, 20) thin films.

with photon energy are shown in figures 3.8 and 3.9 respectively for $Ge_{20}Se_{80-x}In_x$ (x = 0, 5) and (x = 10, 15, 20) thin films.

The optical band gap has been estimated from absorption coefficient data as a function of wavelength by using Tauc relation [17]

$$\alpha h\nu = B(h\nu - E_g^{opt})^n \tag{3.13}$$

where $h\upsilon$ is the photon energy, α is the absorption coefficient, E_g^{opt} is the optical band gap, B is band tailing parameter and n = 1/2 and 2 for direct and indirect band gap respectively. Figure 3.10 shows the variation of $(\alpha h\nu)^{1/2}$ with $h\nu$. Optical band gap E_g^{opt} can be determined by the extrapolation of best fit line between $(\alpha h\nu)^{1/2}$ and $h\nu$ to intercept the $h\nu$ - axis $(\alpha = 0)$ for $Ge_{20}Se_{80-x}In_x$ system. Variation of optical band gap with different In concentration is given in table 3.2 and plotted in figure 3.11. It is found that the optical band gap increases with increase in concentration of In up to 10 at. % and at higher concentration of In (>10 at. %), it decreases subsequently.

The variation in optical parameters with In incorporation is mainly attributed to change in stoichiometry. The In additives in $Ge_{20}Se_{80-x}In_x$ must bring about a compositional change in host network of Ge-Se *i.e.* the alloying effect. According to Phillips [28], molecular structure of melt-quenched Ge_xSe_{100-x} is much more ordered and may be expected from a continuous random network model. As per the model, Ge_xSe_{100-x} alloys may be described by chemically ordered clusters embedded in a continuous network. Some of these clusters are $(Se)_n$ chains, $Ge(Se_{1/2})_4$ corner sharing tetrahedral and $Ge_2(Se_{1/2})_6$ ethane like structural units. $(Se)_n$ chains, $Ge(Se_{1/2})_4$ structure dominate for $x \leq 33$ and third type is expected to occur at higher concentration of Ge *i.e.* $x > 33$. In our present system *a*-$Ge_{20}Se_{80-x}In_x$, since Ge is at 20 at. %, hence first two structures are possible. At lower concentration of In (≤ 10 at. %), In atoms may enter into Se chain and rearrange in the network of host Se to satisfy their bonding states and therefore reducing the concentration of defects states. This leads to an increase in optical band gap (E_g^{opt}) with addition of In upto 10 at. %. With further increase of In (>10 at. %), In enters into Ge-Se system and saturates In-Se bonds which exist in the glass. Perhaps some unsaturated In atoms may also act as

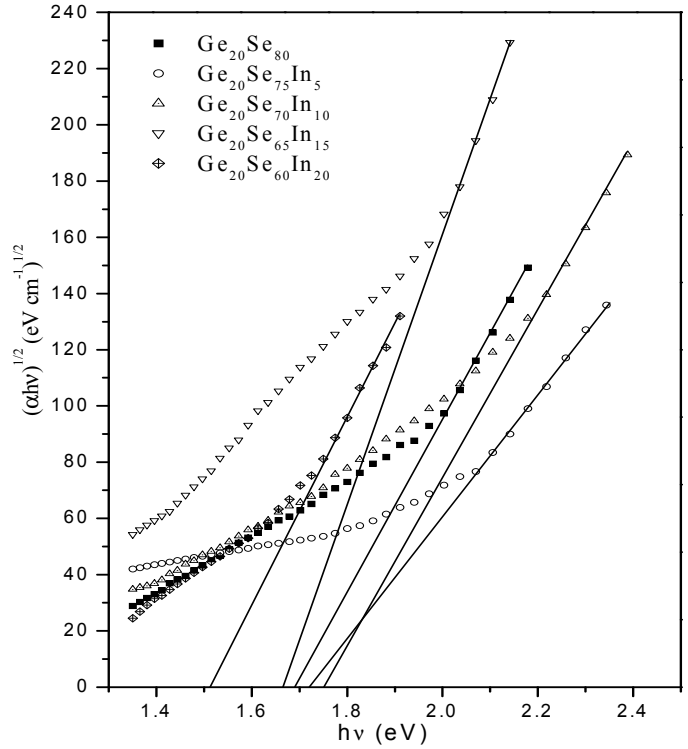

Figure 3.10 Plot of $(\alpha h\nu)^{1/2}$ versus $h\nu$ for $Ge_{20}Se_{80-x}In_x$ (x = 0, 5, 10, 15, 20) thin films.

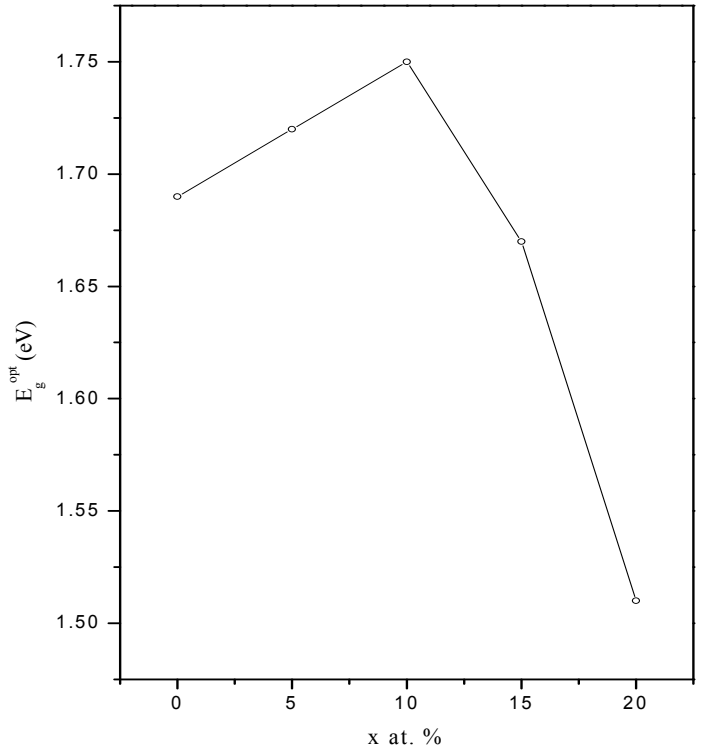

Figure 3.11 Plot of optical band gap (E_g^{opt}) versus In content (x at. %).

Table 3.2 Values of absorption coefficient (α), optical band gap (E_g^{opt}), real part of dielectric constant (ε_r), imaginary part of dielectric constant (ε_i) and optical conductivity (σ) are given at 1000 nm for $Ge_{20}Se_{80-x}In_x$ (x = 0, 5, 10, 15, 20) thin films.

x	α (cm^{-1})	E_g^{opt} (eV)	ε_r	ε_i	σ (s^{-1}) x 10^{13}
0	1551.5	1.69	7.51	0.0118	0.17
5	1499.4	1.72	8.13	0.0537	0.81
10	1718.1	1.75	9.06	0.0311	0.53
15	4659.5	1.67	8.70	0.0927	1.39
20	1560.5	1.51	8.90	0.005	0.07

defect center. This may result in perturbation in the system, broadening of valence and conduction band edges in the mobility gap [29, 30].

So decreases of E_g^{opt} may be attributed to the formation of more number of defect centers and increase of disorder with increase in In concentration (>10 at. %). This is in accordance with Mott and Davis model [20] which states that the width of the localized states near the mobility edges depends on the degrees of disorder and the defects present in the amorphous structure. In particular, it is known that unsaturated bonds along with some saturated bonds (like dative bonds [31]) are produced because of an insufficient number of atoms deposited in the amorphous films. These unsaturated bonds are responsible for the formation of some defects in the films. Such defects produce localized states in the amorphous solids. The presence of a high concentration of localized states in the band structure is responsible for the low value of E_g^{opt}. The change in optical band gap and single oscillator energy may also be understood in terms of change in average bond energy of the system with In incorporation. Upto 10 at. % of In, In atoms may enter into Se chain resulting in the systematic replacement of Se-Se bond (bond energy of 44 kcal mol^{-1}) with Se-In bonds (bond energy of 48.2 kcal mol^{-1}). Since energy of Se-In bond is higher than Se-Se bond, the average bond energy of the system increases. The optical band gap is a bond sensitive property [32]. Thus an increase in the average bond energy results in the increase in optical band gap and single oscillator energy in *a*-$Ge_{20}Se_{80-x}In_x$ at x = 0, 5, 10 at. % thin films.

The dielectric constant of *a*-$Ge_{20}Se_{80-x}In_x$ thin films can be calculated with the help of refractive index and extinction coefficient. Real dielectric constant can be calculated from the relation $\varepsilon_r = n^2 - k^2$ while the imaginary dielectric constant can be calculated from relation $\varepsilon_i = 2nk$. The variation of both real and imaginary dielectric constants with energy for *a*-$Ge_{20}Se_{80-x}In_x$ thin films is shown in figures 3.12 and 3.13 respectively. For *a*-$Ge_{20}Se_{80-x}In_x$ thin films the variation of both real and imaginary dielectric constants (ε_r and ε_i) with energy follows the same trend as that of refractive index and extinction coefficient. The optical parameters *i.e.* n, k, ε_r and ε_i decrease with increasing wavelength. The optical conductivity is determined

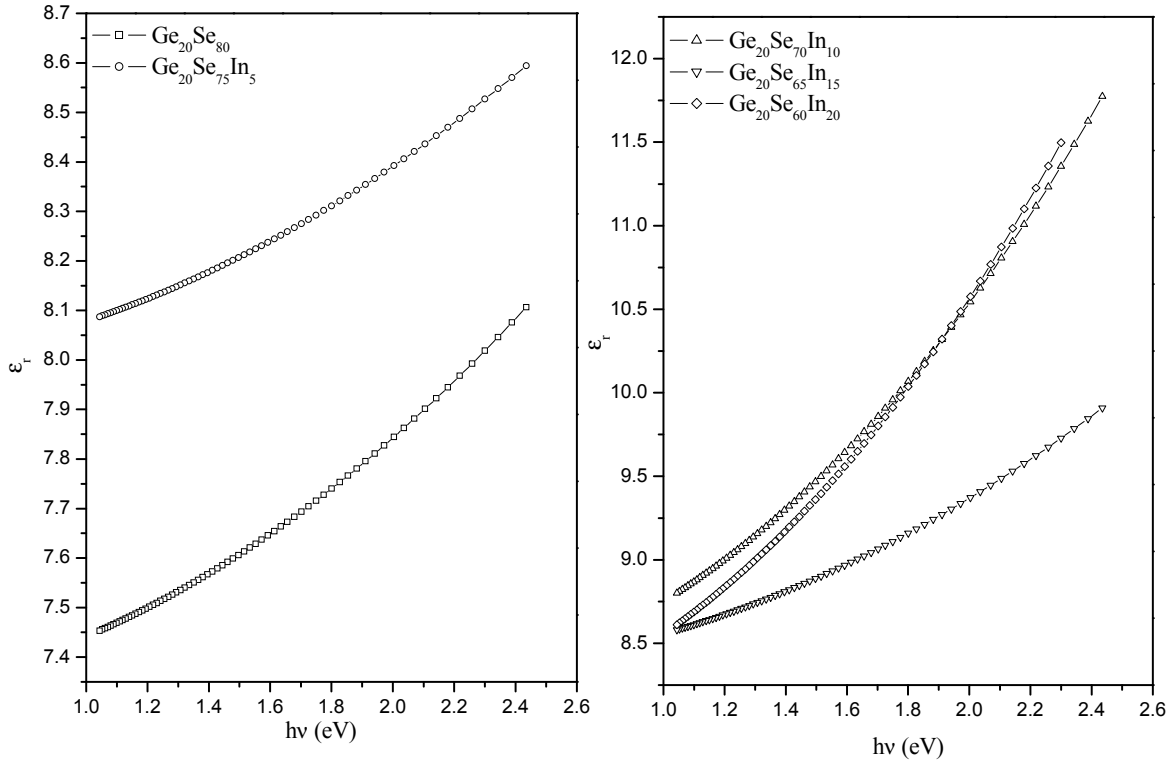

Figure 3.12 Plot of real part of dielectric constant (ε_r) versus *hυ* (eV) for $Ge_{20}Se_{80-x}In_x$ (x = 0, 5, 10, 15, 20) thin films.

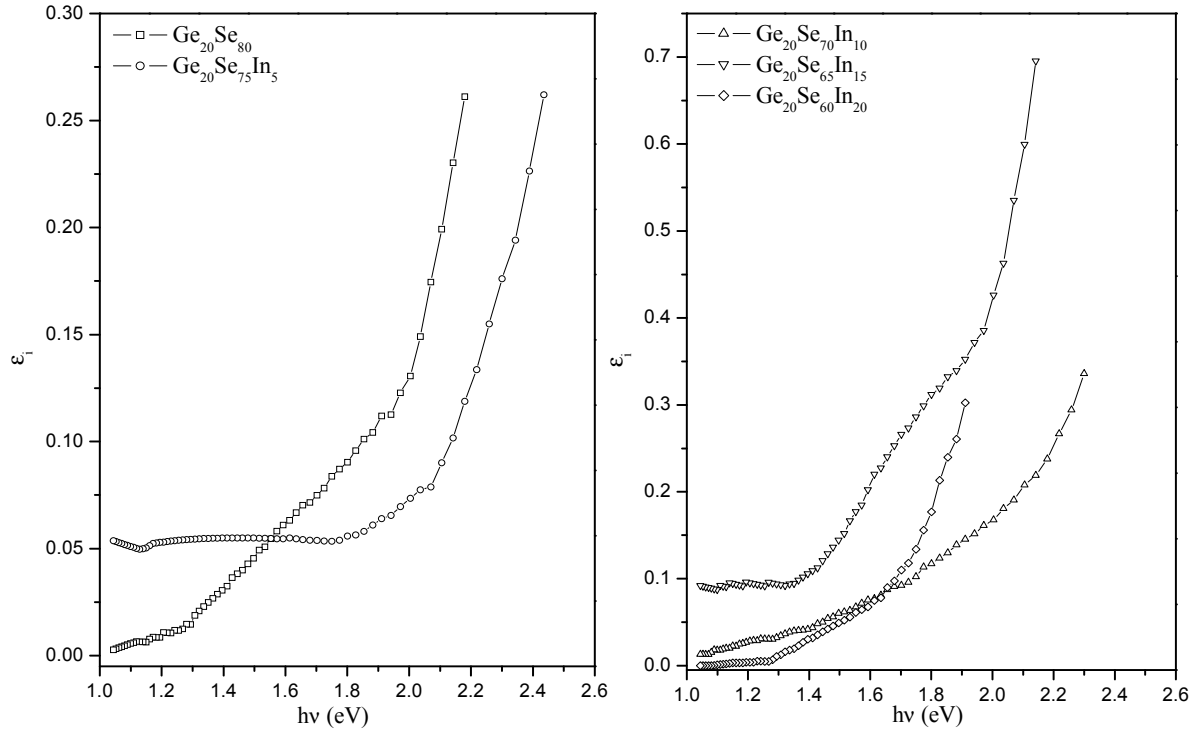

Figure 3.13 Plot of imaginary part of dielectric constant (ε_i) versus *hυ* (eV) for $Ge_{20}Se_{80-x}In_x$ (x = 0, 5, 10, 15, 20) thin films.

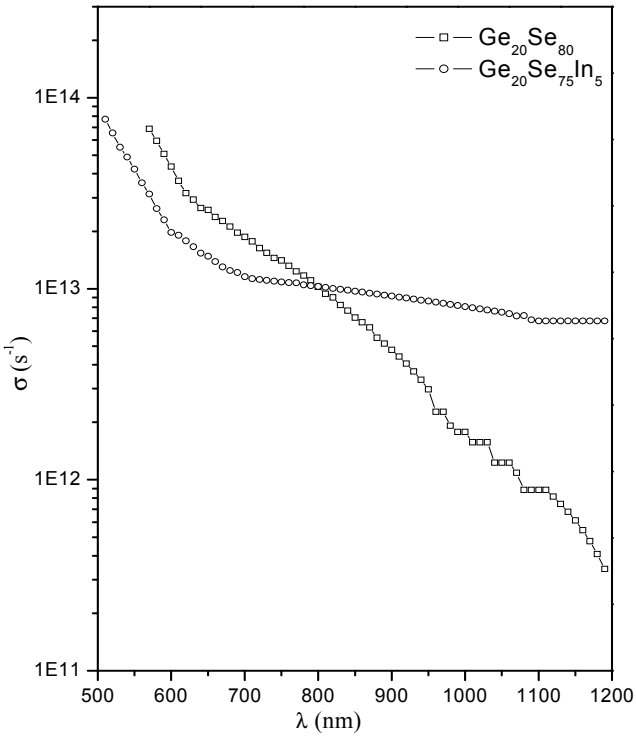

Figure 3.14 Plot of optical conductivity (σ) versus λ (nm) for $Ge_{20}Se_{80-x}In_x$ (x = 0, 5) thin films.

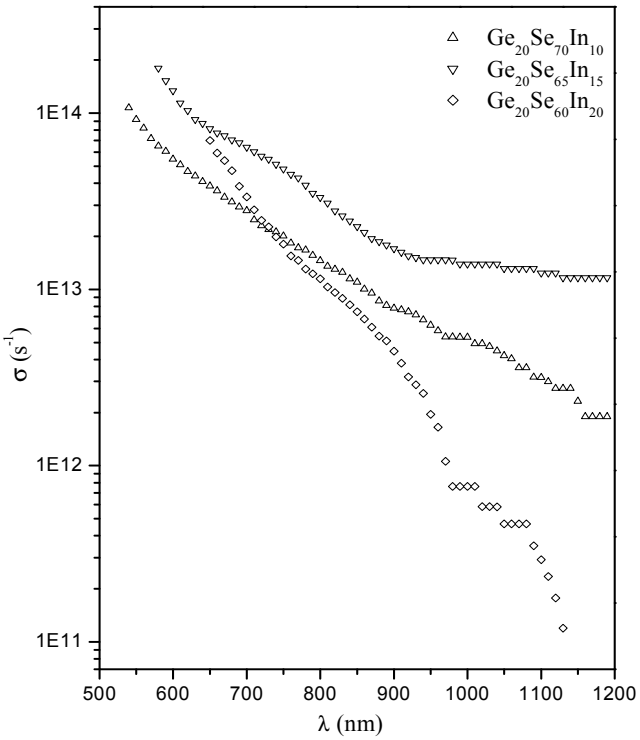

Figure 3.15 Plot of optical conductivity (σ) versus λ (nm) for $Ge_{20}Se_{80-x}In_x$ (x = 10, 15, 20) thin films.

using the relation [25], $\sigma = \alpha nc/4\pi$, where 'c' is the velocity of light, 'α' is absorption coefficient and 'n' is refractive index. Optical response is most conveniently studied in terms of optical conductivity. It has the dimensions of frequency which are valid only in Gaussian system of units. The optical conductivity directly depends on the absorption coefficient and refractive index and is found to increase sharply for higher energy values due to large absorption coefficient and refractive index for these values. The plots of optical conductivity versus wavelength for $Ge_{20}Se_{80-x}In_x$ (x = 0, 5) and (x = 10, 15, 20) thin films are given in figure 3.14 and 3.15 respectively. The variation of ε_r, ε_i and σ (at λ = 1000 nm) with In at. % is given in table 3.2.

3.2 Electrical Properties of Ge-Se-In Thin Films

Common feature of chalcogenide glasses is the presence of localized states in the mobility gap due to the absence of long range order as well as inherent defects. Photocurrent measurements have been widely used to understand the defect states in chalcogenides glasses [33,34]. In chalcogenides, these defect centers are with negative correlation energy. The study of the photoconductivity (PC) provides an understanding of the photo generations and transport of the free carriers. The PC represents a valuable tool in understanding the recombination kinetics which in turn provides information about the localized states in the amorphous materials [35]. In many non crystalline materials and for large temperature range the dc conduction as a function of temperature, can be expressed by the relation $\sigma = \sigma_0 \exp(-\Delta E/T)$ with constant activation energy ΔE over the whole temperature range of the measurements. The activation energy is usually referred to half of the energy gap. The activation energy is usually situated in the range of 0.5 – 1.0 eV although values are as low as 0.2 eV and as high as 1.5 eV have been observed. The pre exponential factor is often situated in the range 10^3 to 10^4 $\Omega^{-1}cm^{-1}$ but it can be as low as 10^{-5} $\Omega^{-1}cm^{-1}$ and as high as 10^8 $\Omega^{-1}cm^{-1}$. Generally the annealing of the chalcogenides leads to decrease of the electrical conductivity and to a small increase of activation energy [36].

In this section temperature dependent (303 – 375 K) steady state photoconductivity and intensity dependent (3 - 1035 Lux) photocurrent is measured for Ge-Se-In system. The variation of different parameters as dark conductivity (σ_d), photoconductivity (σ_{ph}), dc-activation energy (ΔE_d), photoactivation energy (ΔE_{ph}), photosensitivity, pre exponential factor (σ_0) have been studied. These measurements give valuable information regarding the defect states and other mechanism responsible for conductivity and photoconductivity behavior of alloy.

3.2.1 Experimental Details

Thin films of the glassy alloys $Ge_{20}Se_{80-x}In_x$ (x = 0, 5, 10, 15, 20) have been prepared by vacuum evaporation technique, keeping the substrates at room temperature and a base pressure ~ 10^{-4} Pa. Amorphous nature of the thin films was confirmed by X-ray diffraction technique as no sharp peak was observed. Pre-deposited thick indium electrodes on well-degassed Corning 7059 glass substrates have been used for the electrical contacts. A planar geometry of the film (length ~ 2.4 cm; electrode gap ~ 4×10^{-2} cm) is used for the electrical measurements. The thickness of the film is ~ 2000 A^o. After deposition thin films were kept in the deposition chamber in dark for 24 h before mounting in the metallic sample holder to attain thermodynamic equilibrium *i.e.* to avoid any irregularity and inconsistency in the behavior of the film during various measurements. Thin films are annealed at 375 K for 1 hour in a vacuum of about 10^{-3} mbar. This temperature is less than the glass transition temperature of *a*-$Ge_{20}Se_{80-x}In_x$ glassy alloys. Dark conductivity measurement is carried out over the films after mounting in the metallic sample holder which is already described in previous chapter.

3.2.2 Results and Discussion

DC conductivity measurements yield valuable information about conduction mechanism in amorphous semiconductors. The temperature dependent dc dark conductivity (σ_d) for glassy thin films of *a*-$Ge_{20}Se_{80-x}In_x$ is shown in figure 3.16. The plots of $\ln\sigma_d$ vs. $1000/T$ are found to be straight indicating that conduction is

through an activated process having single activation energy value in the temperature range 303 – 375 K. In most of the chalcogenide glasses, σ_d can therefore be expressed by the Arrhenius relation;

$$\sigma_d = \sigma_0 \exp\left(\frac{-\Delta E_d}{k_B T}\right) \tag{3.23}$$

where, σ_0 is the pre-exponential factor, ΔE_d is the activation energy for dc conduction, k_B is the Boltzmann's constant and T is the absolute temperature. The values of ΔE_d at 303 K are calculated from slope of the curves of figure 3.16 and are given in table 3.3. Figure 3.17 shows the compositional dependence of ΔE_d. The value of ΔE_d increases up to 10 at. % of In addition and thereafter decreases with further alloying of In to Ge-Se base. This variation of activation energy also follows the same trend as that of optical band gap (figure 3.17). Variation of steady state photoconductivity (σ_{ph}) of $Ge_{20}Se_{80-x}In_x$ thin films with temperature (*i.e.* σ_{ph} vs. $1000/T$) at a particular intensity (1035 Lux) is shown in figure 3.18. The values of σ_{ph} are given in table 3.3. It is clear from the figure 3.18 that the photoconductivity is an activated process and the activation energy (ΔE_{ph}) for photoconduction is much smaller than dark conduction in all samples.

Photoconductivity simply increases solely and monotonically with increasing temperature (figure 3.18). It can be described as a thermally activated process which is explained on the basis of bimolecular recombination. In chalcogenide glasses, changes in composition bring structural changes in the network due to absence of long range order which in turn induce modification in the density and distribution of localized states in the glassy system. The net effect of these modifications is to increase or decrease the defect density participating in the electrical conduction. With the addition of In to Ge-Se, the variation in photoconductive parameters is mainly because of change in stoichiometry of the base glass. The In additives in $Ge_{20}Se_{80-x}In_x$ thin films must bring about a compositional change of host network of Ge-Se as discussed in section 3.1.3. At lower concentration of In (≤ 10 at. %), In atoms may enter into Se chain and rearrange the network of host Se. It makes bonds with Se to satisfy their bonding states and therefore reducing the number of defects states. With

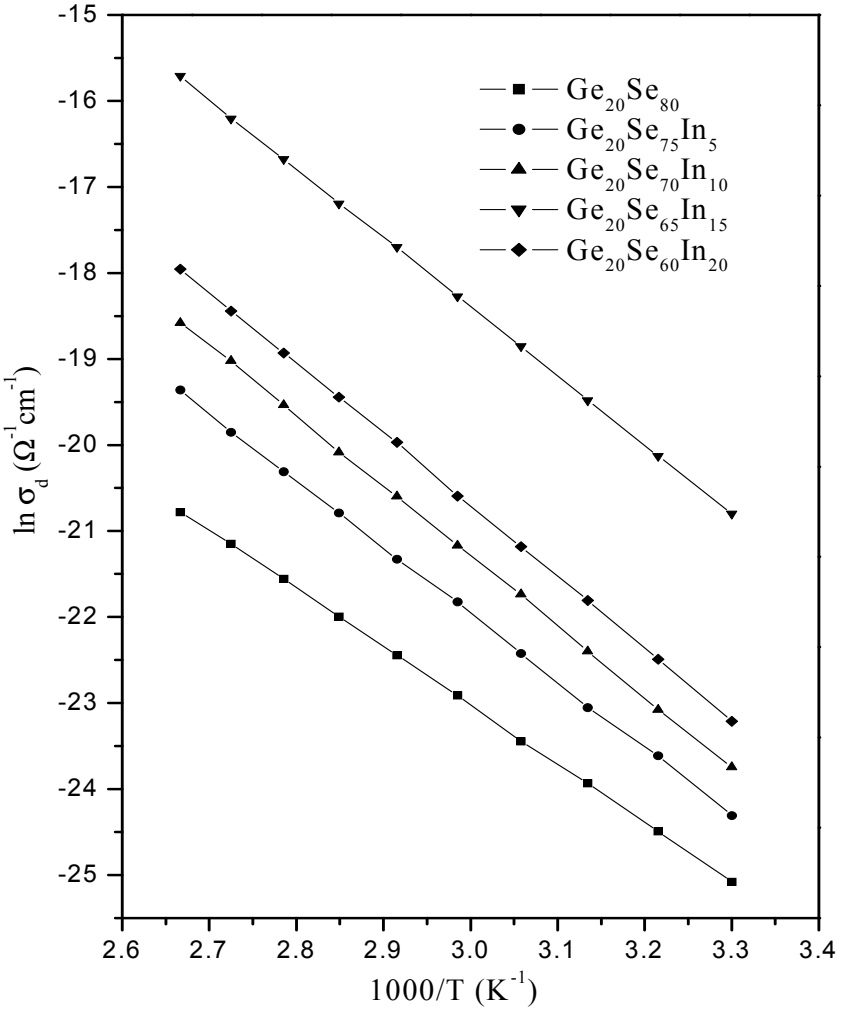

Figure 3.16 Temperature dependence of dark conductivity of $Ge_{20}Se_{80-x}In_x$ (x = 0, 5, 10, 15, 20) thin films.

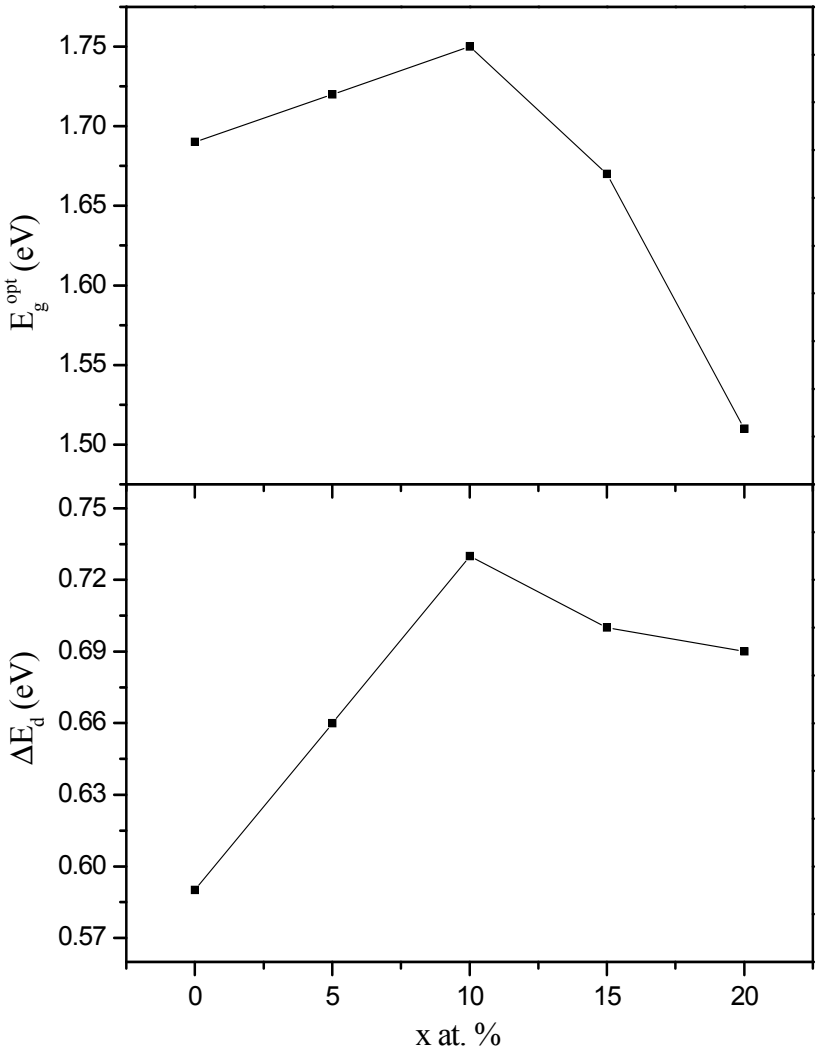

Figure 3.17 Variation of dark activation energy (ΔE_d) and optical band gap (E_g^{opt}) with *x* at. %.

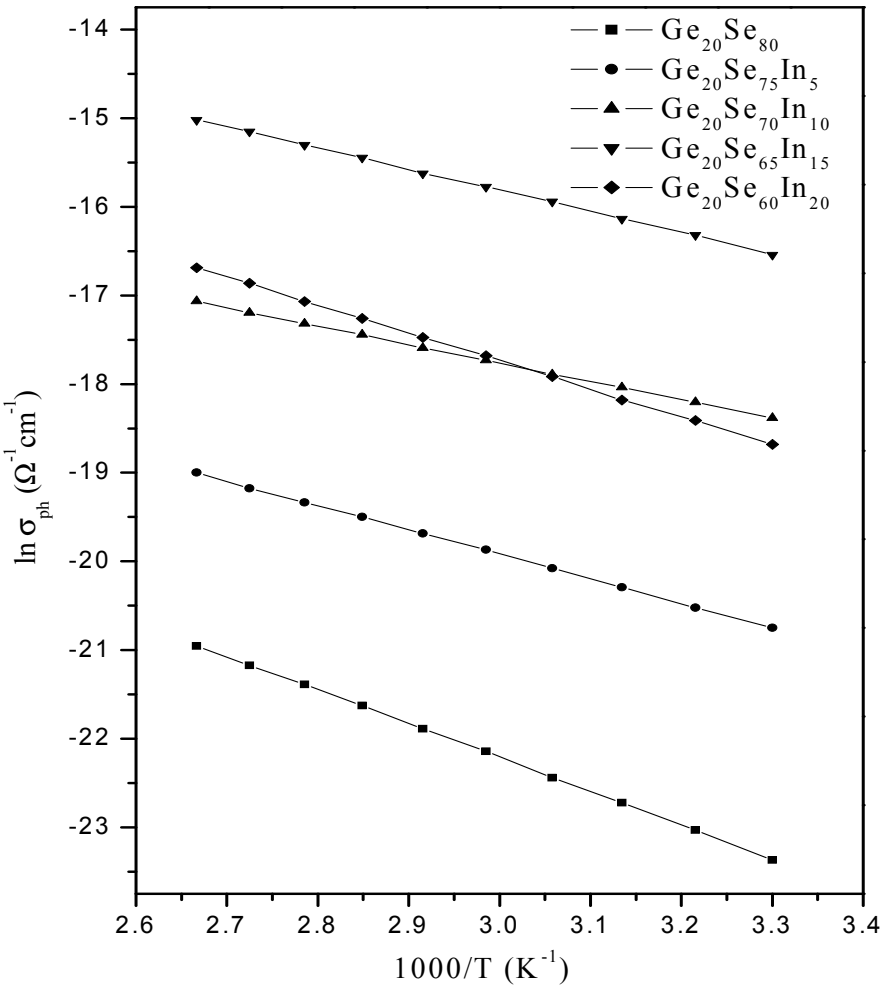

Figure 3.18 Temperature dependence of photo conductivity for $Ge_{20}Se_{80-x}In_x$ (x = 0, 5, 10, 15, 20) thin films.

the reduction of defect states, system becomes more and more rigid. This results in the increase in dark conductivity, photoconductivity and activation energy up to certain concentration of In (*i.e.* 10 at. %). With further addition of In (>10 at. %), In enters into Ge-Se system and saturates In-Se bonds. Perhaps some unsaturated In atoms might act as defect centers. This may result in perturbation in system and broadening of valence and conduction band edges in the mobility gap [29, 30]. So, the decrease of activation energies at higher concentration of In (> 10 at. %) may be attributed to the formation of more number of defect centers with increase of disorder in the system.

Intensity (F) dependence of steady state photoconductivity has also been studied at room temperature (303 K) to investigate the nature of recombination processes in $Ge_{20}Se_{80-x}In_x$ thin films. The plots of $\ln \sigma_{ph}$ vs. $\ln F$ are straight lines for all the compositions and are shown in figure 3.19, which indicate that photoconductivity (σ_{ph}) follows a power law with intensity (F) *i.e.*

$$\sigma_{ph} \alpha F^{\gamma} \tag{3.25}$$

For γ = 0.5, the recombination is predominantly bimolecular in nature,

1.0, the recombination is monomolecular in nature.

According to Rose [37], for $0.5 \leq \gamma \leq 1.0$, the value of γ can not be interpreted by assuming a set of discrete trap levels, but considering the existence of continuous distribution of trap levels in the band gap. In *a*-$Ge_{20}Se_{80-x}In_x$ films, the value of γ is calculated from the slope of $\ln \sigma_{ph}$ vs. $\ln F$ and are found to be close to 0.5 for all compositions. This square root dependence of photocurrent on intensities indicates the existence of bimolecular recombination on illumination of thin films with light in which recombination rate of electron is proportional to number of holes. In non-equilibrium condition, most of the electrons and holes are generated after shining light and are located at D^0 centers. These centers decrease by recombination process $\left[2D^0 \rightarrow D^+ + D^-\right]$ when the illumination is stopped [38].

Photosensitivity (σ_{ph}/σ_d) is an important parameter to describe the usefulness of a particular material from optoelectronic device point of view. The values of σ_{ph}/σ_d for $Ge_{20}Se_{80-x}In_x$ thin films at room temperature (303 K) and at intensity 1035 Lux are calculated and are tabulated in table 3.3. It is clear from the

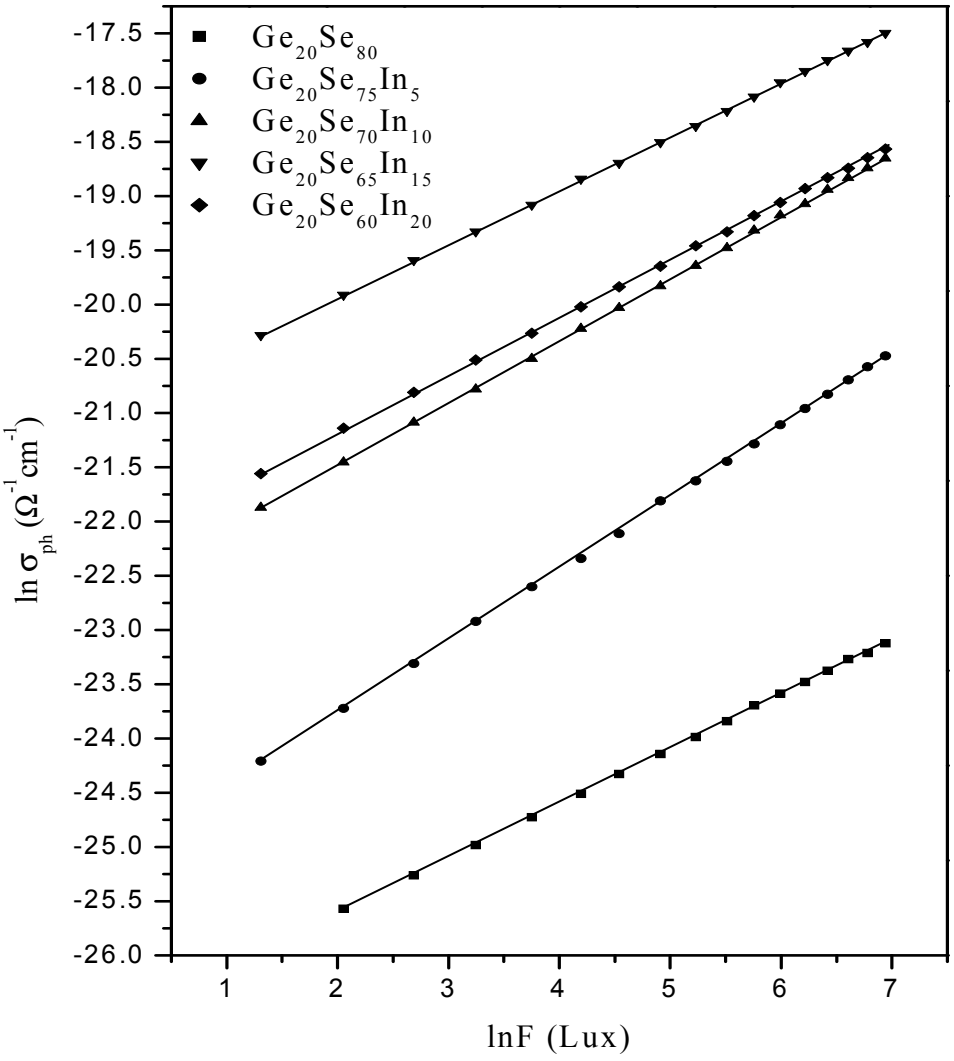

Figure 3.19 Intensity dependence of photoconductivity for $Ge_{20}Se_{80-x}In_x$ (x = 0, 5, 10, 15, 20) thin films at 303 K.

Table 3.3 The dc dark conductivity (σ_d), the pre-exponential factor (σ_0), the activation energy for dc conduction (ΔE_d), photoconductivity (σ_{ph}), the activation energy of photoconduction (ΔE_{ph}), power exponent (γ), photosensitivity (σ_{ph}/σ_d), refractive index (n), charge carrier density for $Ge_{20}Se_{80-x}In_x$ (x = 0, 5, 10, 15, 20) thin films.

x	σ_d ($\Omega^{-1}cm^{-1}$) (303K)	σ_0 ($\Omega^{-1}cm^{-1}$)	ΔE_d (eV)	σ_{ph} ($\Omega^{-1}cm^{-1}$)	ΔE_{ph} (eV)	γ	σ_{ph}/σ_d (303K)	n_σ (cm^{-3})
0	1.4×10^{-11}	0.08	0.59	7.2×10^{-11}	0.34	0.51	5	4.8×10^{15}
5	2.8×10^{-11}	3.01	0.66	9.8×10^{-10}	0.21	0.66	35	2.4×10^{14}
10	4.8×10^{-11}	12.50	0.73	1.1×10^{-8}	0.18	0.57	217	2.0×10^{13}
15	9.8×10^{-10}	36.83	0.70	6.6×10^{-8}	0.19	0.50	67	6.9×10^{13}
20	8.3×10^{-11}	29.21	0.69	7.8×10^{-9}	0.28	0.54	94	9.4×10^{13}

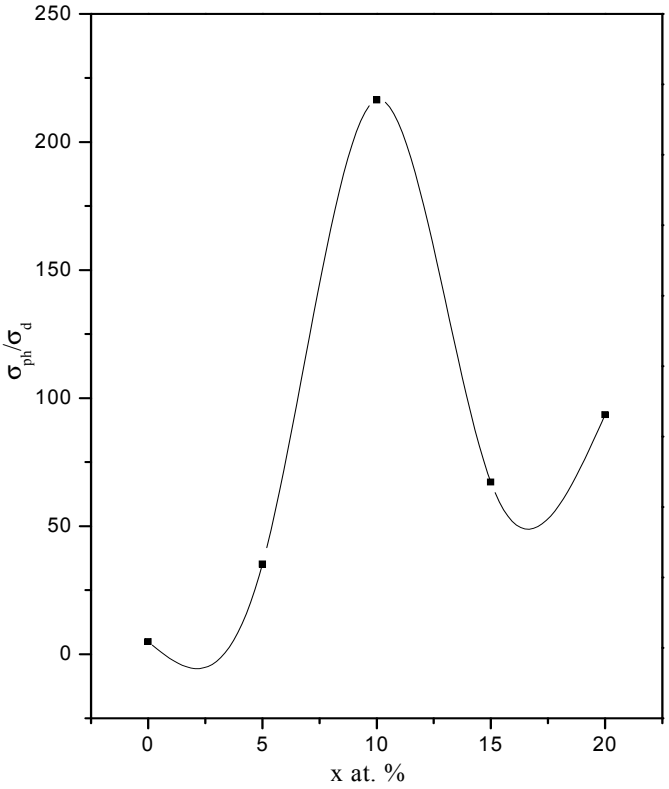

Figure 3.20 Variation of photosensitivity versus In content (x at. %).

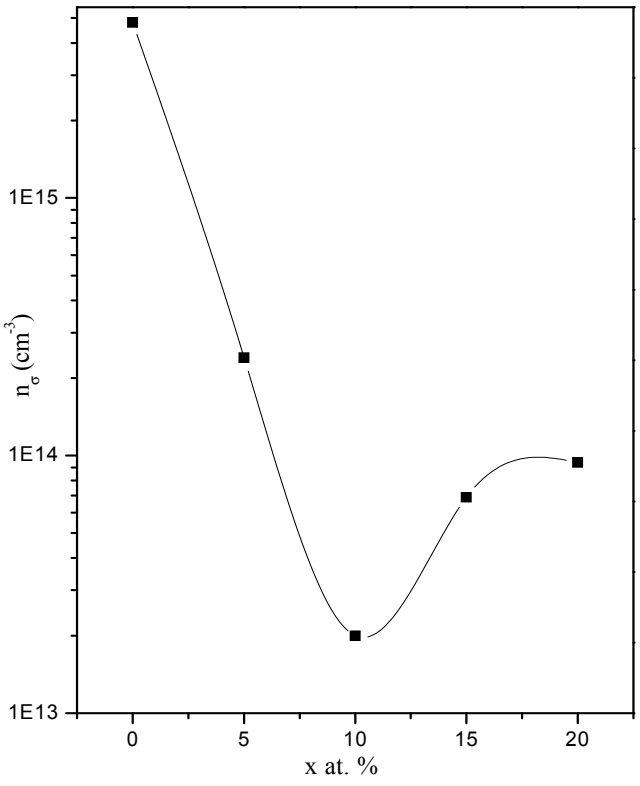

Figure 3.21 Variation of carrier charge density versus In content (x at. %).

table that at a particular intensity, photosensitivity increases from 5 to 217 up to 10 at. % of In addition to Ge-Se alloy and then subsequently decreases to 94 with further In addition. Similar trend with In addition have also been obtained in the optical measurement (sec. 3.1.3). The refractive index increases up to 10 at. % of In addition and above this In concentration, it shows irregular trend. Variation in σ_{ph}/σ_d with x at. % is shown in figure 3.20.

The charge carrier concentration (n_σ) for different samples is calculated using the equation [39,40]

$$n_\sigma = 2\left(\frac{2\pi m k_B T}{h^2}\right)^{\frac{3}{2}} \exp\left(\frac{-\Delta E_\sigma}{k_B T}\right) \tag{3.26}$$

where m is the mass of charge carrier and k_B is the Boltzmann's constant.

Using equation (3.26), free charge carrier concentration has been calculated for $Ge_{20}Se_{80-x}In_x$ thin films. The calculated values of n_σ are listed in table 3.3. Figure 3.21 shows the plot of n_σ vs. In concentration. It is clear from the figure that the value of n_σ decreases with the increase of In concentration up to 10 at. % and with further In addition to Ge-Se alloy it increases. The value of n_σ decreases after the addition of In (≤ 10 at. %) which indicates that the number of localized states decreases. Our optical studies also show increase in the optical gap and the refractive index (see table 3.3). Density of charge carriers increases on addition of In (> 10 at. %) which indicates an increase in the localized states. The presence of high concentration of localized states (> 10 at. %) in the band gap is responsible for the decrease in the value of E_g^{opt}. Due to this, the photosensitivity of $Ge_{20}Se_{80-x}In_x$ thin films first increases (≤ 10 at. %) and then further decreases (> 10 at. %) at a particular temperature and intensity.

3.3 Conclusion

Various parameters related to optical and electrical properties have been calculated for *a*-$Ge_{20}Se_{80-x}In_x$ (x = 0, 5, 10, 15, 20) thin films. The optical absorption is of non direct type and absorption coefficient is of the order of 10^4 cm^{-1}. n and k

for the thin films were calculated and found to decrease with the increase of wavelength. The optical parameters *viz.* E_g^{opt}, n_0, E_d and E_0 found to increase up to 10 at. % of In incorporation in Ge-Se system and then decrease with further addition of In. The change in optical parameters with In incorporation is explained on the basis of Mott and Davis model and change in average bond energy of the system. The dielectric constants and optical conductivity have also been determined from the optical parameters and found to decrease with the increase in wavelength. The study of dark and photoconductivity of $Ge_{20}Se_{80-x}In_x$ thin films as a function of temperature reveals that the conduction is through an activated process with single activation energy in the temperature range 303 to 375 K. ΔE_d increases up to 10 at. % of In addition and thereafter it decreases. The intensity dependence of photocurrent indicates the existence of bimolecular recombination in $Ge_{20}Se_{80-x}In_x$ thin films in which recombination rate of electrons is proportional to the number of holes. Charge carrier concentration (n_σ) decreases up to 10 at. % of In addition and then increases. Photosensitivity (σ_{ph}/σ_d) also shows maximum value at 10 at. % of In addition, indicating that the Ge-Se-In system becomes more rigid.

References

1. Lankhorst M H R, Ketelaars B W S M M and Wolters R A M 2005 *Nat. Mater*. **4** 347
2. Klude M, Alexe G, Kruse C, Passow T, Heinke H and Hommel D 2002 *Phys. Stat. Soli. b* **229** 935
3. Trnovcona V, Furar I and Lezal D 2007 *J. Non-Cryst. Solids* **353** 1311
4. Zakery A and Elliott S R 2003 *J. Non-Cryst. Solids* **330** 1
5. Aggarwal I D and Sanghera J S 2002 *J. Optoelectron. Adv. Mater.* **4** 665
6. Liu Q M, Gan F X, Zhao X J, Tanaka K, Narazaki A and Hirao K 2001 *Opt. Lett.* **26** 1347
7. Boolchand P, Georgiev D G and Goodman B 2001 *J. Optoelectron. Adv. Mater.* **3** 703
8. Goyal N, Zolanvari A and Tripathi S K 2001 *J. Mater. Sci.: Mater. Electr.* **12** 523
9. Marquez E, Wagner T, Gonzalez-Leal J M, Bernal A M, Prieto-Aleon R, Jimenez-Garay R and Ewen P J S 2000 *J. Non-Cryst. Solids* **274** 62
10. Ovshinsky S R 1976 *Structure and Excitation of Amorphous Solids* (New York: American Institute of Physics)
11. Fritzsche H 1976 *Structure and Excitation of Amorphous Solids* (New York: American Institute of Physics)
12. Khan Z H, Zulfiquar M, Hyas M, Husain M and Begum K S 2002 *Current Appl. Phys.* **2** 164
13. Borisova Z U 1981 *Glassy Semiconductors* (New York: Plenum Press)
14. Manificier J C, Gasiot J and Fillard J P 1976 *J. Phys. E: Sci. Instrum* **9** 1002
15. Swanepoel R 1983 *J. Phys. E : Sci. Instrum.* **16** 1214
16. Ambrico M, Smaldone D, Spezzacatenna C, Stagno V, Perna G and Capozzi V 1998 *Semicond. Sci. Technol.* **13** 1446
17. Tauc J 1970 *The optical properties of solids* (Amsterdam: North-Holland)
18. Urbach R 1953 *Phys. Rev.* **92** 1324
19. Al-Ani S K J, Al-Hassany I H O and Al-Dahan Z T 1995 *J. Mater. Sci*. **30** 3720

20. Mott N F and Davis E A 1979 *Electronic Processes in Non-Crystalline Materials* (Oxford: Clarendon Press)
21. Abdelghany A, Elsayed S N and Mousa N H 1996 *Vacuum* **47** 243
22. Morigaki K 1999 *Physics of Amorphous Semiconductors* (London: Imperial College Press)
23. Andriesh A M and Iovu M S 2003 *Moldavian J. of Physical Sciences* **2** 3
24. Pankove J I 1975 *Optical Processes in Semiconductors* (New York: Dover)
25. Wemple S H and DiDomenico M 1971 *Phys. Rev. B* **3** 1338
26. Wemple S H 1973 *Phys. Rev. B* **7** 3767
27. Tanaka K 1980 *Thin Solid Films* **66** 271
28. Philips J C 1981 *J. Non-Cryst. Solids* **43** 37
29. El-Ocker M M, El-Fouly M H, Fayek S A, Talaat H and Amin G A M 1995 *Appl. Phys. A* **60** 233
30. Fayek S A, El-Ocker M M, Fouad S S, El-Fouly M H and Amin G A M 1995 *J. Phys. D: Appl. Phys.* **28** 2150
31. Ovshinsky S R and Alder D 1978 *Contemp. Phys.* **19** 109
32. Pattanaik A K and Srinivasan A 2003 *J.Optoelectron. Adv. Mater.* **5** 1161
33. Thakur A, Sharma V, Chandel P S, Goyal N, Saini G S S and Tripathi S K 2006 *J. Mater. Sci.* **41** 2327
34. Murugavel S and Asokan S 2002 *J. Non-Cryst. Solids* **303** 296
35. Dahshan A, Amer H H, Moharam A H and Othman A A 2006 *Thin Solid Films* **513** 369
36. Popescu M 2000 *Non Crystalline Chalcogenides* (Dordrecht: Kluwer Academic)
37. Rose A 1963 *Concepts in Photoconductivity and Allied Problems* (New York: Interscience)
38. Shimakawa K 1985 *J. Non-Cryst. Solids* **77** 1253
39. El-Korashy A, El-Zahed H, Zayed H A and Kenawy M A 1995 *Solid State Commun.* **95** 335
40. Sharma V, Thakur A, Goyal N, Saini G S S and Tripathi S K 2005 *Semicond. Sci. Technol.* **20** 103

CHAPTER IV*

Effect of Bi on Optical and Electrical Properties of *a*-Ge-Se-In Thin Films

*
- **Ishu Sharma**, S. K. Tripathi and P. B. Barman, "*Effect of Bi Addition on the Optical Behavior of Thin Films of a-Ge-Se-In Glassy Alloys*" **Applied Surface Science** (2008) [Communicated].

- **Ishu Sharma**, A. Kumar, S. K. Tripathi and P. B. Barman, "*Effect of Bi Addition on the electrical properties of a-Ge-Se-In Thin Films*" **Journal of Physics D: Applied Physics** (2008) [Communicated].

4.0 Introduction

Optical and electrical study of *a*-$Ge_{20}Se_{80-x}In_x$ (x = 0, 5, 10, 15, 20) thin films have already been discussed in chapter III. The non linear and photosensitive properties together offer numerous applications to a number of integrated optical functions. Since $Ge_{20}Se_{70}In_{10}$ system shows maximum value of optical band gap and photosensitivity, so in continuation with this, the effect of Bi addition to *a*-$Ge_{20}Se_{70}In_{10}$ system has been considered for optical and electrical study. Addition of Bi to Ge-Se system increases the chemical durability and broadening the IR transparency range *i.e.* multiphonon absorption edge gets extended towards NIR region [1-3]. The replacement of Se with Bi in Ge-Se host matrix leads to the decrease in optical band gap [4]. Optical constants of $Ge_{25}Sb_{15-x}Bi_xS_{60}$ $(0 \le x \le 15)$ have been studied [5] and were found that with the increase of Bi content, the optical band gap decreases and refractive index increases. Earlier experiments have shown that the addition of Bi in Ge-Se system brings down the optical band gap upto 1.2 eV for *n*-type conducting samples, resulting in an enhancement of photoconduction [6,7]. Electrical and optical properties of *n*-type semiconducting chalcogenide glasses in the system Ge-Se-Bi have been studied by Tohge *et al*. [8]. They found that 13 at. % is the maximum limit for the incorporation of Bi content in glasses containing 20 at. % of Ge. In this chapter the effect of Bi addition on the optical and electrical properties of $Ge_{20}Se_{70-x}In_{10}Bi_x$ (x = 2, 4, 6, 8, 10) system have been investigated.

4.1 Optical Properties of Ge-Se-In-Bi Thin Films

In this section optical band gap (E_g^{opt}), absorption coefficient (α), refractive index (n) and extinction coefficient (k) for $Ge_{20}Se_{70-x}In_{10}Bi_x$ (x = 2, 4, 6, 8, 10) thin films have been determined by analyzing transmission spectrum in the wavelength range from $400-1800$ nm. The dispersion of refractive index was analyzed with Wemple - DiDomenico single oscillator model. The dielectric constants and optical conductivity were also analyzed using n, k and α.

4.1.1 Experimental Details

Bulk samples of the $Ge_{20}Se_{70-x}In_{10}Bi_x$ (x = 2, 4, 6, 8, 10) chalcogenide system were prepared using melt quench technique. Thin films of the alloys were prepared by thermal evaporation technique [Vacuum coating unit HINDHIVAC 12A4D Model] at room temperature and base pressure of $\sim 10^{-4}$ Pa using a molybdenum boat. The thickness of the deposited thin films has been measured by thickness monitor (DTM-101). Amorphous nature of the bulk samples and thin films was confirmed by XRD technique. No prominent peak was observed in the bulk as well as in thin films. The normal incidence transmission spectra of $Ge_{20}Se_{70-x}In_{10}Bi_x$ thin films were obtained by a double beam ultraviolet-visible-near infrared spectrophotometer [Perkin Elmer Lambda 750], in the transmission range 400-1800 nm. Repeated characterizations on the thin films of same composition (grown at different times), were carried out and the results only varied within ± 1-2 %. All optical measurements were performed at room temperature (300 K).

4.1.2 Results and Discussion

Figures 4.1 and 4.2 show the optical transmission spectra of $Ge_{20}Se_{70-x}In_{10}Bi_x$ thin films for (x = 2, 4) and (x = 6, 8, 10) respectively. A clear cut red shift is observed in the interference free region of the spectra with the increase of Bi content. The values of the thickness (d), refractive index (n), extinction coefficient (k) and absorption coefficient (α) have been determined using the envelope method as discussed in chapter III.

The thickness of films calculated from the transmission spectrum is reported in table 4.1. It is in consistent with the thickness (d^*) measured directly from the thickness monitor while depositing the films. The difference between the mechanically measured and the optically-calculated values only varied within 2-3 % which shows the precision of reported results.

The variation of refractive index (n) and extinction coefficient (k) with wavelength is shown in figures 4.3 and 4.4 respectively. From the figures 4.3 and 4.4, it is clear that both refractive index and extinction coefficient decrease with the increase of wavelength for all thin films.

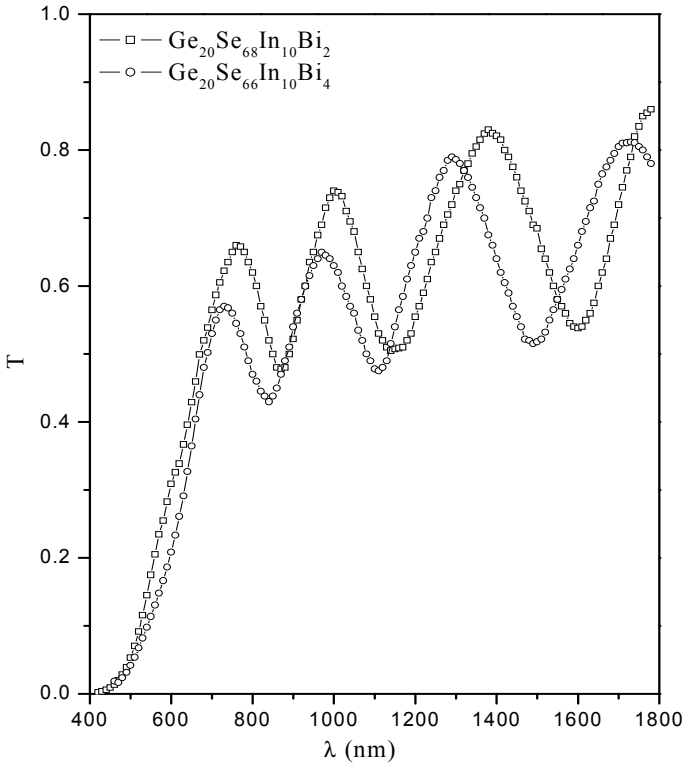

Figure 4.1 Plot of transmission versus wavelength (nm) for $Ge_{20}Se_{70-x}In_{10}Bi_x$ (x = 2, 4) thin films.

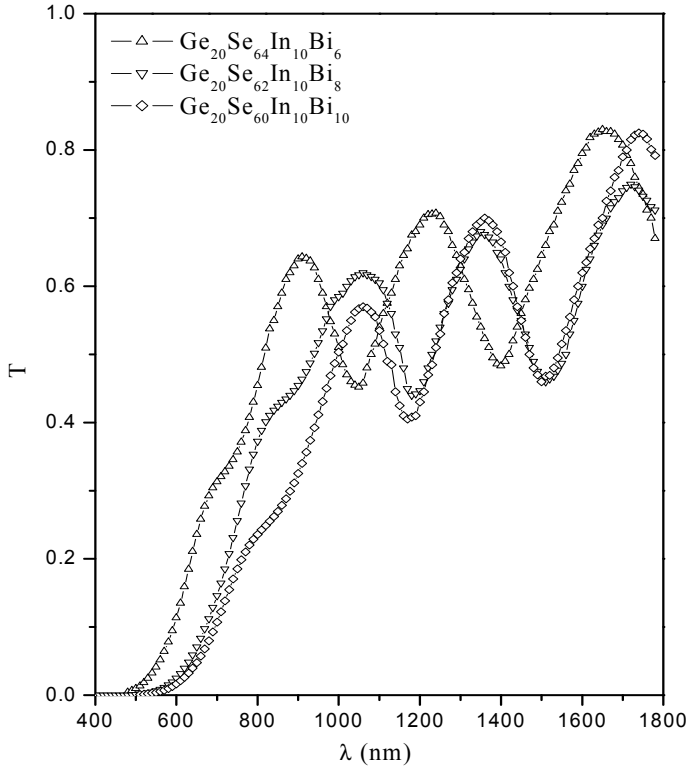

Figure 4.2 Plot of transmission versus wavelength (nm) for $Ge_{20}Se_{70-x}In_{10}Bi_x$ (x = 6, 8, 10) thin films.

This decrease in the value of the refractive index with wavelength attributes to the significant normal dispersion behavior of the material. Figure 4.3 also indicates that with the increase of Bi content, refractive index increases for entire wavelength range under investigation. This high refractive index value is advantageous for strong optical field confinement which allows small waveguide bend radii (leading to compact circuit designs) and enhanced optical intensities (for efficient non-linear interactions). The increase in the refractive index with the increase in Bi content at 1000 nm is reported in table 4.1 and can be attributed to the increase in valence of current carriers and also presumable due to the increased polarizability [9] associated with the larger Bi atom. Larger the atomic radius of the atom, larger will be its polarizability and consequently, according to Lorentz - Lorenz relation [10],

$$\frac{n^2-1}{n^2+2}=\frac{1}{3\varepsilon_0}\sum_i N_i\alpha_{pi} \tag{4.1}$$

(where ε_0 is the vacuum permittivity, N_i is the number of polarizable units of type *i* per unit volume with polarizability α_{pi}) larger will be the refractive index. The atomic radius of Se is 1.16 A^o and Bi is 1.46 A^o. On the other hand, a clear red-shift of the optical absorption edge is observed in figures 4.1 and 4.2, with increasing Bi content. It is stressed that, following the fundamental Kramers – Kronig relationships for n and k, the red-shift in the absorption spectrum must necessarily gives an increased refractive index value. It is worth to quote here the fundamental relationship, $n_0-1=\left(1/2\pi^2\right)\int_0^\infty \alpha\, d\lambda$ as experimentally obtained [9] which allows checking the consistency of the values of refractive index. Lezal [11] has also correlated the refractive index with transparency range. As the transmission range increases, corresponding to it refractive index also increases. This increase in the refractive index with increase of Bi content may be ascribed to the addition of heavier Bi (density = 9.8 g/cc at 20 ^oC) atoms to Se (density = 4.79 g/cc at 20 ^oC) matrix leading to make the system more compact. It is also clearly observed that the extinction coefficient (k) increases significantly with increasing Bi content.

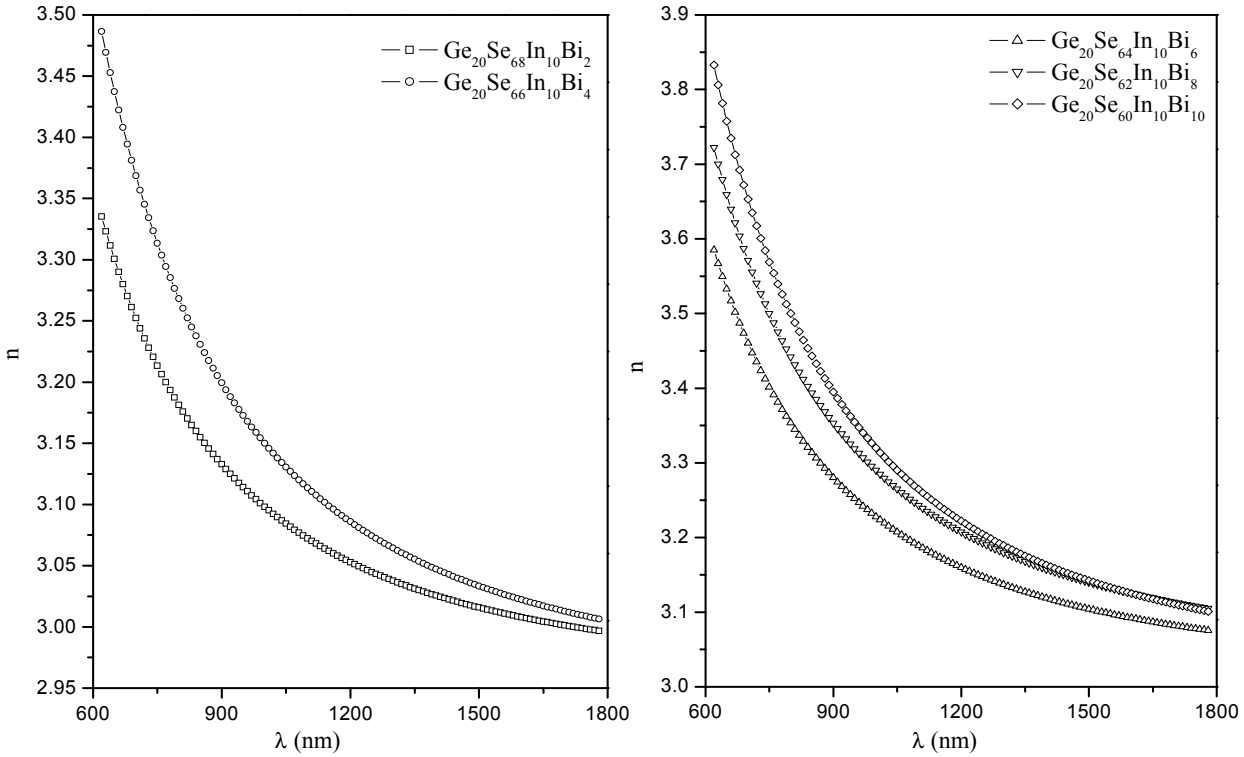

Figure 4.3 Plot of refractive index versus λ (nm) for $Ge_{20}Se_{70-x}In_{10}Bi_x$ (x = 2, 4, 6, 8, 10) thin films.

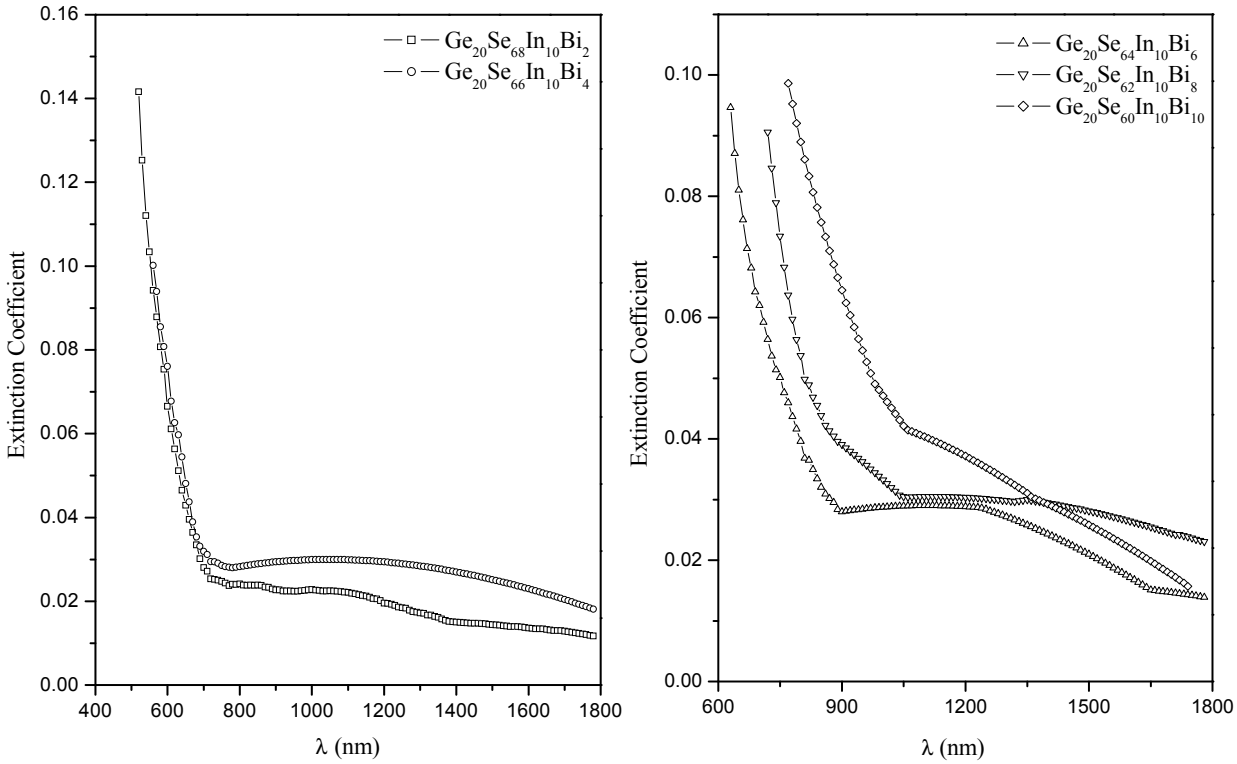

Figure 4.4 Plot of extinction coefficient versus λ (nm) for $Ge_{20}Se_{70-x}In_{10}Bi_x$ (x = 2, 4, 6, 8, 10) thin films.

The spectral dependence (dispersion) of refractive index values for each sample has been fitted to Wemple - DiDomenico single-oscillator model as given in equation 3.22. Plotting refractive index factors $(n^2-1)^{-1}$ against $(h\nu)^2$, for all films, given in figure 4.5, allows us to determine the oscillator parameters by linear fits to the larger wavelength data. The calculated values of E_0 and E_d from the slope and intercept of above plots for all the compositions are given in table 4.1. E_0 is related to bond energy of the different chemical bonds present in the material. Thus the decrease observed in the values of E_0 with the addition of Bi content for the films under study, is mainly presumably due to the lower bond energies of Bi-Se (40.7 kcal/mol) and Bi-Bi (25.0 kcal/mol) as compared to Ge-Se (49.1 kcal/mol), In-Se (48.2 kcal/mol) and Se-Se (44 kcal/mol) bonds. According to Tanaka [12], $E_0 \approx 2\ E_g^{opt}$, which is quite reasonably supported by our results also.

The values of static refractive indices n_0 for $Ge_{20}Se_{70-x}In_{10}Bi_x$ thin films have been calculated from WDD dispersion parameters E_0 and E_d by using equation 3.23. The values of n_0 and high frequency dielectric constant $\varepsilon_\infty = n_0^2$ are given in table 4.1. It is clear from the table that, increase in Bi content clearly contributes to the increase of the optical parameter n_0, as it is expected, taking into account the impact of its relatively high covalent radius of Bi.

The absorption coefficient (α) of $Ge_{20}Se_{70-x}In_{10}Bi_x$ thin films can be calculated using the well-known relation given by equation (3.10). The variation of absorption coefficient with photon energy for $Ge_{20}Se_{70-x}In_{10}Bi_x$ thin films is shown in figure 4.6 and 4.7 for (x = 2, 4) and (x = 6, 8, 10) respectively. The optical band gap (E_g^{opt}), has been estimated according to generally accepted 'non-direct transition' model for amorphous semiconductor from absorption coefficient data as a function of wavelength by using Tauc relation [13] (equation 3.13). This relationship assumes that the densities of electron states in the valence and conduction bands near the band gap have a parabolic distribution and the matrix elements for the interband transitions associated with the photon absorption are equal for all the transitions.

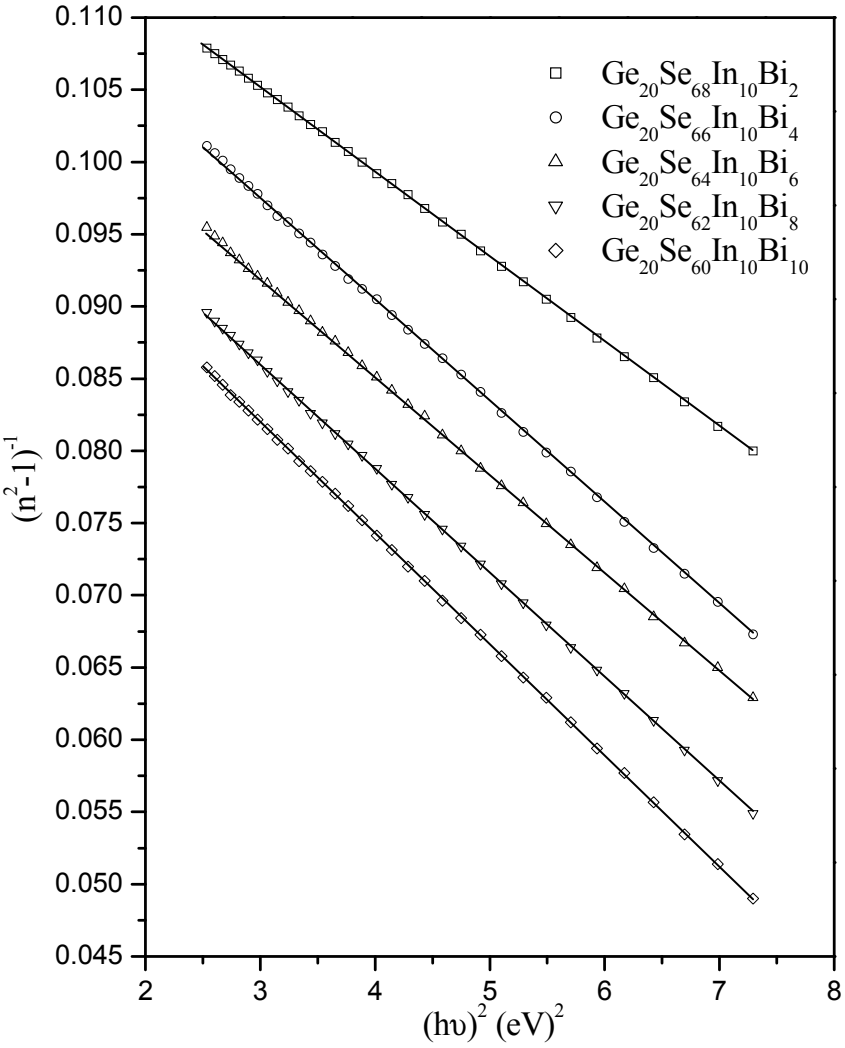

Figure 4.5 Plot of $(n^2-1)^{-1}$ versus $(h\nu)^2$ for $Ge_{20}Se_{70-x}In_{10}Bi_x$ (x = 2, 4, 6, 8, 10) thin films.

Table 4.1 Values of thickness (d^*) and (d), refractive index (n), extinction coefficient (k), dispersion energy (E_d), oscillator strength (E_0) at 1000 nm and static refractive index (n_0) for $Ge_{20}Se_{70-x}In_{10}Bi_x$ (x = 2, 4, 6, 8, 10) thin films.

x	$d^* \pm 25$ (nm)	d (nm)	n	k	E_d (eV)	E_0 (eV)	n_0
2	700	679	3.18	0.0242	35.78	4.44	3.01
4	700	723	3.26	0.0283	32.76	3.96	3.04
6	700	692	3.35	0.0396	34.21	3.92	3.12
8	700	707	3.44	0.0537	33.67	3.72	3.17
10	700	695	3.50	0.0889	32.69	3.54	3.19

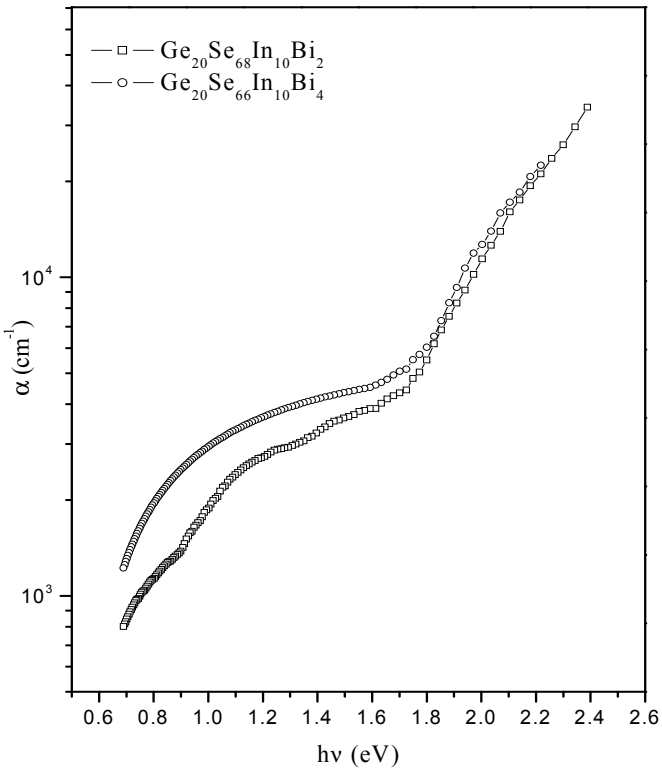

Figure 4.6 Plot of α versus $h\nu$ for $Ge_{20}Se_{70-x}In_{10}Bi_x$ (x = 2, 4) thin films.

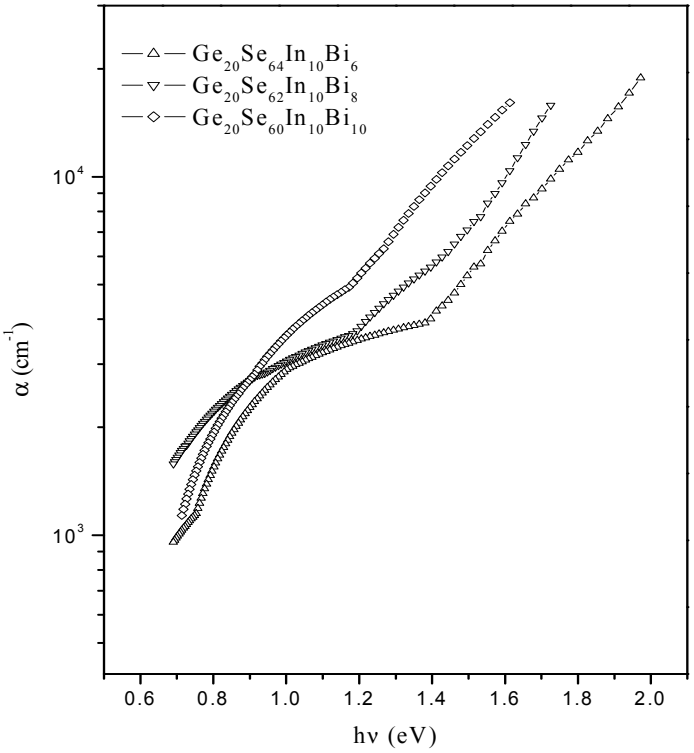

Figure 4.7 Plot of α versus $h\nu$ for $Ge_{20}Se_{70-x}In_{10}Bi_x$ (x = 6, 8, 10) thin films.

Figure 4.8 shows the variation of $(\alpha h\nu)^{1/2}$ with $h\nu$. Optical band gap E_g^{opt} can be determined by the extrapolation of best fit line between $(\alpha h\nu)^{1/2}$ and $h\nu$ to intercept the $h\nu$ axis $(\alpha = 0)$ for $Ge_{20}Se_{70-x}In_{10}Bi_x$ system. Variation of optical band gap with different Bi concentration is given in table 4.2. It is clear from the table that with the incorporation of Bi content, optical band decreases from 1.63 to 0.87 eV. Bi impurities induce structural modifications in the parent matrix which are clearly reflected in the optical band gap values. It is also suggested by Kitao *et al.* [14], that the decrease in the band-gap is caused by an alloying effect, namely a compositional change in the host material itself. This effect is due to the change in bond angles and/or bond lengths. Bi addition to Ge-Se system gives rise to the reduction in the width of two broader transitions. This is natural if we recall that the broader transitions are assigned to random VAPs (D^+ and D^-) which are more likely to get influenced by the external dopants unlike IVAPs (non-random D^+ and D^-). The lowering of energy of transitions associated with random VAPs might be due to higher atomic radii of Bi atoms added which can push the corresponding energy levels away from the band edges towards the Fermi level. The lowering of band gap with the Bi addition to Ge-Se-In matrix can also be explained in accordance with Mott and Davis model [15] which states that the width of the localized states near the mobility edges depends on the degrees of disorder and the defects present in the amorphous structure. The Bi incorporation to Ge-Se-In matrix thus tends to increase monotonically the degree of disorder in the glassy structure. The addition of Bi leads to Bi-Se bonding which introduces the large number of defects in the system [16]. Moreover this reduction in optical band gap of the system is also reflected in the reduction in average bond energy with the increase in Bi content.

The dielectric constant of *a*-$Ge_{20}Se_{70-x}In_{10}Bi_x$ thin films can be calculated with the help of refractive index (n) and extinction coefficient (k) [17]. Real dielectric constant can be calculated from the relation $\varepsilon_r = n^2 - k^2$ and the imaginary dielectric constant can be calculated from the following relation $\varepsilon_i = 2nk$. For $Ge_{20}Se_{70-x}In_{10}Bi_x$ thin films the variation of both real and imaginary dielectric constants (ε_r and ε_i) with

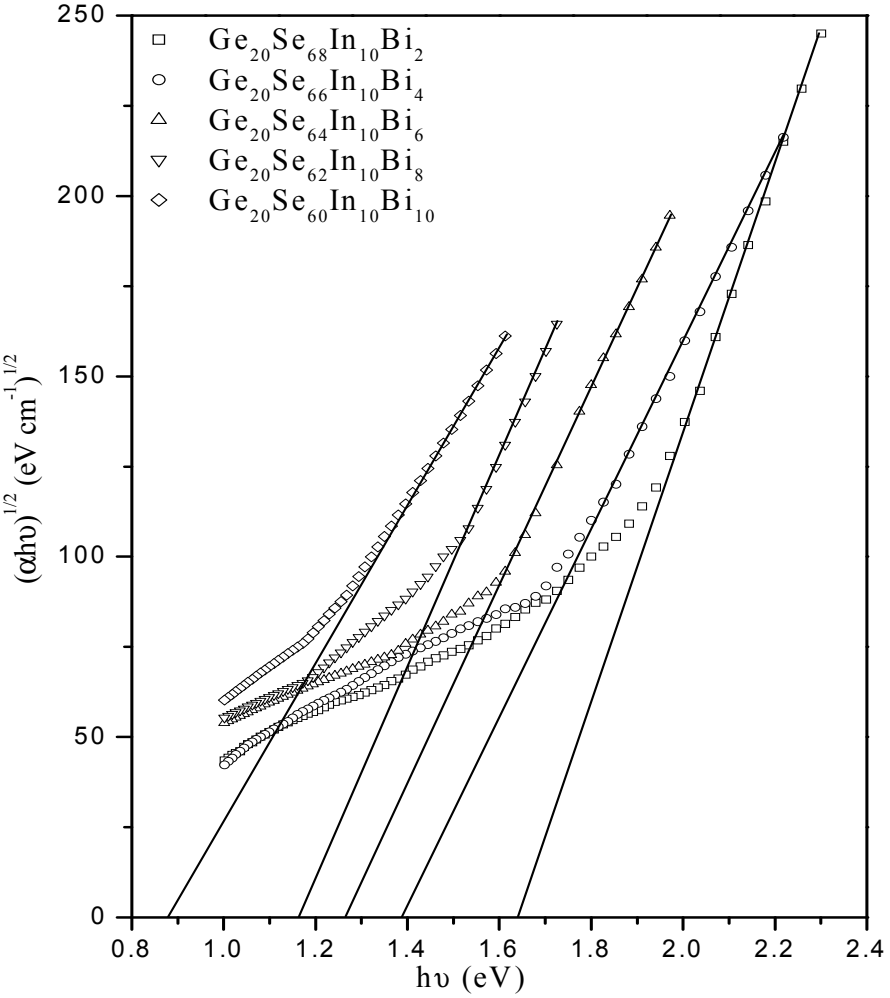

Figure 4.8 Plot of $(\alpha h\nu)^{1/2}$ versus $h\nu$ for $Ge_{20}Se_{70-x}In_{10}Bi_x$ (x = 2, 4, 6, 8, 10) thin films.

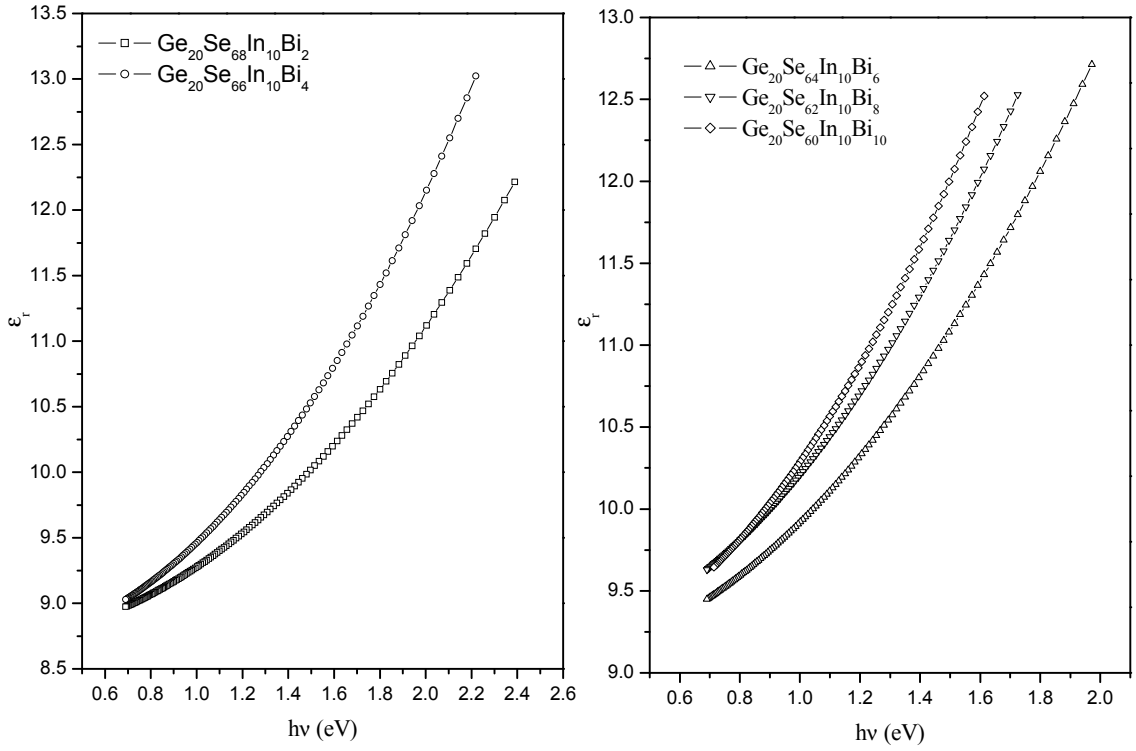

Figure 4.9 Plot of real part of dielectric constant (ε_r) versus $h\nu$ for $Ge_{20}Se_{70-x}In_{10}Bi_x$ (x = 2, 4, 6, 8, 10) thin films.

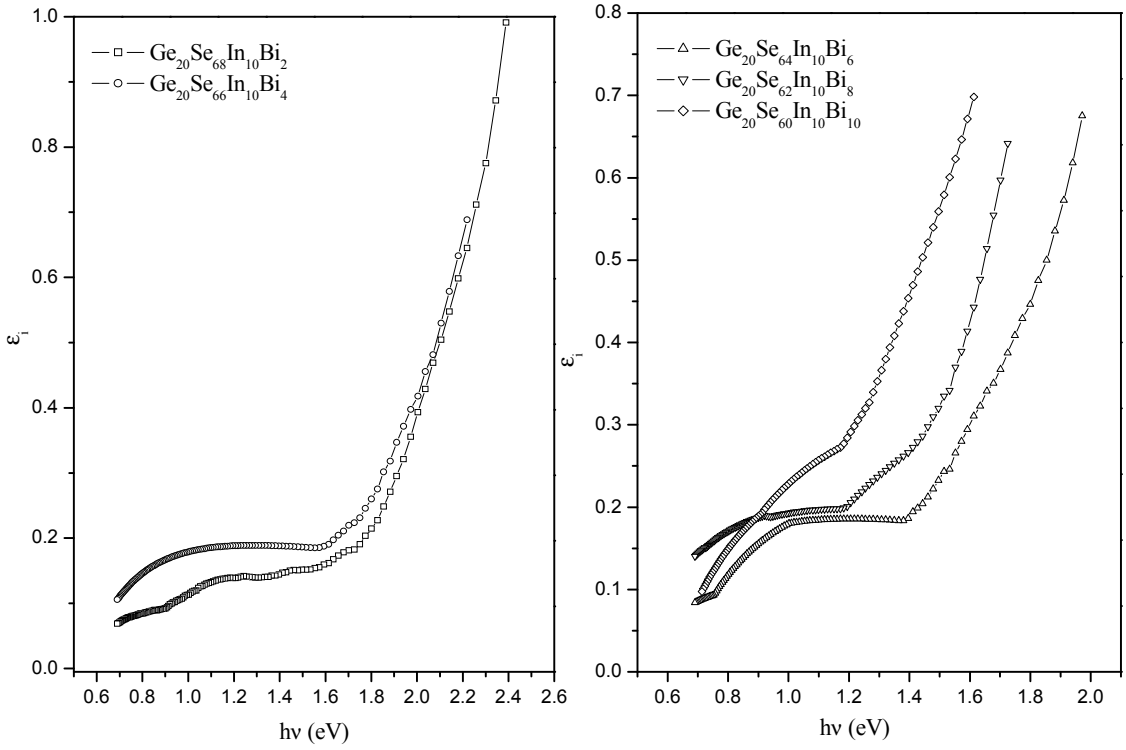

Figure 4.10 Plot of imaginary part of dielectric constant (ε_i) versus $h\nu$ for $Ge_{20}Se_{70-x}In_{10}Bi_x$ (x = 2, 4, 6, 8, 10) thin films.

Table 4.2 Values of absorption coefficient (α), optical band gap (E_g^{opt}), real part of dielectric constant (ε_r), imaginary part of dielectric constant (ε_i), and optical conductivity (σ) are given at 1000 nm for $Ge_{20}Se_{70-x}In_{10}Bi_x$ (x = 2, 4, 6, 8, 10) thin films.

x	α (cm^{-1})	E_g^{opt} (eV)	ε_r	ε_i	σ (s^{-1}) x 10^{13}
2	3801.5	1.63	10.12	0.153	2.88
4	4447.4	1.39	10.68	0.185	3.52
6	6222.4	1.27	11.24	0.265	4.97
8	8443.3	1.16	11.84	0.369	6.93
10	13983.1	0.87	12.24	0.623	11.6

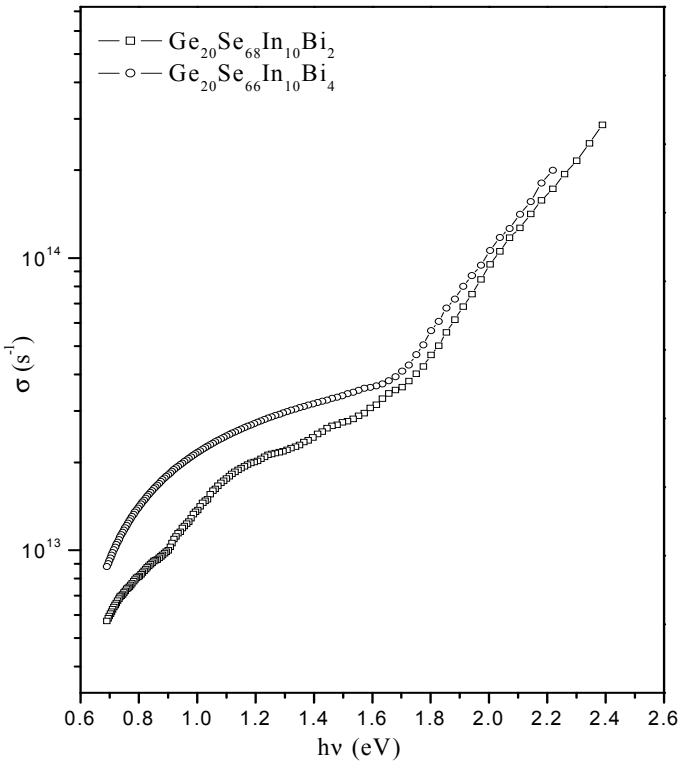

Figure 4.11 Plot of optical conductivity (σ) versus $h\nu$ for $Ge_{20}Se_{70-x}In_{10}Bi_x$ (x = 2, 4) thin films.

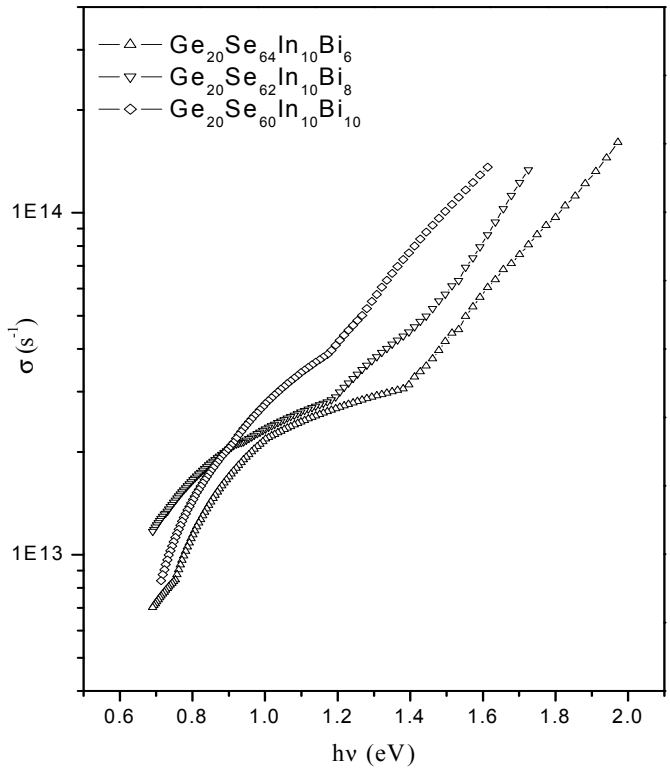

Figure 4.12 Plot of optical conductivity (σ) versus $h\nu$ for $Ge_{20}Se_{70-x}In_{10}Bi_x$ (x = 6, 8, 10) thin films.

energy, given in figures 4.9 and 4.10, follows the same trend as that of refractive index and extinction coefficient. The values of ε_r and ε_i for all compositions at λ = 1000 nm are tabulated in table 4.2. Optical response is most conveniently studied in terms of optical conductivity. Figure 4.11 and 4.12 shows the frequency (energy) dependent optical conductivity 'σ' obtained from absorption coefficient (α), velocity of light (c) and refractive index (n) and is given by the relation [18] *i.e.* $\sigma = \alpha nc/4\pi$. It has the dimensions of frequency which are valid only in Gaussian system of units. σ is almost proportional to square of frequency/energy which indicates that the system may be ascribed by a single relaxation time [19]. The optical conductivity directly depends on the absorption coefficient and refractive index and found to increase sharply for higher energy values due to large absorption coefficient and refractive index for these values. With the increase of Bi content optical conductivity increases and is tabulated in table 4.2.

4.2 Electrical Properties of Ge-Se-In-Bi Thin Films

The optical band gap slightly decreases in contrast with decrease of activation energy. It is well documented that carrier type reversal occurs after fairly large concentration of Bi (x ≥ 7 at. %). Recently, the influence of metal impurities on transient characteristics of photoconductivity and optical absorption was studied by Iovu *et al*. [20]. These impurities are supposed to create new defect states and/or change the short- and medium-range order in the film. It has been known for a long time that chalcogenide glasses are *p*-type semiconductors. In these materials, the valence band is constituted by the chalcogen lone-pair orbitals [21,22]. The effect of structural disorder is less on the lone pair band compared to that on the antibonding orbitals *i.e.* conduction band. Therefore, the range of localized tail states at the valence-band edge is smaller in comparison to the localized states at the conduction-band edge. As a consequence, the number of electrons excited above the conduction-band mobility edge is less than the number of holes excited below the valence-band mobility edge and the chalcogenide glasses behave as *p*-type semiconductors [23]. Chalcogenide glasses also contain positively and negatively charged defect states, known as valence-alternation pairs (VAPs) [24]. Amorphous chalcogenides are

generally insensitive to doping, because of the pinning of the Fermi level at mid gap by the valence-alternation pairs [25]. However, it has been realized by Mott [26] that charged additives could change the ratio of valence-alternation pairs to such an extent that the Fermi energy could become unpinned. Metallic additives such as Bi and Pb in chalcogenide glasses enter the network as charged species, altering the concentration of valence-alternation pairs [24]. When the concentration of charged additives exceeds that of valence-alternation pairs, the chalcogenide glasses can exhibit carrier-type reversal. $p \rightarrow n$ transition has been observed in Ge-Se and In-Se glasses with the addition of Bi and Pb [27,28]. Since Bi addition to Ge-Se system increases the chemical durability, the replacement of Se with Bi in Ge-Se host matrix leads to the decrease in the activation energy and also exhibits electronic switching [29].

In present section photoconductive properties of $Ge_{20}Se_{70-x}In_{10}Bi_x$ system (x = 2, 4, 6, 8, 10) are measured in detail which is very important from the basic physics as well as application point of view. The steady state and transient photoconductivity measurements on thermally evaporated $Ge_{20}Se_{70-x}In_{10}Bi_x$ thin films have been done. Temperature (300 – 360 K) and intensity (3 - 1035 Lux) dependent steady state photoconductivity measurements have been carried out for all compositions. Rise and decay of photocurrent has also been measured at room temperature at 1035 Lux intensity for all compositions.

4.2.1 Experimental Details

Thin films of the glassy alloys have been prepared by vacuum evaporation technique, keeping the substrates at room temperature with a base pressure ~ 10^{-4} Pa. Amorphous nature of films was confirmed by X-ray diffraction technique as no sharp peak was observed. Pre-deposited thick indium electrodes on well-degassed Corning 7059 glass substrates have been used for the electrical contacts. A planar geometry of the film (length ~ 2.4 cm; electrode gap ~ 1×10^{-2} cm) with thickness of the film is ~ 6000 A^{o} is used for the electrical measurements. Experimental details for electrical measurements are described in previous chapters.

4.2.2 Results and Discussion

4.2.2.1 Temperature Dependent Electrical Conductivity

The temperature dependent dark conductivity (σ_d) measurements for $Ge_{20}Se_{70-x}In_{10}Bi_x$ thin films are shown in figure 4.13. The plots of $\ln\sigma_d$ vs. $1000/T$ are found to be straight line indicating that conduction is through an activated process having single activation energy in the temperature range 303 – 360 K. In most of the chalcogenide glasses σ_d can be expressed by the Arrhenius relation, $\sigma_d = \sigma_0 \exp(-\Delta E_d / k_B T)$. The values of dark activation energy (ΔE_d) were estimated from slope of $\ln\sigma_d$ vs. $1000/T$ curves and are plotted as a function of *x* in figure 4.14. The values of ΔE_d and σ_d are also given in table 4.3 along with the pre exponential factor (σ_0). The values of ΔE_d were found to decrease with the increase in Bi content. The compositional dependence of dark conductivity at room temperature is shown in figure 4.15. It is interesting to see from the figure that with the substitution of Bi to Ge-Se-In alloys (replacing Se), there is an appreciable increase in electrical conductivity at x ≥ 8 at. %. However, without thermoelectric power measurements it is difficult to assess this abrupt enhancement in conductivity for x ≥ 8 at. % of Bi. This increase in conductivity may be attributed to current due to electrons only. It is observed that binding energy of the studied compositions decreases with the increase of Bi content which is presumably due to lower bond energies of Bi-Se (40.7 kcal/mol) and Bi-Bi (25.0 kcal/mol) as compared to Ge-Se (49.1 kcal/mol), In-Se (48.2 kcal/mol) and Se-Se (44 kcal/mol) bonds. This explains the obtained increase of σ_d at 300 K and consequent decrease of ΔE_d with increase in Bi content. With the addition of Bi, there is an increase in the ionic bonds (Bi-Se). Moreover the larger polarizability of dopants helps the formation of partially ionic bonds with the chalcogen likely and also accounts for the increase in the conductivity. The sharp change in the conductivity at x ≥ 8 is linked with the discontinuity in the activation energy. This sudden decrease in activation energy can be understood by considering the effect of charged impurities on the defect density and carrier concentration. According to Mott and Davis [15], increase in the density of localized states leads to the formation of compositions with higher degree of disorder.

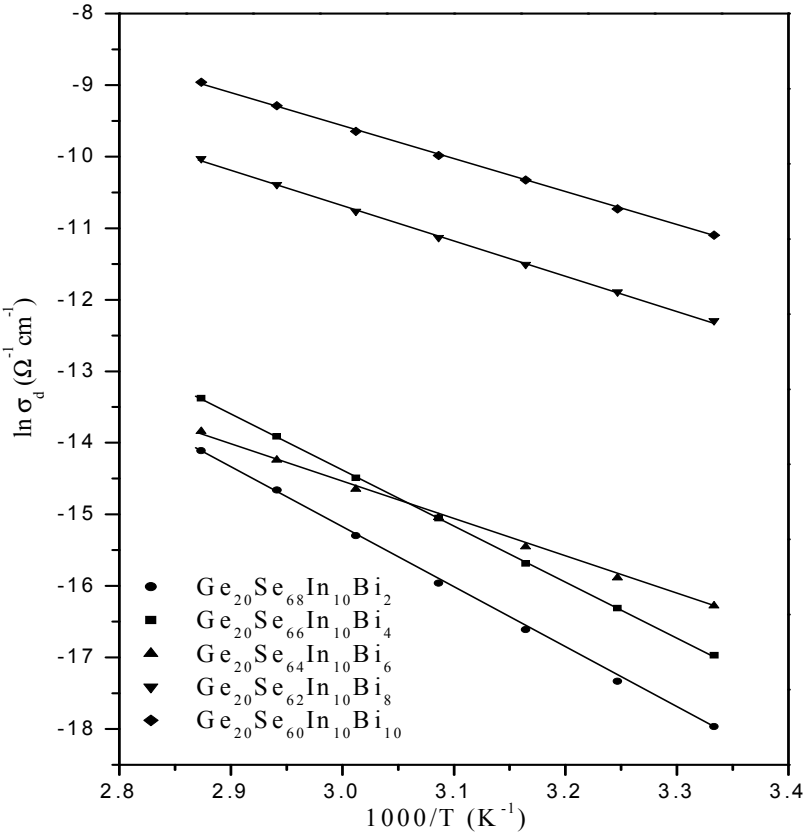

Figure 4.13 Temperature dependence of dark conductivity of $Ge_{20}Se_{70-x}In_{10}Bi_x$ thin films.

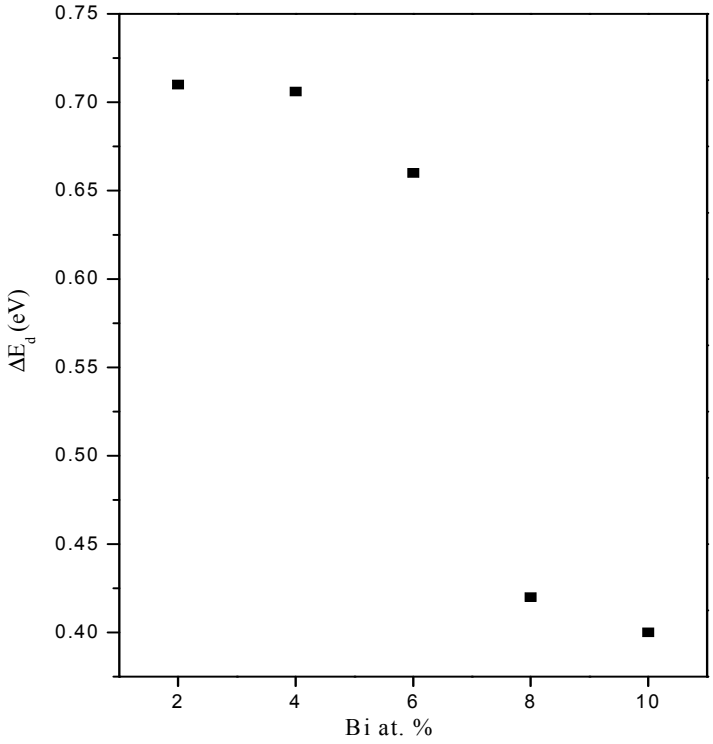

Figure 4.14 Variations of ΔE_d with Bi at. %.

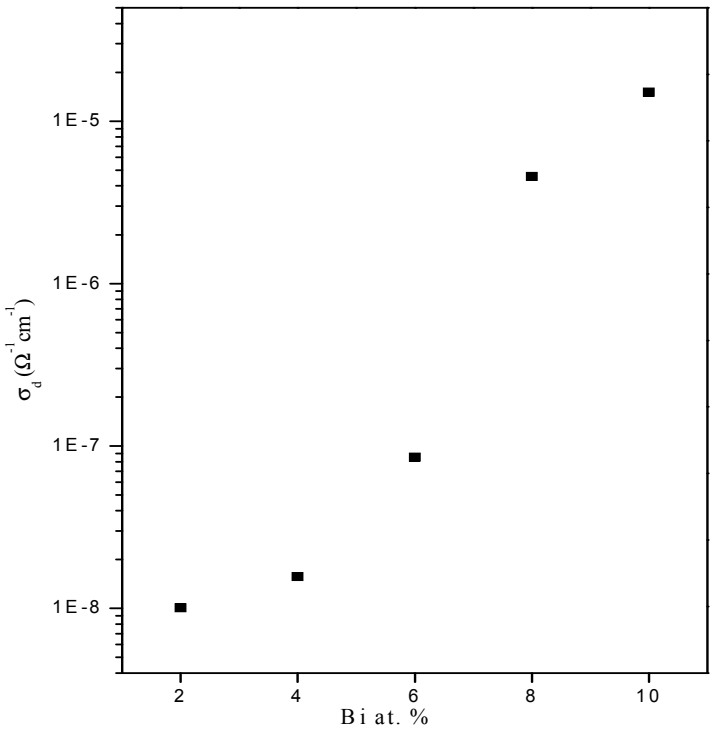

Figure 4.15 Variations of σ_d with Bi at. %.

Table 4.3 The dc dark conductivity (σ_d), the pre-exponential factor (σ_0), the activation energy for dc conduction (ΔE_d), photoconductivity (σ_{ph}), the activation energy of photoconduction (ΔE_{ph}) and optical band gap (E_g^{opt}) for $Ge_{20}Se_{70-x}In_{10}Bi_x$ (x = 2, 4, 6, 8, 10) thin films at 300 K.

x	σ_d ($\Omega^{-1}cm^{-1}$)	σ_0 ($\Omega^{-1}cm^{-1}$)	ΔE_d (eV)	σ_{ph} ($\Omega^{-1}cm^{-1}$)	ΔE_{ph} (eV)	E_g^{opt} (eV)
2	1.01×10^{-8}	8.3×10^{3}	0.71	3.14×10^{-7}	0.32	1.63
4	1.57×10^{-8}	11.1×10^{3}	0.706	2.53×10^{-7}	0.24	1.39
6	8.52×10^{-8}	10.2×10^{3}	0.66	1.09×10^{-7}	0.26	1.27
8	4.57×10^{-6}	51.20	0.42	4.34×10^{-6}	0.18	1.16
10	1.51×10^{-5}	78.11	0.40	6.71×10^{-6}	0.07	0.87

The variation of dc parameters with Bi for the investigated compositions may be explained by assuming that Bi atoms act as impurity centers (gives rise to some non-radiative defect centers) in the mobility gap. This induces structural changes in the network which may disturb the balance of the charged defects and consequently change the electric conduction. In such a situation the distribution and density of localized states are modified and even some new trap states can be created into the mobility gap [30]. Addition of Bi brings about a reduction in the relative concentration of D^+ as compared to D^- defects. This imbalance accompanied by contribution of extra electrons brings about dominant electron conduction in Bi doped glasses.

Variation of steady state photoconductivity (σ_{ph}) of $Ge_{20}Se_{70-x}In_{10}Bi_x$ thin films with temperature (*i.e.* σ_{ph} vs. 1000/*T*) at a particular intensity (1035 Lux) is shown in figure 4.16. The values of ΔE_{ph} are calculated from the slope of the curves of figure 4.16 and are given in table 4.3 along with the values of σ_{ph}. It is clear from the figure that the photoconductivity is an activated process. The value of activation energy (ΔE_{ph}) for photoconduction also follows the same trend, with incorporation of Bi, as that of ΔE_d for all samples.

Photosensitivity is an important parameter for characterizing a photoconductor from optoelectronic device point of view. This is defined by the product of μ (free carrier mobility) and τ (free carrier life time or recombination time). The values of photosensitivity (σ_{ph}/σ_d) for $Ge_{20}Se_{70-x}In_{10}Bi_x$ thin films at ambient temperature (300 K) and at intensity 1035 Lux are calculated and inserted in table 4.4. The values of photosensitivity are plotted in figure 4.17 against Bi content. It is clear from the table that at a particular intensity, photosensitivity decreases from 31 to 0.44 with the addition of Bi to the glassy thin films. So, this decrease of photosensitivity may be attributed to the formation of more number of defect centers with increase of disorder in the system.

Free charge carrier concentration has been calculated for $Ge_{20}Se_{70-x}In_{10}Bi_x$ thin films. The calculated values of n_σ are also plotted in figure 4.18 and listed in table 4.4.

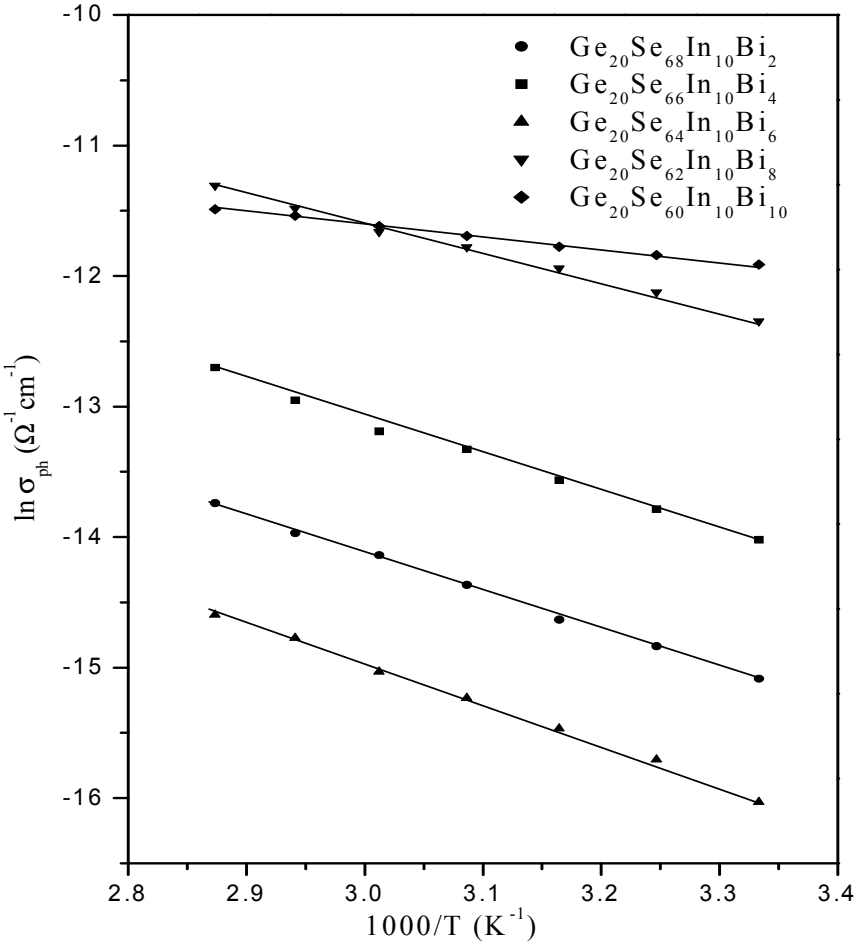

Figure 4.16 Temperature dependence of photo conductivity of $Ge_{20}Se_{70-x}In_{10}Bi_x$ (x = 2, 4, 6, 8, 10) thin films.

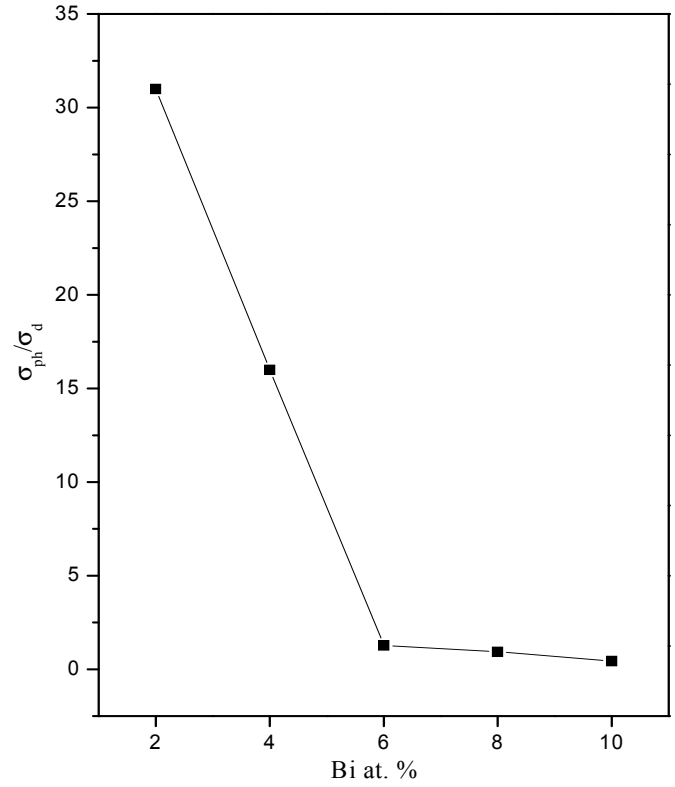

Figure 4.17 Variation of photosensitivity (σ_{ph} / σ_d) with Bi at. %.

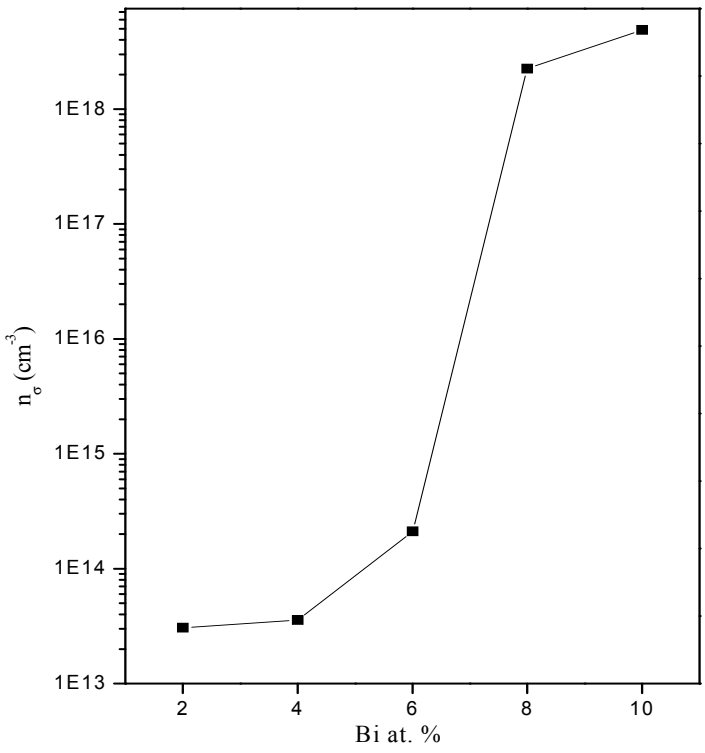

Figure 4.18 Variation of carrier charge density (n_σ) with Bi at. %.

It is clear from the figure that the value of n_σ increases with the increase of Bi concentration, indicating the increase in number of localized states.

Our optical studies (sec. 4.1.2) also show decrease in the optical gap with the increase of Bi content. Density of charge carriers increases on addition of Bi which attributes to an increase in the localized states which also accounts for the decrease in the activation energy with increasing Bi content. The presence of high concentration of localized states in the band gap is responsible for the decrease in the value of optical gap (E_g^{opt}). Due to this, the photosensitivity of $Ge_{20}Se_{70-x}In_{10}Bi_x$ thin films also decreases with the substitution of Bi at a particular temperature and intensity.

Thus σ_{ph}/σ_d at a particular temperature and intensity will be maximum when the density of states will be minimum. For 2 at. % of Bi substitution, the value of σ_{ph}/σ_d is maximum which otherwise shows that density of states is minimum. This result is further confirmed by the minimum value of n_σ at this particular concentration. Moreover this increase in conductivity might also be due to an increase in carrier density. The increase in photoconductivity is also primarily due to this increase in carrier density.

4.2.2.2 Intensity Dependent Steady State Photoconductivity

Investigating the light intensity dependence of the photocurrents at room temperature is normally a way to confirm the internal consistency of the recombination model. Figure 4.19 shows the intensity (F) dependence of steady state photoconductivity (σ_{ph}) at 300 K for $Ge_{20}Se_{70-x}In_{10}Bi_x$ thin films. The plots of $\ln\sigma_{ph}$ vs. $\ln F$ are straight in nature for all the compositions, which indicate that the photoconductivity (σ_{ph}) follows a power law with intensity (F). For $0.5 \leq \gamma \leq 1.0$, according to Rose [31], the value of γ can not be interpreted by assuming a set of discrete trap levels, but considering the existence of continuous distribution of trap levels in the band gap. In *a*-$Ge_{20}Se_{70-x}In_{10}Bi_x$ thin films also, the value of γ (calculated from the slope of $\ln\sigma_{ph}$ vs. $\ln F$) are found to be ~ 0.5 for all compositions. This square root dependence of photocurrent on intensities indicates the

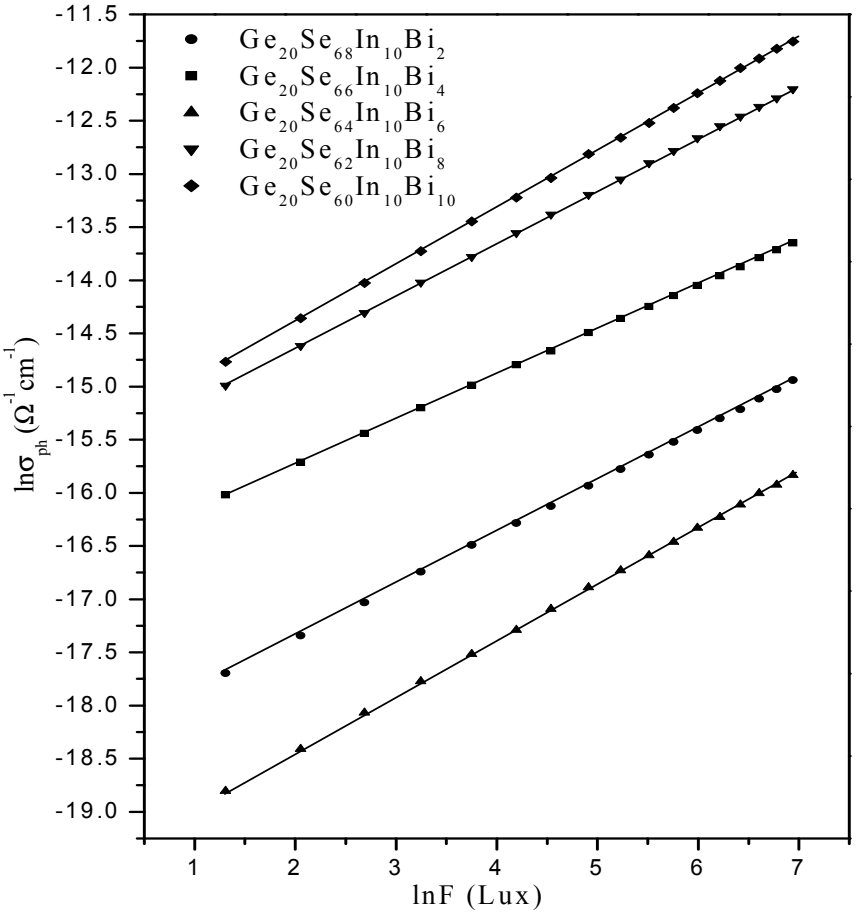

Figure 4.19 Intensity dependence of photoconductivity for $Ge_{20}Se_{70-x}In_{10}Bi_x$ (x = 2, 4, 6, 8, 10) thin films at 300 K.

existence of bimolecular recombination. On illuminating the films with light, direct recombination between electrons and holes takes place without introducing any recombination centers in the band gap. Here, the photoconductivity rate G should be balanced by recombination across the band gap and follows the relation $\sigma_{ph} \alpha \mathrm{G}^{\gamma}$, with $\gamma = 0.5$. In non-equilibrium condition, most of the electrons and holes are generated after shining light and are located at D^0 centers. The charged defect centers D^+ and D^- can act as discrete traps for photogenerated electrons and holes. The majority of excess electrons and holes are trapped by D^+ and D^- according to the reaction, $D^+ + e \rightarrow D^0$ and $D^- + h \rightarrow D^0$ respectively, giving rise to neutral D^0 sites. After the cessation of illumination, the excess density of D^0 decreases due to recombination following $2D^0 \rightarrow D^+ + D^-$. The location of D^0 is thus converted into D^+ and D^-. This type of recombination can be presented by bimolecular recombination.

4.2.3.3 Transient Photoconductivity

For a better understanding of recombination and trapping mechanism, determination of energy distribution of various species of gap states and to disentangle the mobility-lifetime effects from the photogeneration effects, transient photoconductive measurements are conducted by exposing all the samples to light (1035 Lux intensity) at 300 K. Rise and decay of photocurrent for all compositions are shown in figure 4.20. It is clear from the results that the photocurrent rises in monotonous manner upto the steady state value. After cessation of steady illumination, trapped electrons and holes combine and the photoconductivity decay is quite fast initially and then it reaches its steady state value or zero as time elapses. However, a persistent photoconductivity is also observed which takes many hours to decay. This is attributed to some kind of photo-induced effects and not due to trapping of charge carriers in the traps because of the large time constant involved [32]. Photoconductivity relaxation in amorphous chalcogenides has gained satisfactory interpretation in frame of the model of multiple trapping in gap states, as proposed by Iovu *et al.* [33].

Table 4.4 Values of power exponent (γ), photosensitivity (σ_{ph}/σ_d), charge carrier density (n_σ) and decay constant for $Ge_{20}Se_{70-x}In_{10}Bi_x$ (x = 2, 4, 6, 8, 10) thin films at 300 K.

x	γ	σ_{ph}/σ_d	n_σ (cm^{-3})	τ_d (s)
2	0.52	31	3.06×10^{13}	29.14
4	0.51	16	3.57×10^{13}	35.8
6	0.53	1.28	2.11×10^{14}	58.36
8	0.50	0.94	2.25×10^{18}	87.5
10	0.54	0.44	4.89×10^{18}	120

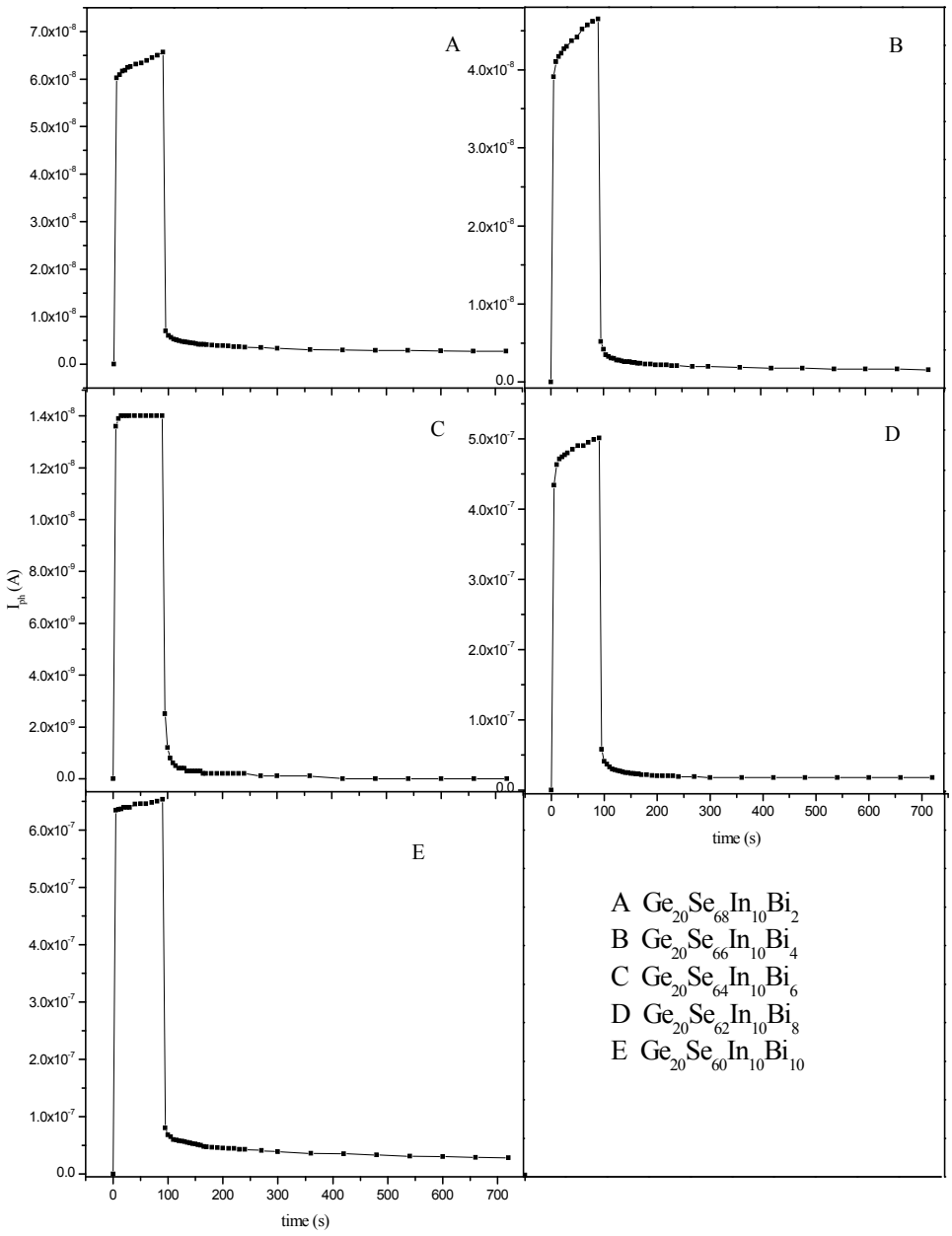

Figure 4.20 Photocurrent rise and decay for $Ge_{20}Se_{70-x}In_{10}Bi_x$ thin films.

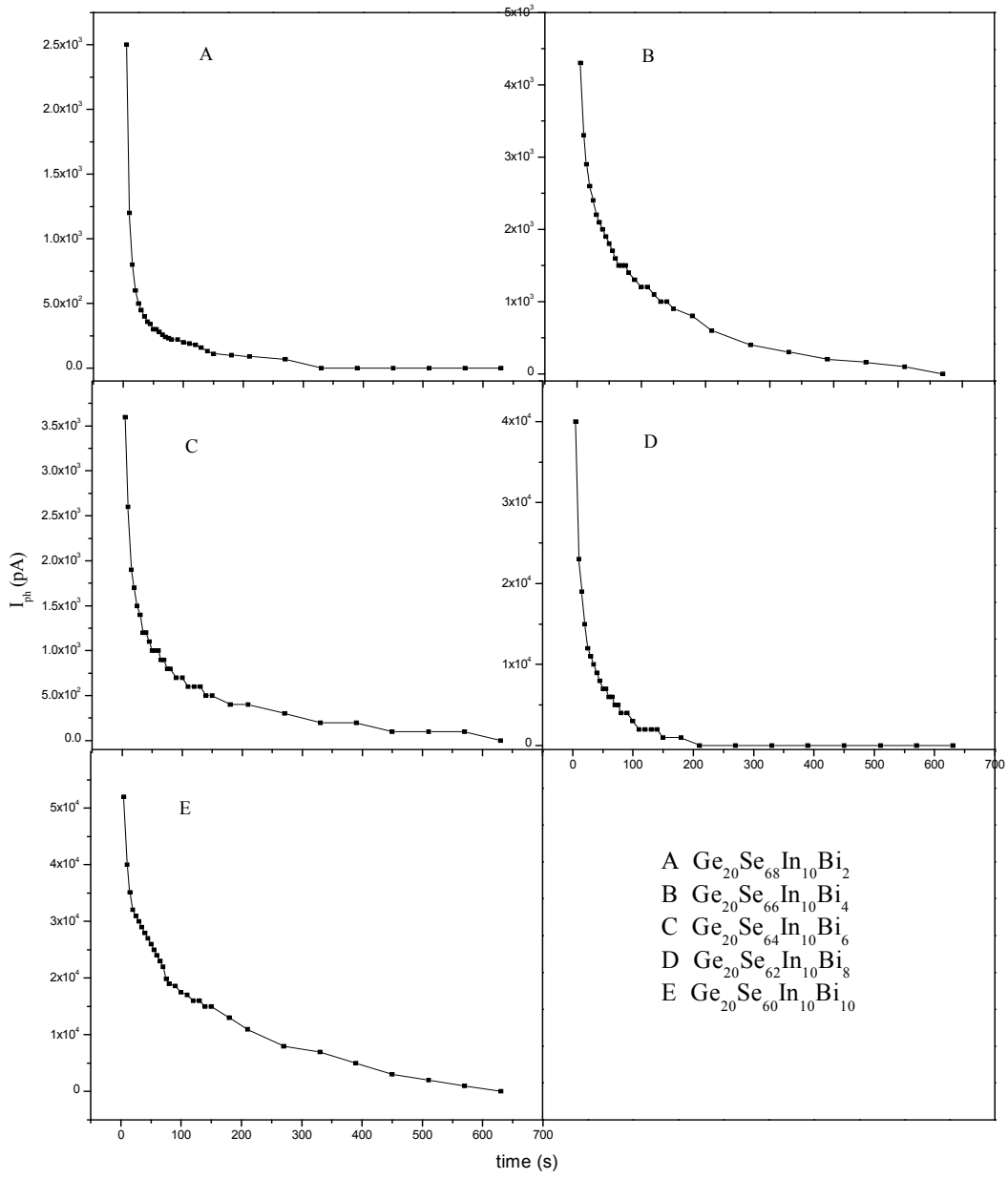

Figure 4.21 Time dependence of photocurrent during decay for $Ge_{20}Se_{70-x}In_{10}Bi_x$ thin films.

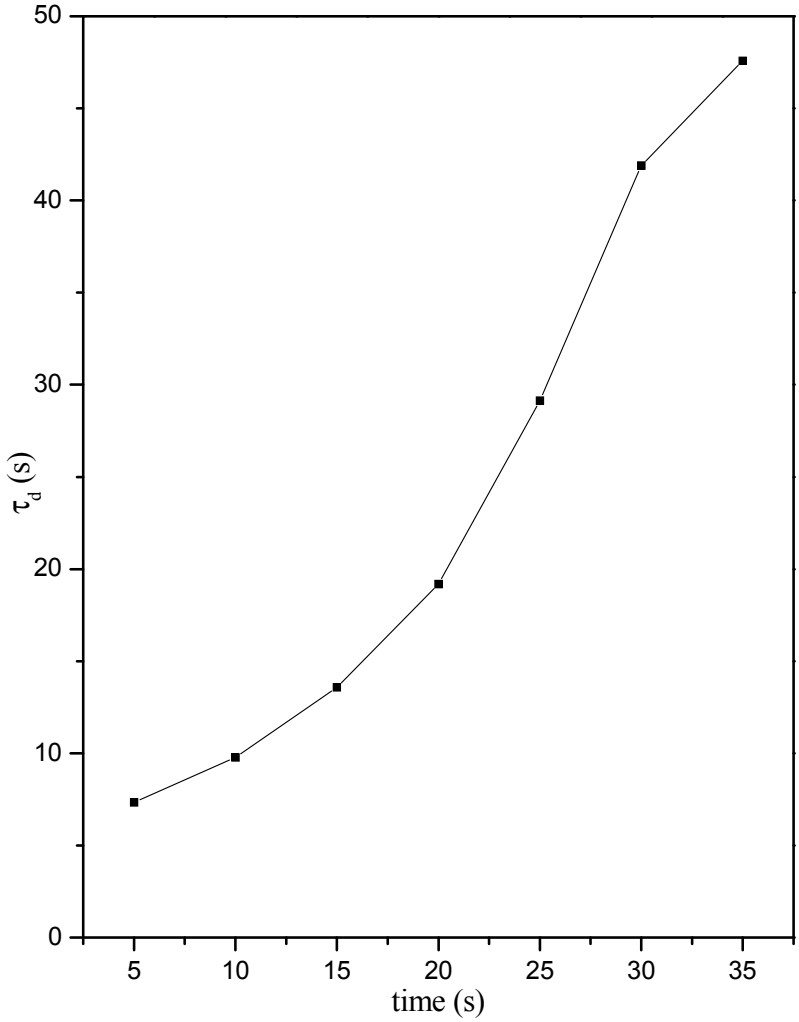

Figure 4.22 Variation of differential life time (τ_d) with time for x = 2 at. %.

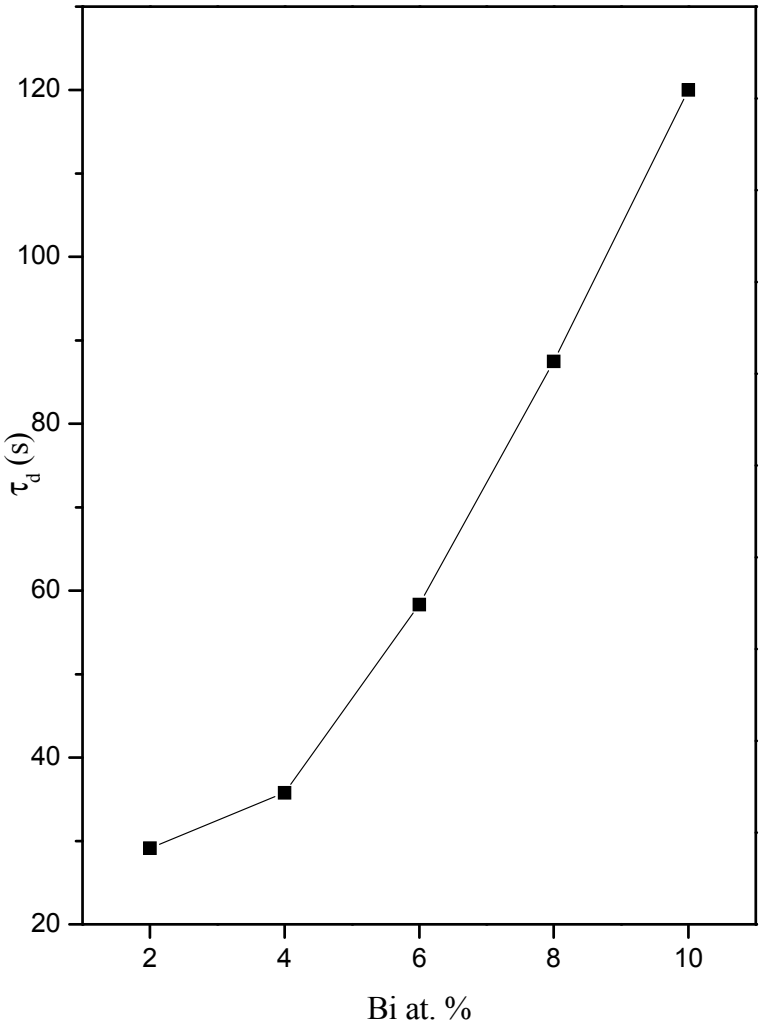

Figure 4.23 Variation of differential life time (τ_d) versus Bi content (x at. %).

To understand the trapping effects, the persistent photoconductivity is subtracted from the measured photoconductivity, and then the corrected photocurrent (pA) against time (s) is plotted for all compositions and shown in figure 4.21. In case of single trap level these curves must be straight lines. However, in the present case, these curves do not maintain same slope and the slope goes on decreasing continuously as the time of decay increases. This indicates that the traps exist at all the energies in the band gap which have different time constant and hence giving the non-exponential decay of photoconductivity. To analyze the decay rates in case of non exponential decay, differential life time (τ_d) has been calculated using the relation given by Fuhs and Stuke [34]

$$\tau_d = -\left[\frac{1}{I_{ph}}\left(\frac{dI_{ph}}{dt}\right)\right]^{-1} \tag{4.2}$$

In the case of exponential decay, the differential lifetime will be equal to the carrier life time. However, in case of a non-exponential decay, τ_d will increase with time and only the value at $t = 0$ will correspond to the carrier lifetime. From the slope of I_{ph} vs. time curves, we have calculated the values of τ_d using equation (4.2) at various times of the decay curves. Figure 4.22 shows the plots of variation of τ_d (for x = 2 at. %) with time at 300 K and at 1035 Lux intensity. It is clear from the figure that τ_d increases with the increase in time. This confirms the non-exponential decay in the present case (as for an exponential decay τ_d should be constant with time). Other compositions also follow the same trend of variation of τ_d with time.

To compare the rate of decay for various samples under investigation, the value of τ_d at t = 25 s has been chosen as at this time the slow decay is predominant in all the films. Figure 4.23 shows the variation of τ_d with the Bi additive at room temperature and also tabulated in table 4.4. The values of τ_d increases with the increase in Bi additive in the $Ge_{20}Se_{70-x}In_{10}Bi_x$ thin films. The higher value of τ_d after Bi incorporation indicates the slower rate of decay of I_{ph}. Simple kinetics involving trapping and recombination centers influence the photoconductivity of solids *i.e.* $2D^0 \rightarrow D^+ + D^-$. Two relevant recombination steps are; (*i*) tunneling of band tail

electrons to neutral dangling bonds D^0, producing D^- states and (*ii*) the diffusion of holes in the tail states to recombine with D^- states formed in step (*i*).

Addition of Bi gives rise to defect centers. These defects could induce more defect localized states which might act as trapping centers. Because of the involvement of electron and hole traps in the recombination process, additional processes of trap filling during the rise and trap emptying during the decay get involved. These traps 'store' the charge carrier and hence delay the recombination rate corresponding to increase in differential life time with the increase of Bi content. Similar conclusions are also drawn from the steady state photo-conductivity measurements. The decrease in photosensitivity value with increasing Bi content is also explained on the basis of increase of localized states.

4.3 Conclusion

Optical and electrical properties of $Ge_{20}Se_{70-x}In_{10}Bi_x$ (x = 2, 4, 6, 8, 10) vacuum evaporated thin films are studied. Optical parameters, in the wavelength range 400 – 1800 nm are studied from their normal incidence transmission spectra. Absorption mechanism is due to indirect transition. It is found that though optical energy gap decreases monotonically, the refractive index increases with the increase of bismuth content. This increase in refractive index is quite favorable for fabricating optical waveguides leading to compact circuit design with high intensities. These results indicate an increase in chemical disorder and a decrease in average bond energy of the system with increasing Bi content. The refractive index values for each sample have been fitted to the single-oscillator model. The values obtained for the single-oscillator energy E_0 are consistent with our optical gap results. The dielectric constants and optical conductivity found to decrease with the increase in wavelength for entire wavelength range under investigation. The study of dark and photoconductivity of $Ge_{20}Se_{70-x}In_{10}Bi_x$ thin films as a function of temperature (300-360 K) reveals that the conduction is through an activated process with single activation energy. Charge carrier concentration (n_σ) increases with increasing Bi content which further accounts for the increase in conductivity. ΔE_d and photosensitivity (σ_{ph}/σ_d) decreases with Bi addition indicating an increase in

localized states in the system. The intensity dependence of photocurrent shows the existence of bimolecular recombination in thin films in which recombination rate of electrons is proportional to the number of holes. The transient photoconductivity measurements for investigating thin films at room temperature and 1035 Lux intensity shows that the photocurrent rises in a monotonous manner upto steady state value and after cessation of illumination, it follows non exponential decay. An increase in differential life time is observed with time (for all composition) as well as with increase in Bi concentration.

References

1. El-Korashy A, El-Kabany N and El-Zahed H 2005 *Physica B* **365** 55
2. El-Zahed H and El-Korashy A 2000 *Thin Solids Films* **376** 236
3. Wang Z, Tu C, Li Y and Chen Q 1995 *J. Non-Cryst. Solids* **191** 132
4. Sharma P, Vashistha M and Jain I P 2005 *J. Optoelectron. Adv. Mat.* **7(5)** 2647
5. El-Samanoudy M M 2003 *Thin Solid Films* **423** 201
6. Tohge N, Minami T and Tanaka M 1980 *J. Non-Cryst. Solids* **37** 23
7. Tohge N, Takahiro T, Yonesakim Y and Minami T 1985 *J. Appl. Phys.* **58** 4225
8. Tohge N, Minami T, Yamamoto Y and Tanaka M 1980 *J. Appl. Phys.* **51** 1048
9. Marquez E, Gonzalez-Leal J M, Bernal-Oliva A M, Jimenez-Garay R and Wagner T 2007 *J. Non-Cryst. Solids* **354** 503
10. Elliott S R 2000 *The Physics and Chemistry of Solids* (Chichester: Wiley)
11. Lezal D 2003 *J. Optoelectron. Adv. Mater.* **5** 23
12. Tanaka K 1980 *Thin Solid Films* **66** 271
13. Tauc J 1979 *Amorphous and Liquid Semiconductors* (New York: Plenum Press)
14. Kitao M, Akao H, Ishikawa T and Yamada S 1981 *Phys. Stat. Soli. (a)* **64** 493
15. Mott N F and Davis E A 1971 *Electronics Process in Non-Crystalline Materials* (Oxford: Clarendon Press)
16. Khan M M A, Zulfequar M and Husain M 2003 *Optical Materials* **22** 21
17. Wakkad M M, Kh. Shokr E and Mohamed S H 2000 *J. Non-Cryst. Solids* **265** 157
18. Pankove J I 1975 *Optical Processes in Semiconductors* (New York: Dover)
19. Shimakawa K, Narushima S, Hosono S and Kawazoe H 1999 *Phil. Mag. Lett.* **79** 755
20. Iovu M S, Shutov S D and Popescu M 2002 *J. Non-Cryst. Solids* **299** 924
21. Kolobov A V 1996 *J. Non-Cryst. Solids* **198-200** 728

22. Kastner M 1972 *Phys. Rev. Lett.* **28** 355
23. Baranovskii S D *et al.* 1984 *Fiz. Tekh. Poluprovodn* **18** 1016
24. Kastner M, Adler D and Fritzsche H 1976 *Phys. Rev. Lett.* **37** 1504
25. Mott N F 1967 *Adv. Phys.* **16** 49
26. Mott N F 1976 *Phil. Mag.* **34** 1101
27. Tohge N, Minami T, Yamamoto Y and Tanaka M 1980 *J. Appl. Phys.* **51** 1048
28. Mehra R M *et al.* 1997 *J. Appl. Phys.* **81** 7842
29. Rehman S and Sastry G S 1992 *Mater. Sci. Eng. B* **12** 219
30. Adler D, Shur M S, Silver M and Ovshinsky S R 1980 *J. Appl. Phys.* **51** 3289
31. Rose A 1963 *Concepts in Photoconductivity and Allied Problems* (New York: Interscience)
32. Igalson M 1982 *Solid State Commun.* **27** 171
33. Iovu M S, Shutov S D, Arkhipov V I and Adriaenssens 2002 *J. Non-Cryst. Solids* **299** 1008
34. Fuhs W and Stuke J 1968 *Phys. Stat. Sol.* **27** 171

CHAPTER V*

Physical Properties of *a*-Ge-Se-In and *a*-Ge-Se-In-Bi Glassy Alloys

* • **Ishu Sharma**, S. K. Tripathi, and P. B. Barman, "*Compositional dependence of physical properties in Ge-Se-In glassy semiconductors*" **Physica B: Condensed Matter** 403 (2008) 624.

- **Ishu**, S. K. Tripathi and P. B. Barman, "*Effect of indium incorporation on the physical parameters of Ge-Se glassy alloy*" **Journal of Optoelectronics and Advanced Materials** 9 (2007) 3039.

- **Ishu Sharma**, S. K. Tripathi and P. B. Barman, "*Correlation between the physical and optical behavior of a-Ge-Se-In-Bi system*" **Philosophical Magazine** (2008) [Communicated].

5.0 Introduction

In chalcogenide glasses, short range inter-atomic forces are predominantly covalent: strong in magnitude and highly directional, whereas weak vander Waal forces contribute significantly to the medium range order. These materials exhibit unique physical properties that make them good candidates for potential technological applications in solid-state devices, as threshold and memory switching, in nanotechnology and infrared transmission and detection, *etc.* [1,2]. In connection with the modification of their properties on doping with metal impurities [3,4], chalcogen semiconductors truly emerged as reference materials in order to develop a better understanding of the glassy state and its specific properties. Moreover, because these materials show a continuous change of their various properties with change in their chemical composition, it is possible to investigate the correlation of the features observed in the property-composition dependence with the structural arrangement in the glass. Recently, variation of physicochemical, mechanical and optical properties of multi component chalcogenide glasses and thin films caused by changes in the average coordination number $(< r >)$, has been the subject of intensive research [5,6]. The model of bond arrangement [7,8] and topological models such as the constraints model [9,10] and the structural transition model [11], have been used in the interpretation of the compositional dependence of these properties. Distinct features such as an extrema or a kink caused by chemical ordering are observed in the compositional dependence at the stochiometric or tie-line compositions (also known as chemical thresholds of the system [12]). The topological model based on the constraints theory is also employed to explain the peculiarities in property-compositional dependence of covalently bonded chalcogenide glasses. In this model the properties are discussed in terms of the average coordination number. At $< r > = 2.4$, the glass network has a mechanical or floppy-to-rigid percolation threshold. At this $< r >$ value the network structure changes from an elastically floppy type to a rigid type [10] Taking into account not only the short range constraints, but also the constraints of the medium range order (MRO), Tanaka [11] has predicted another structural phase transition. It is the transition from two dimensional (2*D*) layer-like structures to 3*D* cross-linked network. This transition is observed at $< r > \approx 2.67$ and

may be regarded as a topological one. The above mentioned thresholds have been observed in several chalcogenide systems.

Optical and electrical study of $Ge_{20}Se_{80-x}In_x$ (x = 0, 5, 10, 15, 20) and $Ge_{20}Se_{70-x}In_{10}Bi_x$ (x = 2, 4, 6, 8, 10) thin films have already been performed in chapters III and IV respectively. In this chapter we have discussed the physical properties of $Ge_{20}Se_{80-x}In_x$ (x = 0, 5, 10, 15, 20) and $Ge_{20}Se_{70-x}In_{10}Bi_x$ (x = 2, 4, 6, 8, 10) glassy alloys.

5.1 Physical Properties of $Ge_{20}Se_{80-x}In_x$ (x = 0, 5, 10, 15, 20) Glassy Alloys

In this section, correlation between glass transition temperature (T_g) and the mean bond energy $(< E >)$ has been studied by using Tichy – Ticha approach [13,14]. Other physical parameters *viz.* cohesive energy (*CE*), average heat of atomization $(\overline{H_s})$, density (ρ), molar volume (V_m) and compactness (δ) of bulk glassy alloys have been determined theoretically. The variation of these parameters have been shown in terms of composition or equivalently with the average coordination number, $< r >$. The relation between photon energy (E_{04}) is discussed in terms of average heat of atomization and average coordination number. The compactness of the structure of the glass is determined from measured density of glasses in order to display the chemical threshold in the system using Phillips – Thorpe topological models.

5.1.1 Experimental Details

Bulk samples of $Ge_{20}Se_{80-x}In_x$ (x = 0, 5, 10, 15, 20) were prepared by melt quenching technique (chapter II). The amorphous nature of the bulk samples was confirmed by the X-ray diffraction technique as no sharp peak was observed in spectra. The density of the glasses were measured by the Archimedes method using double distilled water as a reference liquid, having density 1.0 g/cc at 20 ^oC.

5.1.2 Results and Discussion

5.1.2.1 Correlation between Mean Bond Energy and Glass Transition Temperature

Glass transition temperature of Ge-Se-In glasses has been measured theoretically. T_g represents the temperature above which an amorphous matrix can attain various structural configurations and below which the matrix is frozen into a structure which cannot easily change to another structure. Therefore, it is reasonable to assume that T_g must be related to the magnitude of the cohesive forces within the network, since these forces must overcome to allow atom movement. So, T_g are generally based on simple models in which it is assumed that T_g is proportional to another material parameter (such as mean bond energy) which strongly depends on the cohesive forces or the rigidity of the network.

Tichy and Ticha [15] were the first to point out that the value of glass transition temperature should not only be related to connectedness of the network (which is related to $< r >$) but should also be related to the quality of connections, *i.e.* the mean bond energy between the atoms of the network. From bond energy values (table 5.1) strong heteropolar bonds *i.e.* Ge-Se and In-Se are calculated using Pauling Relation [16] and can be well differentiated from weak homopolar bonds *i.e.* Ge-Ge, In-In and Se-Se bonds [14]. So, chemically ordered networks are expected where the number of heteropolar bonds is maximized *i.e.* they are more favorably formed than homopolar bonds. Since bulk glasses are considered, a chemical bond ordering model is assumed. Based on this assumption mean bond energy is given by

$$< E >= E_c + E_{rm} \tag{5.1}$$

where,

E_c = overall contribution towards bond energy arising from strong heteropolar bonds.

E_{rm} = contribution arising from weaker bonds that remain after the strong bonds have been maximized *i.e.* the average bond energy per atom of the 'remaining matrix'.

For $Ge_xSe_yIn_z$ system (where $x + y + z = 1$);

Case I. In the selenium rich region $(R > 1)$, there are heteropolar bonds and

chalcogenide – chalcogenide bonds.

$$E_c = 4xE_{Ge-Se} + 3zE_{In-Se} \tag{5.2}$$

and

$$E_{rm} = \frac{[2y - 4x - 3z]}{< r >} E_{Se-Se} \tag{5.3}$$

where E_{Se-Se} is the homopolar bond energy of Se-Se bonds.

Case II. In the selenium poor region $(R < 1)$, there are heteropolar and metal – metal bonds present.

$$E_c = \frac{2y(4xE_{Ge-Se} + 3zE_{Se-In})}{4x + 3z} \tag{5.4}$$

and

$$E_{rm} = \frac{(4x + 3z - 2y)}{< r >} E_{Ge-In} \tag{5.5}$$

R is the parameter which determines the deviation of stoichiometry and is expressed by the ratio of covalent bonding possibilities of chalcogen atom to that of non-chalcogen atom. Values of R were found to be larger than unity for glasses which indicate chalcogen-rich materials and less than unity for glasses indicating chalcogen poor material. For $Ge_xSe_yIn_z$ system, the quantity $'R'$ is defined by [13,14]

$$R = \frac{yCN(Se)}{xCN(Ge) + zCN(In)} \tag{5.6}$$

where x, y and z are respectively the atomic fractions of Ge, Se and In.

However, the calculation of $'R'$ also requires the knowledge of coordination number (CN) of all the constituents of glassy alloys. For the investigating system, $CN(Ge)$ and $CN(Se)$ respect the Mott $"8 - N"$ rule [17], where N is the number of outer shell electrons. Coordination number of In in $Ge_xSe_yIn_z$ system has been well discussed by Saiter *et al.* [18]. Values of R and $< E >$ are given in table 5.1.

Nearest-neighbor coordination $< r >$ in a ternary system is particularly suitable for testing the validity of these topological concepts [19], because of its large glass forming region. The average coordination number $< r >$ in our system is defined by

$$< r > = \frac{aX + bY + cZ}{a + b + c} \tag{5.7}$$

Table 5.1 Values of $< r >$, R, $< E >$, T_g for $Ge_{20}Se_{80-x}In_x$ composition and bond energies of their respective bonds.

x	$< r >$	*R*	$< E >$ (eV/atom)	T_g (K)	*Bonds*	*Bond Energies* (kcal/mol)
0	2.40	2.000	2.35	451	*Ge – Se*	49.10
5	2.45	1.579	2.45	484	*Se – Se*	44.00
10	2.50	1.273	2.57	520	*Ge – Ge*	37.60
15	2.55	1.040	2.71	562	*In – Se*	48.20
20	2.60	0.857	2.66	547	*In – In*	29.83
	-	-	-	-	*Ge – In*	33.72

where *a*, *b* and *c* are the percentage at. wt. and $X = 4$, $Y = 2$ and $Z = 3$ are coordination numbers of Ge, Se and In respectively.

Structural measurements of Ge-Se-In system have been done by Ledru *et al.* [20] and Saiter *et al.* [21] and they have found that the coordination number of In is 3 in Ge-Se-In system and In is only coordinated with Se atom. The obtained values of $< r >$ for the five compositions of $Ge_{20}Se_{80-x}In_x$ with x = 0, 5, 10, 15 and 20 are listed in table 5.1.

Using a set of 186 glasses, Tichy and Ticha [13,14] illustrated an impressive correlation of T_g with mean bond energy $< E >$ in the form;

$$T_g = 311[< E > -0.9] \tag{5.8}$$

In particular they demonstrated that the compositional dependence of T_g in numerous glassy systems presents maximum value near the chemical threshold *i.e.* $R = 1$, because the chemical bond energies are maximized at this composition.

Applying this model to $Ge_{20}Se_{80-x}In_x$ system, we evaluated mean bond energy and using above relation (equation 5.8), T_g has been calculated. The values of T_g against In concentration are given in table 5.1. It is clear from the table that with the increase in In content in Ge-Se glassy alloy, the mean bond energy along with glass transition temperature increases, reaches a maximum at $R = 1$, corresponding to composition $Ge_{20}Se_{65}In_{15}$ and then decreases as shown in figures 5.1 and 5.2 respectively. The major limitation of the model is that, it does not account for the molecular interaction, which plays a vital role in the relaxation process in glass transition region. Glass transition and crystallization temperature in Ge-Se-In glass has been calculated by Saffarini [22] and found that the extrema observed in T_g and T_x at $R = 1$ corresponds to chemical threshold. Chemical ordering in $Se_{80}Ge_{20-x}In_x$ (4, 8, 12, 15, 18) glasses has also studied by Rabinal *et al.* [23] and found that T_g increases with increase of In content, reaches a maximum around 15 at. % which is quite close to chemical threshold $x_c = 16$ at. %.

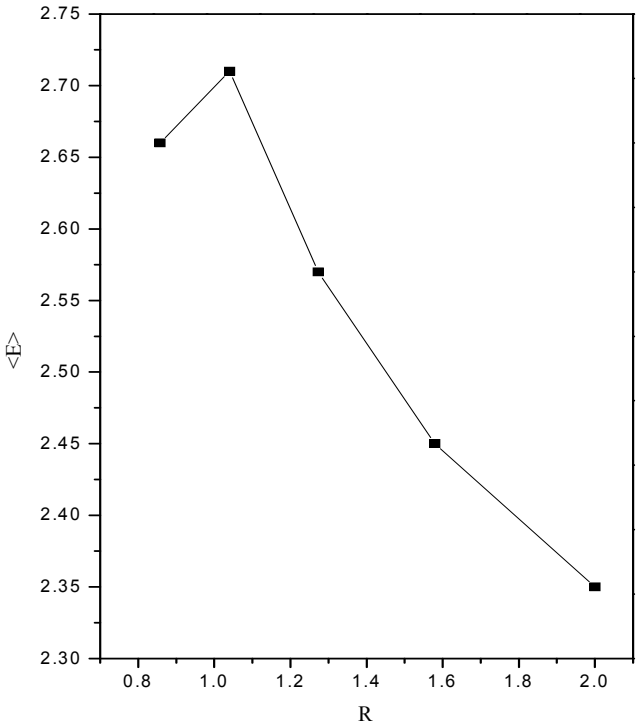

Figure 5.1 Variation of $< E >$ with R for $Ge_{20}Se_{80-x}In_x$ (x = 0, 5, 10, 15, 20).

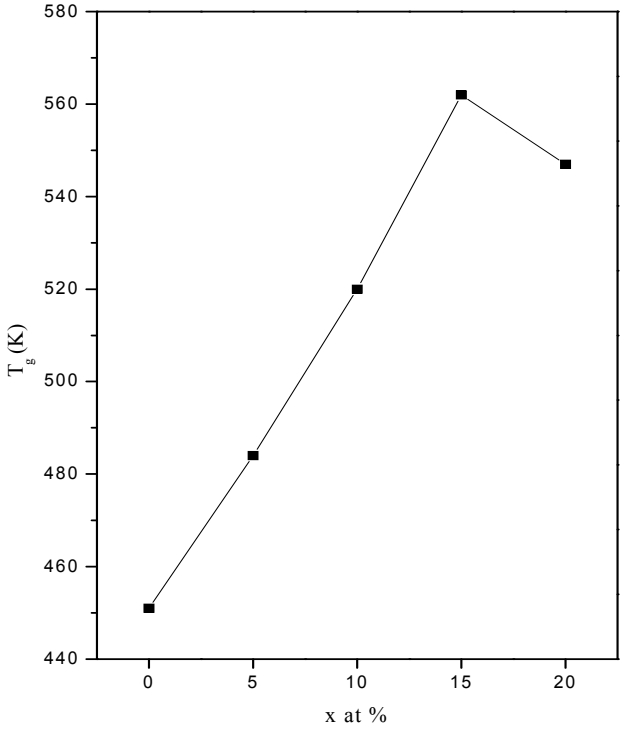

Figure 5.2 Variation of T_g with In content (x at. %).

5.1.2.2 Calculation of Cohesive Energy and Electronegativity

Using the chemical bond approach (*CBA*) method [24], the cohesive energy (the stabilization energy of an infinitely large cluster of material per atom) for investigated samples has been calculated. According to *CBA* the bonds are formed in the sequence of decreasing bond energy until available valence of atoms is satisfied and bond energies are assumed to be additive. Thus cohesive energies were calculated by summing the bond energies over all bonds expected in the material. Calculated values of *CE* along with the chemical bond of distribution for all the compositions are tabulated in table 5.2. The results indicate that, the *CE* of these glassy alloys shows an increase with increasing In content up to 15 at. % and it subsequently decreases at 20 at. % . Change in *CE* with In content follows the same trend as that of mean bond energy $< E >$ calculated above.

It can be concluded that increase of E_g^{opt} with increasing In content is due to increase of average stabilization energy and decrease of electronegativity of the system which is calculated by using Sanderson's principle [25]. According to this principle electronegativity of the alloy is the geometric mean of electronegativity of its constituent elements. It is evident from the table 5.2, electronegativity decreases as the optical band gap decreases.

5.1.2.3 Relation between E_{04}, $\overline{H_s}$ and $< r >$

It is interesting to relate the E_{04} (the photon energy) with average single bond energy, ($\overline{H_s}/< r >$). E_{04} is the arbitrary quantity defined as photon energy at which optical absorption coefficient has the value of $10^4 cm^{-1}$. The photon energy at $\alpha = 10^4 cm^{-1}$ is about 0.2 eV larger than the optical band gap (E_g^{opt}) [26]. The obtained E_{04} values along with calculated E_g^{opt} values, are given in table 5.3. To correlate these values for $Ge_{20}Se_{80-x}In_x$ system, we calculate the average heat of atomization.

Table 5.2 χ, E_g^{opt}, distribution of chemical bonds and cohesive energy (*CE*) in $Ge_{20}Se_{80-x}In_x$ (x = 0, 5, 10, 15, 20) system.

x	χ	E_g^{opt} (eV)	Distribution of chemical bonds				*CE* (kcal/mol)
			Ge – Se	*In – Se*	*Se – Se*	*In – In*	
0	2.43	1.69	0.5000	-	0.5000	-	46.55
5	2.38	1.72	0.5333	0.1000	0.3667	-	47.14
10	2.34	1.75	0.5714	0.2143	0.2143	-	47.81
15	2.30	1.67	0.6153	0.3461	0.0386	-	48.59
20	2.26	1.51	0.6667	0.2222	-	0.1111	46.76

Table 5.3 Values of E_g^{opt}, E_{04}, $\overline{H_s}$ and $\overline{H_s}/< r >$ for $Ge_{20}Se_{80-x}In_x$ (x = 0, 5, 10, 15, 20) system.

x	E_g^{opt} (eV)	E_{04} (eV)	$\overline{H_s}$ (kcal/g-atom)	$\overline{Hs}/< r >$ (kcal/g-atom)
0	1.69	1.89	57.52	23.96
5	1.72	1.92	57.95	23.65
10	1.75	1.95	58.38	23.35
15	1.67	1.87	58.81	23.06
20	1.51	1.71	59.24	22.78

According to Pauling [16], the heat of atomization $\overline{H_s}(A-B)$ at standard temperature and pressure of a binary semiconductor formed from atoms A and B is the sum of heat of formation (ΔH) and the average heats of atomization $\overline{H_s^A}$ and $\overline{H_s^B}$. Where, $\overline{H_s^A}$ and $\overline{H_s^B}$ corresponds to the average non-polar bond energy of *A* and *B*.

$$\overline{H_s}(A-B) = \Delta H + \frac{1}{2}\left(\overline{H}_s^A + \overline{H}_s^B\right) \tag{5.9}$$

The term (ΔH) in above equation is proportional to the square of the difference between the electronegativities χ_A and χ_B of the two atoms *i.e.*

$$\Delta H \quad \alpha \quad (\chi_A - \chi_B)^2 \tag{5.10}$$

In order to extend this idea to ternary and higher order semiconductor compounds [27], the average heat of atomization $\overline{H}_s$ (kcal/gram-atom) is defined for a compound $A_\alpha B_\beta C_\gamma$ as a direct measure of the cohesive energy and thus of average bond strength and is given by

$$\overline{H}_s = \frac{\alpha H_s^A + \beta H_s^B + \gamma H_s^C}{\alpha + \beta + \gamma} \tag{5.11}$$

where α, β and γ are the atomic ratios of A, B and C respectively. In the present ternary glassy system, the average heat of atomization is calculated by equation (5.11) using the values of heat of atomization 90, 49.4 and 58 in kcal/g-atom for Ge, Se and In respectively. Average heat of atomization $\overline{H}_s$ (kcal/g-atom) and average single bond energy $(\overline{H}_s / < r >)$ are given in table 5.3.

In semiconductors, the bonding band forms the valence band and the antibonding forms the conduction band. However, in chalcogenide glasses containing a high concentration of a group VI "Se in our case", valance band $(\sigma - bonding)$ originates from lone pair (*LP*) electron states whereas the conduction band arises from antibonding (σ^*) states [28]. It is therefore interesting to relate the optical band gap with the average single bond energy, and the parameters we use to specify the bonding are $\overline{H_s}$ and $< r >$. The relation between the energy gap and the average heat of atomization was discussed by Aigrain *et al.* [29]. According to them there exists a

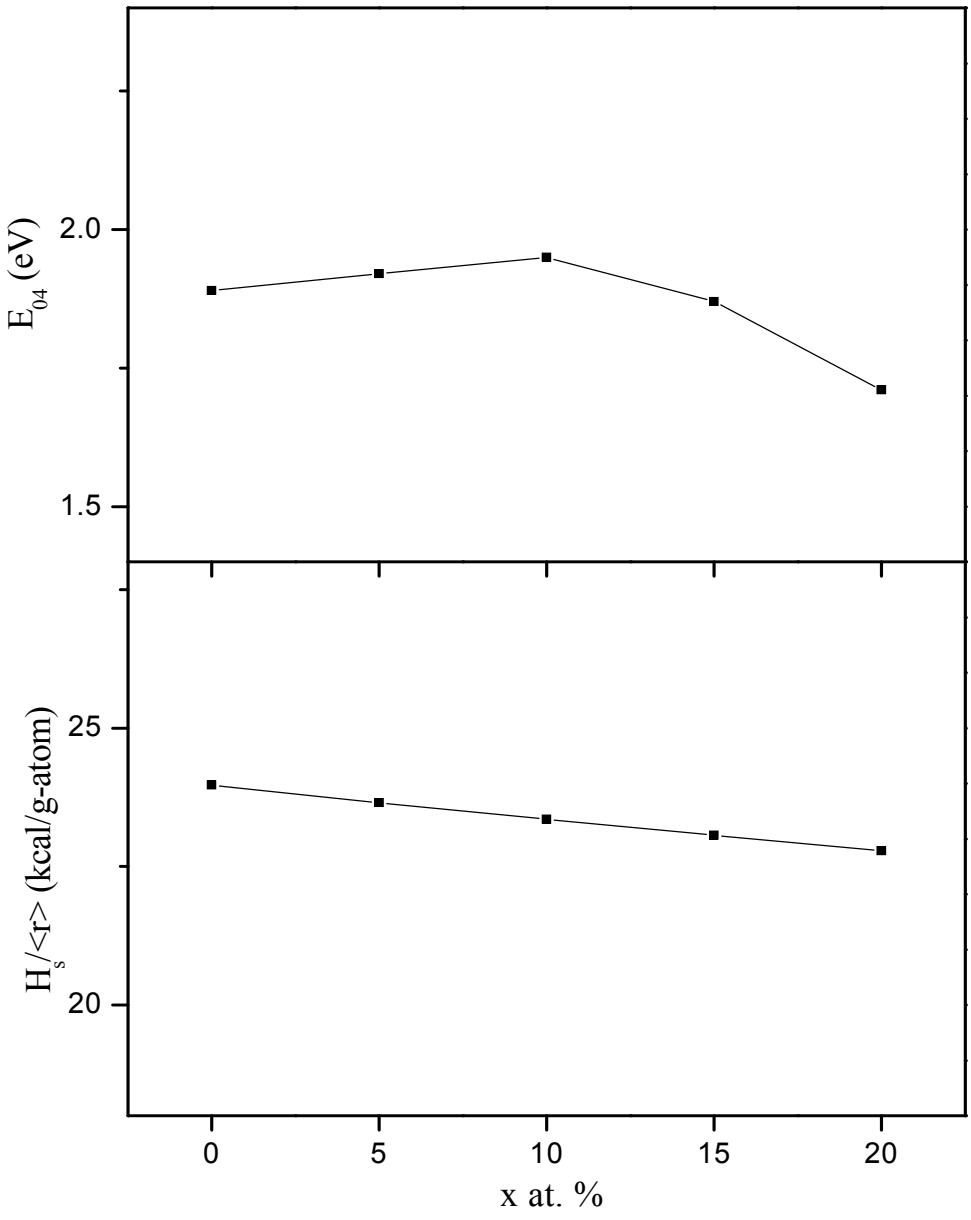

Figure 5.3 Variation of E_{04} and $\overline{H_s}/< r >$ with In content (*x* at. %).

linear correlation, $\Delta E = a\left(H_s - b\right)$ where a and b are characteristic constants. It is suggested from the above equation that the average heat of atomization is a measure of the cohesive energy and represents the relative bond strength, which in turn is correlated with the energy gap of semiconductors. Figure 5.3 represents the variation of E_{04} and average heat of atomization per single bond as a function of composition parameter x (at. %) in Ge-Se-In glassy system. Furthermore, comparing E_{04} with $\overline{H}_s$ (given in table 5.3), there is an increase in E_{04} up to 10 at. % of In and then it decreases with further In addition. However, the average heat of atomization shows very small increment with In addition. But according to Kastner [28], E_{04} for over constrained materials with higher connectivity *i.e.* $3 \leq < r > \leq 4$ depends more strongly on $\overline{H}_s$ than for glasses with lower connectivity, $2 \leq < r > \leq 3$. In our case, the value of $< r >$ varies from $2.4 - 2.6$, which lies in low connectivity region. This further suggests that the parameter $\overline{H}_s / < r >$ is almost constant with x at. % and has a very negligible effect on E_{04} which is also evident from the figure 5.3. Similar results have also been reported for Te-As-Ge-Si and As-Sb-Se-Te systems [30,31].

5.1.2.4 Compactness and Molar Volume

The density was calculated from the formula

$$\rho = \left[\frac{w_1}{w_1 - w_2}\right]\rho_{water} \tag{5.12}$$

where w_1 and w_2 are the weight of the sample in air and weight of sample in reference liquid respectively. The calculated density values are reported in table 5.4. The error in the density measurement and consequently in δ, obtained by measuring the density of some pure elements were estimated to be less than $\pm 1\%$. The compactness δ was calculated by the formula [32]

$$\delta = \frac{\sum_i \frac{c_i A_i}{\rho_i} - \sum_i \frac{c_i A_i}{\rho}}{\sum_i \frac{c_i A_i}{\rho}} \tag{5.13}$$

Table 5.4 Density (ρ), molar mass (m), molar volume (V_m) and compactness (δ) for $Ge_{20}Se_{80-x}In_x$ (x = 0, 5, 10, 15, 20) system.

x	ρ (g/cc)	M (g/mol)	V_m (cc/mol)	δ
0	4.268	77.696	18.20	-0.13002
5	4.226	79.489	18.81	-0.15985
10	4.200	81.282	19.35	-0.18515
15	4.380	83.075	18.97	-0.17036
20	4.640	84.867	18.29	-0.14153

where, c_i is the atomic fraction, A_i is the atomic weight, ρ_i is the atomic density of the i^{th} element of the glass and ρ is the measured density of the glass. Thus, δ is a measure of the normalized change of the mean atomic volume due to chemical interactions of the elements forming the network of a given solid [14]. Consequently, δ is more sensitive to structural changes in glass network as compared to the mean atomic volume.

The molar volume (V_m) was determined from the density data by the equation

$$V_m = \frac{1}{\rho}\sum_i x_i M_i \tag{5.14}$$

where M_i is the molecular weight of the i^{th} component and x_i is the atomic percentage of the same element in the sample.

Table 5.4 summarizes the density of the investigated compositions, their corresponding compactness and molar volume. The compositional variation of compactness, characterized by $< r >$ of the investigated glassy alloys is shown in figure 5.4. From the figure, it is evident that maxima of the compactness occurs at $< r >= 2.4$, which can be well understood in light of constraint theory and rigidity percolation concept [33,34]. The stability of the network with $< r >= 2.4$, where the mechanical threshold takes place can be associated with atomic arrangements that become more tightly bound with shorter bond lengths resulting to smallest mean atomic volume of the network and hence compactness rises to the maximum. Thus, this maximum observed compactness at $< r >= 2.4$ for $Ge_{20}Se_{80}$ glassy alloy, is attributed to the floppy-to-rigid transition occurring in these network glasses.

The variation of molar volume (V_m) with composition (x at. %) is shown in figure 5.5. From the figure it is clear that molar volume first increases upto 10 at. % In concentration and then decreases with further In addition. The variation of optical band gap also follows the same trend with In concentration. In chalcogenide glasses, the energy of the conduction band edge is decided by number of atoms per unit volume (N). A decrease in N leads to an increase in the energy of conduction band edge hence increase optical band gap. From figure 5.5, N decreases up to 10 at. % In, corresponds to increase in optical band gap and with more In addition, N increases with subsequent decrease in optical band gap.

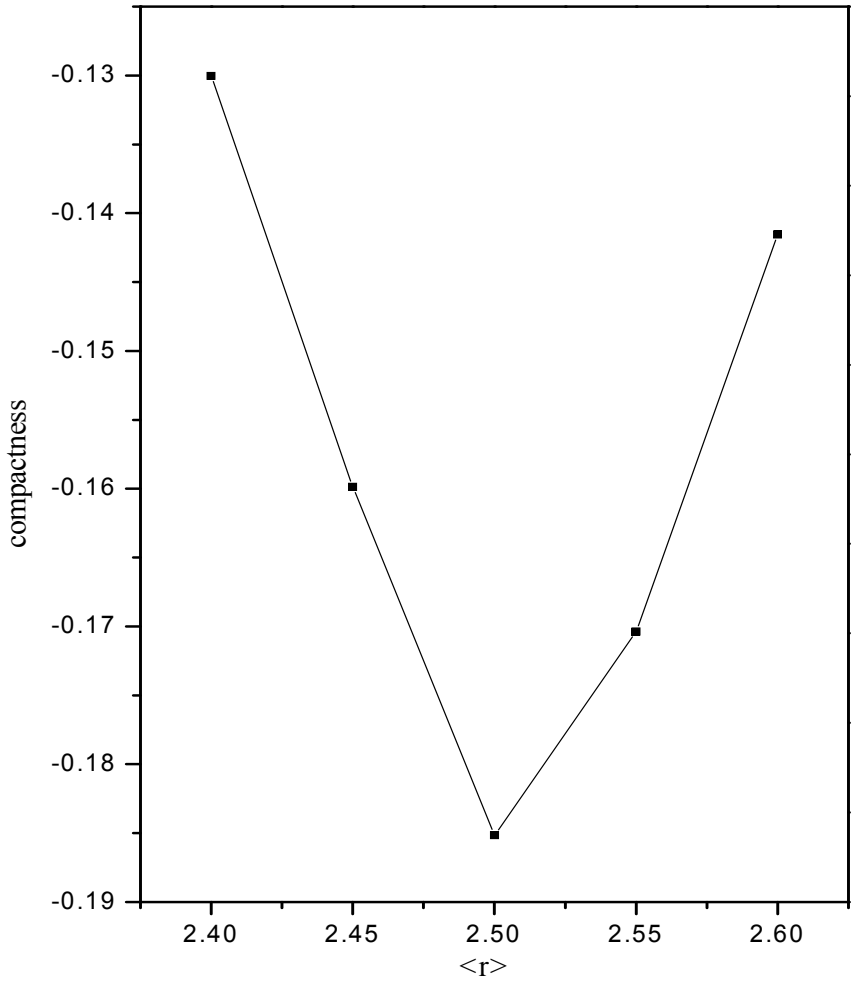

Figure 5.4 Variation of compactness with average coordination number $< r >$.

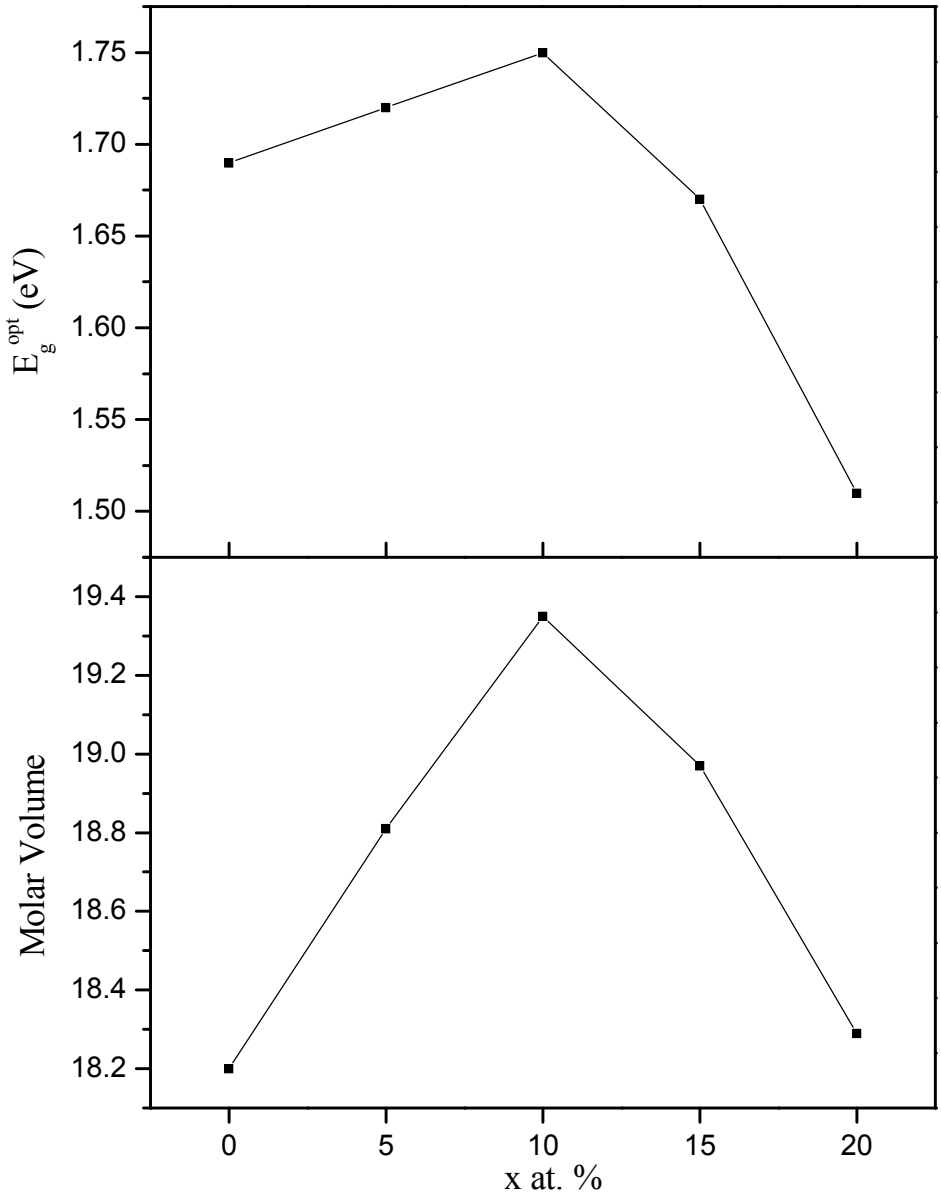

Figure 5.5 Variation of molar volume and optical band gap with *x* at. %

5.2 Physical Properties of $Ge_{20}Se_{70-x}In_{10}Bi_x$ (x = 2, 4, 6, 8, 10) Glassy Alloys

Subtle changes in selected physical properties around the critical Bi concentration, which is seen to occur in the vicinity of Bi = 7 at. % in $Ge_{20}Se_{80-x}Bi_x$ glass has been reported. Electric resistance, thermoelectric power and optical absorption coefficient show a gradual decrease in resistivity with Bi content upto 7 at. % and decrease by four order of magnitude at x = 7.5 at. %. In this section physical properties of amorphous $Ge_{20}Se_{70-x}In_{10}Bi_x$ (x = 2, 4, 6, 8, 10) system have been measured. Physical properties *viz.* density, molar volume, compactness, cohesive energy, average heat of atomization, mean bond energy and glass transition temperature of $Ge_{20}Se_{70-x}In_{10}Bi_{10}$ (x = 2, 4, 6, 8, 10) bulk glassy alloys have been examined theoretically. The cohesive energy of the investigated samples has been calculated using the chemical bond approach method. The relation between photon energy is discussed in terms of average heat of atomization and average coordination number.

5.2.1 Experimental Details

Bulk samples of the $Ge_{20}Se_{70-x}In_{10}Bi_x$ (x = 2, 4, 6, 8, 10) system were prepared by melt quench technique. Amorphous nature of the bulk samples and thin films was checked by XRD technique. No prominent peak is observed in the bulk as well as in thin films. The density of the glasses was measured by the Archimedes method using double distilled water as a reference liquid, which has a density of 1.0 g/cc at 20 ^{o}C.

5.2.2 Results and Discussion

The average coordination number $< r >$ in quaternary system is calculated from

$$< r > = \frac{\alpha X + \beta Y + \gamma Z + \delta A}{\alpha + \beta + \gamma + \delta} \tag{5.14}$$

where $\alpha, \beta, \gamma \; and \; \delta$ are the % at. wt. and $X = 4$, $Y = 2$, $Z = 3$ and $A = 3$ are coordination numbers of Ge, Se, In and Bi respectively. The obtained values of $< r >$ for $Ge_{20}Se_{70-x}In_{10}Bi_x$ are listed in table 5.5.

Table 5.5 Average coordination number $< r >$, density (ρ), refractive index (n), compactness (δ), molar mass (M) and molar volume (V_m) for $Ge_{20}Se_{70-x}In_{10}Bi_x$ (x = 0, 2, 4, 6, 8, 10) system.

x	$< r >$	ρ (g/cc)	n	δ	M (g/mol)	V_m (cc/mol)
0	2.5	4.2	3.01	-0.185	81.28	19.35
2	2.52	4.65	3.09	-0.119	83.88	18.03
4	2.54	4.84	3.15	-0.105	86.48	17.85
6	2.56	5.07	3.23	-0.085	89.08	17.56
8	2.58	5.23	3.29	-0.076	91.68	17.51
10	2.6	5.44	3.32	0.060	94.28	17.30

5.2.2.1 Density, Compactness and Molar Volume

The density, compactness and molar volume were calculated from the formulas given in section 5.1.2.4. The calculated density values are reported in table 5.5. It is clear from the table that measured density increases with the addition of Bi content to *a*-Ge-Se-In alloy. This increase in density also accounts for the increase in refractive index of thin films (table 5.5). This increase in refractive index can be attributed to the increase in valence of current carriers and also presumable due to the increased polarizability associated with the larger Bi atom. Larger the atomic radius of the atom, larger will be its polarizability and consequently, according to Lorentz - Lorenz relation, larger will be the refractive index. The calculated values of compactness, from measured density data, are found to increase with increase of Bi content. The molar volume (V_m) was determined from the density data.

Table 5.5 summarizes the density of the investigated compositions, their corresponding compactness and molar volume. It is evident that compactness goes on increasing as the average coordination number approaches Tanaka threshold [11]. Tanaka modified Phillips'-Thorpe balance condition by including intermediate-range order (IRO) interactions and predicted the existence of a threshold at $< r > = 2.67$. At this $< r >$ value, 2*D* layered structures are fully evolved and the structure is transformed to a 3*D* network for higher $< r >$ values. Thus, it can be supposed that the increasing value of δ (as $< r >$ approaches 2.67), marks the 2*D*→3*D* structural transition in these glasses. It can be associated with atomic arrangements that become more tightly bound with shorter bond lengths resulting smallest mean atomic volume of the network and hence rise in compactness value. Concerning the variation of the refractive index with composition, it can be shown that refractive index increases with increasing Bi ratio, which can be attributed to the increasing compactness of the material or the material aggregation.

The variation of molar volume with composition is shown in figure 5.6. From the figure it is clear that molar volume decreases from 19.35 cc/mol to 17.3 cc/mol with the increase of Bi content. The variation of optical gap also follows the same trend with increases in Bi concentration (chapter IV). In chalcogenide glasses, the

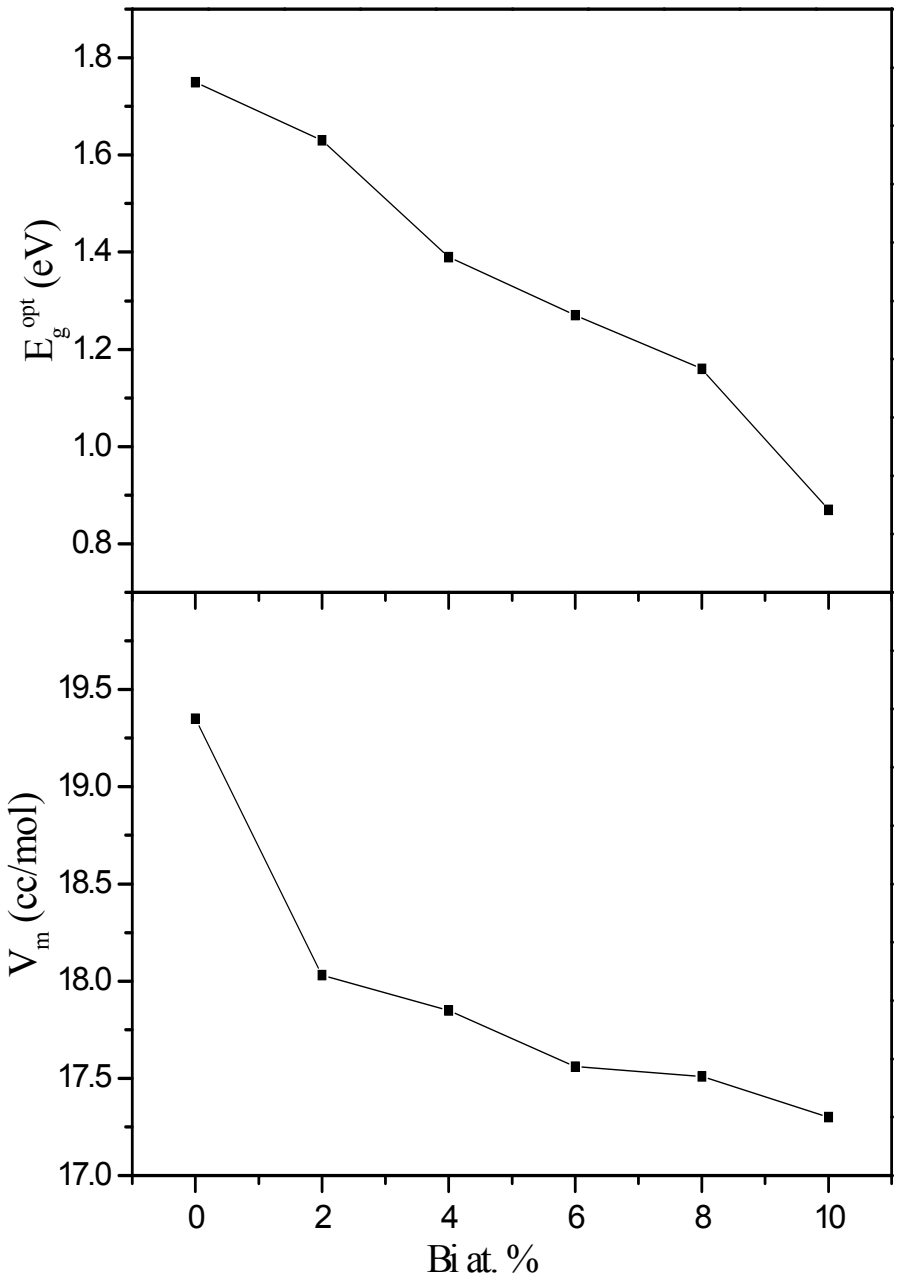

Figure 5.6 Variation of molar volume (V_m) and optical gap (E_g^{opt}) with Bi content.

energy of the conduction band edge is decided by number of atoms per unit volume (N). An increase in N, with decrease of V_m, leads to decrease in the energy of conduction band edge which corresponds to decrease in optical gap subsequently.

5.2.2.2 Correlation between Cohesive Energy and Optical Gap

Explanation of optical behaviour of *a*-Ge-Se-In-Bi glasses has been given in terms of cohesive energy using the chemical bond approach (*CBA*) method [24]. The cohesive energy is the stabilization energy of an infinitely large cluster of material per atom and also reflects the average bond strength. At the same time it allows to determine the number of possible bonds and their type *i.e.* heteropolar or homopolar. According to *CBA*, (*i*) atoms combine more easily with atoms of different type rather than the same type, (*ii*) the heteropolar bonds are formed in the sequence of decreasing bond energy until the available valence of atoms is satisfied, (*iii*) each constituent atom is coordinated by 8 - *N* atoms, where *N* is the number of outer shell electrons and this is equivalent to neglecting the dangling bonds and the other valence defects as a first approximation. Also, vander Waal's interactions are neglected which can provide a means for further stabilization by the formation of much weaker links than regular covalent bonds. Based on *CBA*, the bond energies are assumed to be additive. Thus the cohesive energies were calculated by summing the bond energies over all bonds expected in the material. In *a*-Ge-Se-In-Bi system, the Ge-Se bonds with highest possible energy are expected to occur first, followed by In-Se, Se-Bi and Se-Se. At $x \geq 8$ at. % there are still some unsatisfied Bi-Bi bonds which acts as a defect homopolar bonds. Calculated values of *CE* along with chemical bond distribution for all compositions are tabulated in table 5.6. From table it is found that *CE* of these glassy alloys decreases with increasing Bi content. Therefore, it can be concluded that the decrease of optical gap with increasing Bi content is most probably due to reduction of average stabilization energy. The decrease of *CE* implies lower bonding strength, *i.e.* high defect bonds. The optical band gap is a bond sensitive property [35]. So, the decrease of *CE* accounts for the gradual decrease of optical gap with the addition of Bi at the expense of Se. This behavior is also consistent with theoretical band gap.

Table 5.6 Values of electronegativity (χ), theoretical band gap (E_g^{th}), distribution of chemical bonds, cohesive energy (kcal/mol) and optical gap (E_g^{opt}) for $Ge_{20}Se_{70-x}In_{10}Bi_x$ (x = 0, 2, 4, 6, 8, 10) system.

x	χ	E_g^{th} (eV)	Distribution of chemical bonds					*CE*	E_g^{opt} (eV)
			$Ge-Se$	$In-Se$	$Bi-Se$	$Se-Se$	$Bi-Bi$		
0	2.34	1.58	0.5714	0.2143	-	0.2143	-	47.81	1.75
2	2.33	1.54	0.5882	0.2206	0.0441	0.1471	-	47.78	1.63
4	2.32	1.51	0.6061	0.2273	0.0909	0.0757	-	47.75	1.39
6	2.31	1.47	0.6250	0.2344	0.1406	-	-	47.71	1.27
8	2.30	1.43	0.6122	0.2296	0.1071	-	0.0511	46.76	1.16
10	2.29	1.40	0.5999	0.2250	0.0750	-	0.100	45.86	0.87

It was found that the variation in the theoretical values of the energy gap (E_g^{th}) with composition for quaternary alloys can be described by the relation [29]

$$E_g^{th}(ABCD) = aE_g(A) + bE_g(B) + cE_g(C) + dE_g(D) \tag{5.15}$$

where *a*, *b*, *c* and *d* are the volume fraction and $E_g(A)$, $E_g(B)$, $E_g(C)$ and $E_g(D)$ are optical gaps of *A*, *B*, *C* and *D* elements respectively. The conversion from volume fraction to atomic percentage is made by using atomic weight and densities. The values of E_g^{th} for all the compositions are tabulated in table 5.6 and are plotted in inset of figure 5.7 as a function of Bi at. %, which reveals that addition of Bi leads to decrease in E_g^{th}. This decrease of E_g^{th} and E_g^{opt} with increasing Bi content might be due to decrease of average stabilization energy and decrease of electronegativity of the system as calculated from Sanderson's principle. According to this principle, electronegativity of the alloy is the geometric mean of electronegativities of its constituent elements. It is also evident from the table 5.6 that electronegativity decreases as the optical band gap decreases.

5.2.2.3 Relation between E_{04}, $\overline{H_s}$ *and* $< r >$

An attempt has been made to find the relation between E_{04} and average single bond energy. The obtained E_{04} values are given in table 5.7. To correlate these values with average single bond energy for $Ge_{20}Se_{70-x}In_{10}Bi_x$ system, average heat of atomization has been calculated.

For quaternary semiconductor compounds [36], the average heat of atomization $\overline{H}_s$ (kcal/g-atom) for $A_\alpha B_\beta C_\gamma D_\delta$ compound is given by

$$\overline{H}_s = \frac{\alpha H_s^A + \beta H_s^B + \gamma H_s^C + \delta H_s^D}{\alpha + \beta + \gamma + \delta} \tag{5.16}$$

where α, β, γ and δ are the at. ratios of A, B, C and D respectively. In the present quaternary glassy system, the average heat of atomization is calculated by equation (5.16) using the values of heat of atomization 90, 49.4, 58 and 49.1 in kcal/g-atom for Ge, Se, In and Bi respectively. Average heat of atomization (kcal/g-atom) and average single bond energy are tabulated in table 5.7.

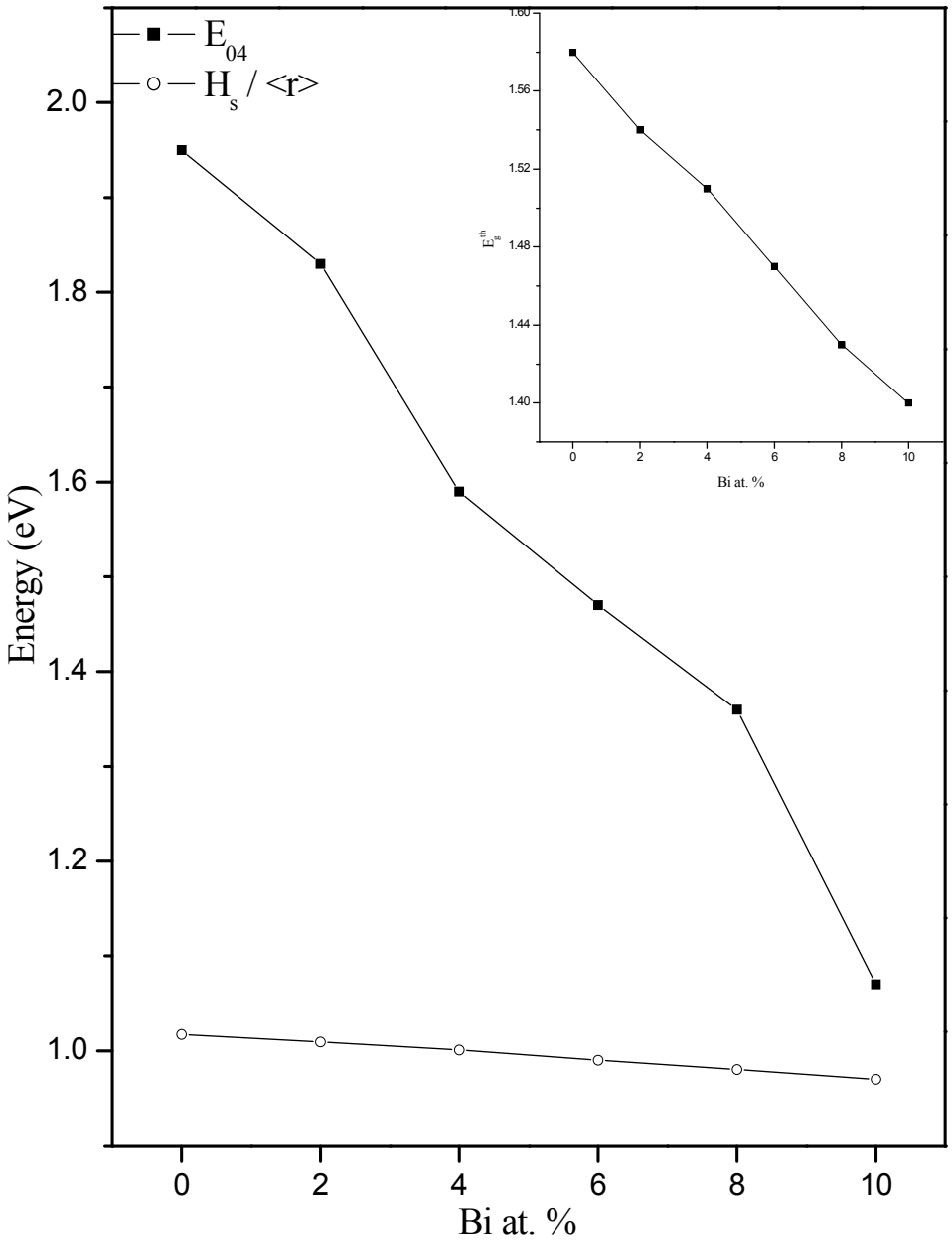

Figure 5.7 Variation of E_{04} and $\overline{H_s}/< r >$ with Bi content and inset shows the variation of theoretical band gap (E_g^{th}) as a function of composition.

Table 5.7 Values of R, $< E >$, T_g, $\overline{H_s}$, $\overline{H_s}/< r >$ and E_{04} for $Ge_{20}Se_{70-x}In_{10}Bi_x$ (x = 0, 2, 4, 6, 8, 10) system and bond energies of their respective bonds.

x	R	$< E >$ (kcal/mol)	T_g (K)	$\overline{H_s}$ (kcal/g-atom)	$\overline{Hs}/< r >$ (kcal/g-atom)	E_{04} (eV)
0	1.27	59.02	520	58.38	23.35	1.95
2	1.17	59.67	529	58.374	23.16	1.83
4	1.08	60.35	538	58.368	22.98	1.59
6	1	61.06	547	58.362	22.79	1.47
8	0.92	59.85	532	58.356	22.62	1.36
10	0.85	58.67	515	58.35	22.44	1.07

Bonds	*Bond Energies* (kcal/mol)
Ge – Se	49.10
Se – Se	44.00
Ge – Ge	37.60
In – Se	48.20
In – In	21.02
Bi – Bi	25.0
Se – Bi	40.7

In chalcogenide it is interesting to relate the optical gap with the average single bond energy. According to Aigrain *et al.* [29] there exists a linear correlation between the energy gap and the average heat of atomization. It is suggested that the average heat of atomization is a measure of the cohesive energy and represents the relative bond strength, which in turn are correlated with the energy gap of semiconductors. Figure 5.7 represents the variation of E_{04} and $\overline{H_s}/< r >$ with composition in Ge-Se-In-Bi glassy alloys. It is clear from the figure that there is decrease in E_{04} with the addition of Bi. However, the average heat of atomization shows negligible deceases with Bi addition. As already discussed in section 5.1.2.3, E_{04} depends more strongly on $\overline{H}_s$ for higher connectivity glasses as lower connectivity glasses. In this case, the value of $< r >$ varies from $2.5 - 2.6$, which can be correlated with low connectivity glasses. This further suggests that the parameter $\overline{H}_s/< r >$ is almost constant with composition and has a very negligible effect on E_{04}. Similar results have also been reported for Ge-Se-In system in section 5.1.2.3.

5.2.2.4 Correlation between Mean Bond Energy and Glass Transition Temperature

Tichy and Ticha recognize that in chemically ordered system, glass transition temperature should not only be related to $< r >$ but there should also be an excellent empirical correlation between T_g and overall mean bond energy. In Ge-Se-In-Bi system, there is a significant difference in the bonding energies of heteropolar bonds *i.e.* Ge-Se, In-Se and Bi-Se from homopolar bonds *i.e.* Se-Se and Bi-Bi bonds. Thus a chemical ordered network is expected. Considerable attention has been devoted to predict T_g of chalcogenide based glasses. It is assumed that T_g is proportional to another material parameter (such as mean bond energy) which strongly depends on the cohesive forces or rigidity of the network (here chemical bond ordering model is assumed). Mean bond energy is given by $< E >= E_c + E_{rm}$, where, E_c = overall contribution towards bond energy arising from strong heteropolar bonds and E_{rm} = contribution arising from weaker bonds that remain after the strong bonds have been maximized *i.e.* the average bond energy per atom of the 'remaining matrix'. Detailed

discussion for calculating $< E >$ is given elsewhere [14]. A correlation between T_g and mean bond energy is given by; $T_g = 311[< E > -0.9]$. In particular, the compositional dependence of T_g in numerous glassy system presents maximum value near $R = 1$, because the chemical bond energies are maximized at this composition. R is the parameter which determines the deviation of stoichiometry and is expressed by the ratio of covalent bonding possibilities of chalcogen atom to non-chalcogen atom. For $Ge_xSe_yIn_zBi_\delta$ system, the quantity $'R'$ is defined by

$$R = \frac{yCN(Se)}{xCN(Ge) + zCN(In) + \delta CN(Bi)} \tag{5.17}$$

where x, y, z and δ are respectively the atomic fractions of Ge, Se, In and Bi. The threshold at $R = 1$ (the point of existence of only heteropolar bonds) is evident. For $R > 1$, the system is chalcogen rich and for $R < 1$, the system is chalcogen poor. The values of R, $< E >$ and T_g are tabulated in table 5.7. With the increase in Bi content in Ge-Se-In glassy alloy, both mean bond energy and glass transition temperature increases and reach as maximum at $R = 1$ and then decreases. For composition $Ge_{20}Se_{64}In_{10}Bi_6$, $R = 1$ marks the minimum selenium content at which chemically ordered network is possible without metal-metal bond formation. The major limitation of the model is that it does not account for the molecular interaction, which plays a vital role in the relaxation process in glass transition region.

5.3 Conclusion

The addition of In to $Ge_{20}Se_{80}$ glassy alloy leads to change in physical properties. Mean bond energy and hence glass transition temperature increases in chalcogenide rich region while decreases in chalcogenide poor region. The cohesive energy of the composition has been calculated using *CBA* and follows the same trend as that of mean bond energy with In content. An increase in photon energy was observed upto 10 at. % of In and it subsequently decreases thereafter. Average single bond energy shows almost constant trend with composition. No correlation between photon energy and average single bond energy was found for low connectivity glasses. The density and the compactness vary with In content in the glassy alloy. Compactness has been observed maximum at percolation threshold. Molar volume

first increases to its maximum value up to 10 at. % of In content and then decreases with further In addition to Ge-Se alloy. Variation of molar volume shows the same trend as that of optical band gap. Physical parameters support the optical data. For addition of Bi to $Ge_{20}Se_{70}In_{10}$ system, density and compactness are found to increase which accounts for an increase in refractive index with Bi content. Molar volume decreases with Bi content follows the same trend as that of optical gap. The cohesive energy of the composition has been calculated using *CBA* and decreases with increase in Bi content. This change is in same fashion to optical gap calculated theoretically and experimentally. Electronegativity also decreases with Bi content. No correlation between photon energy and average single bond energy was found in this system also. Average single bond energy shows almost constant trend whereas a decrease in photon energy with composition was observed. Mean bond energy and glass transition temperature increases in chalcogen rich region and decreases in chalcogen poor region.

References

1. Shiryaev V S, Boussard-Pl'edel C, Houizot P, Jouan T, Adam J L and Lucas J 2006 *Mater. Sci. Eng. B* **127** 138
2. Wang F, Zhang Z, Liu R, Wang X, Zhu X, Pan A and Zou B 2007 *Nanotechnology* **18** 305705
3. Trnovcona V, Furar I and Lezal D 2007 *J. Non-Cryst. Solids* **353** 1311
4. Harea D V, Vasilev I A, Colomeico E P and Iovu M S 2003 *J. Optoelectron. Adv. Mater.* **5** 1115
5. Mahadevan S, Giridhar A and Singh A K 1994 *J. Non-Cryst. Solids* **169** 133
6. Vateva E, Arsova D, Skordeva E and Savova E 1995 *Series Electronic Mat*. (UK: British Academic Press) 604
7. Lucovsky G, Galeener F L, Keezer R C and Six H A 1974 *Phys. Rev. B* **10** 5134
8. Tronc P, Bensoussan M, Brenac A and Sebenne C 1973 *Phys. Rev. B* **8** 5947
9. Phillips J C 1981 *J. Non-Cryst. Solids* **43** 37
10. Phillips J C and Thorpe M F 1985 *Solid State Commun*. **53** 699
11. Tanaka K 1989 *Phys. Rev. B* **39** 1270
12. Mahadevan S and Giridhar A 1989 *J. Non-Cryst. Solids* **110** 118
13. Tichy L and Ticha H 1994 *Mater. Lett.* **21** 313
14. Tichy L and Ticha H 1995 *J. Non-Cryst. Solids* **189** 141
15. Thorpe M F and Tichy L 2001 *Properties and Applications of Amorphous Materials* (London: Kluwer academic Publishers)
16. Pauling L 1960 *The nature of the chemical bond* (New York: Cornell University Press)
17. Mott N F 1969 *Phil. Mag.* **19** 835
18. Saiter J M, Ledru J, Saffarini G and Benazeth S 1996 *Mater. Lett.* **28** 451
19. Fouad S S 1995 *J. Phys. D: Appl. Phys.* **28** 2318
20. Ledru J, Saiter J M, Saffarini G and Benazeth S 1998 *J. Non-Cryst. Solids* **232-234** 634
21. Saiter J M, Ledru J, Saffarini G and Benazeth S 1998 *Mater. Lett.* **35** 309

22. Saffarini G 2002 *Appl. Phys. A* **74** 283
23. Rabinal M K, Sangunni K S and Gopal E S R 1995 *J. Non-Cryst. Solids* **188** 98
24. Bicerano J and Ovshinsky S R 1985 *J. Non-Cryst. Solids* **74** 75
25. Sanderson R T 1971 *Inorganic Chemistry* (New Delhi: Affliated East-West Press)
26. Deneufville J P and Rockstad H K 1974 *Amorphous and liquid semiconductors* ed. Stuke J, Brenig W (London: Taylor & Frances)
27. Sadagopan V and Gotos H C 1965 *Solid St. Electron.* **8** 529
28. Kastner M 1972 *Phys. Rev. Lett.* **28** 355; 1973 *Phys. Rev. B* **7** 5237
29. Benoit C, Aigrain P and Balkanski M 1961 *Selected constants relative to semiconductors* (Pergamon Press: New York)
30. Othman A A, Aly K A and Abousehly A M 2007 *Thin Solid Films* **515** 3507
31. Fouad S S 1999 *Vacuum* **52** 505
32. Vlcek M and Frumar M 1987 *J. Non-Cryst. Solids* **97 & 98** 1223
33. Phillips J C 1979 *J. Non-Cryst. Solids* **34** 153; 1981 **43** 37
34. He H and Thorpe M F 1985 *Phys. Rev. Lett.* **54** 2107
35. Pattanaik A K and Srinivasan A 2003 *J. Optoelectron. Adv. Mater.* **5** 1161
36. Dahshan A and Aly K A 2008 *Phil. Mag.* **88** 361

CHAPTER VI

Summary

Chalcogenide glasses form an important class of materials which are used in various infrared optics and technological applications. Here we have studied two chalcogenide glassy systems *viz.* $Ge_{20}Se_{80-x}In_x$ (x = 0, 5, 10, 15, 20) and $Ge_{20}Se_{70-x}In_{10}Bi_x$ (x = 2, 4, 6, 8, 10). These two glassy systems were studied for their optical properties using UV-Vis-NIR spectroscopy and electrical properties. Physical parameters have also been calculated for $Ge_{20}Se_{80-x}In_x$ and $Ge_{20}Se_{70-x}In_{10}Bi_x$ glassy alloys and are found to be supporting the optical results.

Optical and electrical parameters have been calculated for *a*-$Ge_{20}Se_{80-x}In_x$ (x = 0, 5, 10, 15, 20) thin films. The optical absorption is of non direct type and absorption coefficient is of the order of 10^4 cm^{-1}. n and k for the thin films were calculated and found to decrease with the increase of wavelength. The optical parameters *viz.* E_g^{opt}, n_0, E_d and E_0 found to increase up to 10 at. % of In incorporation in Ge-Se system and then decreases with further addition of In. The change in optical parameters with In incorporation is explained on the basis of Mott and Davis model and change in average bond energy of the system. The dielectric constants and optical conductivity have also been determined from the optical parameters and found to decrease with the increase in wavelength. The study of dark and photoconductivity of $Ge_{20}Se_{80-x}In_x$ thin films as a function of temperature reveals that the conduction is through an activated process with single activation energy in the temperature range 303 to 375 K. ΔE_d increases up to 10 at. % of In addition and thereafter it decreases. The intensity dependence of photocurrent indicates the existence of bimolecular recombination in $Ge_{20}Se_{80-x}In_x$ thin films in which recombination rate of electrons is proportional to the number of holes. Charge carrier concentration (n_σ) decreases up to 10 at. % of In addition and then increases. Photosensitivity (σ_{ph}/σ_d) also shows maximum value at 10 at. % of In addition, indicating that the Ge-Se-In system becomes more rigid at this very composition.

Various parameters related to optical and electrical properties of $Ge_{20}Se_{70-x}In_{10}Bi_x$ (x = 2, 4, 6, 8, 10) vacuum evaporated thin films have also been studied. Optical parameters, in the wavelength range 400 – 1800 nm, are studied from their normal incidence transmission spectra. Absorption mechanism is due to indirect transition. It is found that with the addition of Bi, there is a red shift in the

transmission fringes. Optical energy gap decreases monotonically and the refractive index increases with the increase of bismuth content. This increase in refractive index is quite favorable for fabricating optical waveguides leading to compact circuit design with high intensities. These results indicate an increase in chemical disorder and a decrease in average bond energy of the system with increasing Bi content. The refractive index values for each sample have been fitted to the single-oscillator model. The values obtained for the single-oscillator energy E_0 are consistent with our optical gap results. The dielectric constants and optical conductivity found to decrease with the increase in wavelength for entire wavelength range under investigation. The study of dark and photoconductivity of $Ge_{20}Se_{70-x}In_{10}Bi_x$ thin films as a function of temperature (300 - 360K) reveals that the conduction is through an activated process with single activation energy. Charge carrier concentration (n_σ) increases with increasing Bi content which further accounts for the increase in conductivity. ΔE_d and photosensitivity (σ_{ph}/σ_d) decreases with Bi addition indicating an increase in localized states in the system. The intensity dependence of photocurrent shows the existence of bimolecular recombination in thin films in which recombination rate of electrons is proportional to the number of holes. The transient photoconductivity measurements for investigating thin films at room temperature and typically at 1035 Lux intensity shows that the photocurrent rises in a monotonous manner upto steady state value and after cessation of illumination, it follows non exponential decay. An increase in differential life time is observed with time (for all compositions) as well as with increase in Bi concentration.

The addition of In to $Ge_{20}Se_{80}$ glassy alloy leads to change in physical properties. Mean bond energy and hence glass transition temperature increases in chalcogenide rich region while decreases in chalcogenide poor region. The cohesive energy of the composition has been calculated using CBA and follows the same trend as that of mean bond energy with In content. An increase in photon energy was observed upto 10 at. % of In and it subsequently decreases thereafter. Average single bond energy shows almost constant trend with composition. No correlation between photon energy and average single bond energy was found for low connectivity glasses. The density and the compactness vary with In content in the glassy alloy.

Compactness has been observed maximum at percolation threshold. Molar volume first increases to its maximum value up to 10 at. % of In content and then decreases with further In addition to Ge-Se alloy. Variation of molar volume shows the same trend as that of optical band gap. Physical parameters support the optical data. For addition of Bi to $Ge_{20}Se_{70}In_{10}$ system, density and compactness are found to increase which accounts for an increase in refractive index with Bi content. Molar volume decreases with Bi content follows the same trend as that of optical gap. The cohesive energy of the composition has been calculated using *CBA* and decreases with increase in Bi content. This change is in same fashion as that of optical gap calculated theoretically and experimentally. Electronegativity also decreases with Bi content. No correlation between photon energy and average single bond energy was found in this system. Average single bond energy shows almost constant trend whereas a decrease in photon energy with composition was observed. Mean bond energy and glass transition temperature increases in chalcogen rich region and decreases in chalcogen poor region.